12-2008

Nanostructured Chitosan Membranes for Filtration

Keyur Desai
University of Tennessee - Knoxville

To the Graduate Council:

I am submitting herewith a dissertation written by Keyur Desai entitled "Nanostructured Chitosan Membranes for Filtration." I have examined the final electronic copy of this dissertation for form and content and recommend that it be accepted in partial fulfillment of the requirements for the degree of Doctor of Philosophy, with a major in Materials Science and Engineering.

Kevin M Kit, Major Professor

We have read this dissertation and recommend its acceptance:

Roberto Benson, Gajanan Bhat, Svetlana Zivanovic

Accepted for the Council:
Carolyn R. Hodges

Vice Provost and Dean of the Graduate School

(Original signatures are on file with official student records.)

To the Graduate Council:

I am submitting herewith a dissertation written by Keyur Desai entitled "Nanostructured Chitosan Membranes for Filtration." I have examined the final electronic copy of this dissertation for form and content and recommend that it be accepted in partial fulfillment of the requirements for the degree of Doctor of Philosophy, with a major in Materials Science and Engineering.

_____
Kevin M Kit
Major Professor

We have read this dissertation and recommend its acceptance:

_____
Roberto Benson

_____
Gajanan Bhat

_____
Svetlana Zivanovic

Accepted for the Council:

_____
Carolyn R. Hodges,
Vice Provost and Dean of the Graduate School

(Original signatures are on file with official student records.)

Nanostructured Chitosan Membranes for Filtration

A Dissertation

Presented for the

Doctor of Philosophy Degree

The University of Tennessee, Knoxville

Keyur Desai

December 2008

Dedication

Dedicated to my mother Dr Bhavana Desai

Acknowledgement

Firstly I would like to express my immense gratitude to my thesis advisor, mentor and guide for the past three years Prof. Kevin M Kit who has made my pursuit of a doctorate degree a personally enriching and professionally rewarding experience. Dr Kit has been a very patient, friendly and generous mentor who has given me ample flexibility in designing my work and always been there to guide me through the technical, experimental and personal challenges encountered during the course of my research. I would also like to thank my other committee members Prof. Svetlana Zivanovic of food science and technology department who has been like a co-guide for me on this project always happy and ready to help me address issues related to chitosan chemistry and metal binding experiments, Prof. Gajanan Bhat of materials science and engineering department and UTNRL director, who has helped me with the filtration part of my research and through whom I have learnt all I know about non-woven's processing and characterization and Prof. Roberto Benson, Associate Head of materials science and engineering department and head of the polymer program who has taught me the fundamentals of polymer chemistry, surface modifications of polymers and who has always had his door open to solve any technical or personal issue encountered during the course of my study at UT. I would also like to acknowledge the invaluable guidance and assistance of Prof. P Michael Davidson head food science and technology department for helping me design the experiments for anti-microbial studies and making sense of the obtained results. Thanks to Prof. Weiss and his student Christina from UMASS Amherst who were our co-workers on this project for sharing their data and results. Dr Harry Meyer at the ORNL share user facility has been of immense help in doing the last minute XPS characterization of my samples and correlating surface chemistry with surface binding properties. The author would also like to thank Dr Peter Tsai at UTNRL for his valuable help with the aerosol filtration testing.This work would not have been completed without the assistance of the technical and personnel staff of the MSE department Doug Fielden, Danny Hachwort, Stephen Stiner, Gregory Jones, Brad Snyder, Mike, Sandy, Carla, Frank and Randy. Prof. Dunlap of the SEM facility at UT was also very helpful while doing the SEM imaging of the fibers especially at times when the SEM would just hang up.

I am ever grateful to my family starting with my best friend and mother Dr Bhavana Desai who has been the backbone of my life, and it's all due to her dedication, hard work and

perseverance that I am here today writing this acknowledgement for my doctoral thesis. My maternal grandparents Mr Thakorbhai Desai and Mrs Kusumben Desai have nurtured me and encouraged me to pursue my dreams along with my aunt Dr Smita Desai and they have always been there for me in times of need. This day would not have been realized if not for the love and support provided by my closest friend Sanjay Dube who has been there for me for the past 10 yrs and who has smilingly listened to all my frustrations and problems and help me stay focus. I am deeply grateful for the hospitality and moral support provided by my cousins Sanjay and Parul Desai from Knoxville, TN during my time in Knoxville.

A big thanks to Jiajie Li of the food science department my co-worker on this EPA proposal who has been the person whom I have troubled the most during my PhD work and she has with a big smile and never say no attitude always been there to help me conduct my metal binding and anti-microbial experiments. I would also lastly like to acknowledge the help and support provided by my friends Prabhakar, Raghu, Sameer, Anoop, Bongwoo, Priyadarsi, Shanker, Ranjan, Sandeep,Kan etc. in Knoxville and around the world who have guided and supported me through all my endeavors. A special thank you and sorry to anyone who I may have missed out, it was never my intention though.

This research is funded by U.S. EPA Science To Achieve Results (STAR) program GR832372.

Abstract

Chitosan is a non-toxic and biodegradable biopolymer derived from naturally occurring chitin. It has excellent metal binding and anti-microbial properties which could be beneficial in air and water filtration applications. Nanofibers have distinctly high surface area to volume ratio.

Electrospinning is a process by which nano-sized polymer fibers can be produced using an electrostatically driven jet of polymer solution. The fibers are collected as a non-woven mat and offer a high surface area to volume ratio.

Electrospinning of pure chitosan is hindered by its limited solubility in aqueous acids and high molecular weight with high degree of inter and intra chain hydrogen bonding. We have been able to form nanometer sized fibers without bead defects by electrospinning Chitosan blends with different polymers like poly (ethylene oxide) and poly (acrylamide) with up to 95% chitosan in blend fibers. The electrospinning apparatus was modified so at to be able heat solutions during electrospinning which helps in expanding the processing window. Fiber formation is controlled by polymer molecular weight, blend ratios, polymer concentration and spinning solution temperature.

Surface chemistry of these blend fibers was characterized using XPS. XPS data validated that chitosan content on fiber surface was a function of % chitosan in blend, degree of deacetylation of chitosan, and fiber diameter. A theoretical model was developed which predicted the binding properties of chitosan fibers with known fiber diameter, % chitosan in blend and degree of deacetylation. Surface properties of blend fibers showed a strong correlation with the structure and morphology of the fibers and higher chromium binding capacities compared to similar blend ratio chitosan films were observed. A nanofibrous filter media has been fabricated by electrospinning a layer of chitosan nanofibers onto a non-woven spun bonded poly propylene fabric. These coated filter media have been tested for their metal binding and anti-microbial properties and results showed applicability towards effectively filtering heavy metals and bacteria from waste media. The filtration performance of these nanofibrous filter media have been tested against latex polystyrene beads and aerosol particles and filtration efficiencies of these media were a function of pore size, fiber diameter and size of filtrate.

Table of Contents

List of Tables

List of Figures

1. Introduction

With growing environmental concerns for global warming there is an urgent requirement for cleaner air and water around the world which has sparked immense interest in the development of high efficiency filters. Fibrous media in the form of non-wovens have been widely used for filtration applications. Non-woven filter are made of randomly laid down micron sized fibers which provide a physical sized based separation mechanism for the filtration of air and water borne contaminants[1]. Non-woven nanofibrous filter media (nanofiber is defined as having diameter < 0.5 μm by non-woven's industry[2]) would offer a unique advantage as they have high specific surface area, good interconnectivity of pores, and ease of incorporation of specific functionality on the surface effectively filtering out contaminants by both physical and chemical mechanisms. A number of companies are developing nanofibrous filter media like Donaldson Company (Ultra-Web and Fibra-Web), Finetex Mats™, Amisol EA Air Filters[2].

Chitosan, a polycation, is a non toxic, biodegradable polysaccharide derived from naturally occurring chitin. Chitin is the second most abundant polysaccharide found in the exoskeleton of crustaceans, crab and shrimp shells, insects and fungal mycelia[3,4]. Chitinous biopolymers have also been found in wastes of mushroom like *Agaricus bisporus* (most consumed variety of mushroom in USA)[5]. Based on the mushroom waste generated annually mushrooms could yield up to 1000 metric tons of crude fungal chitin. Chitosan is a copolymer of N-acetyl-D-glucosamine and D-glucosamine, and the D-glucosamine content is dependent on the degree of deacetylation (DDA) of chitin to chitosan. Chitosan has several unique properties; it is anti microbial and inhibits the growth of a wide variety of fungi, yeasts and bacteria [6]. It can also bind toxic metal ions which can be beneficial for use in air and water filtration applications[7].

Electrospinning is a process by which sub-micron sized polymer fibers can be produced using an electrostatically driven jet of polymer solution[8]. The fibers are collected as a non-woven mat. Electrospun nanofiber mats offer a distinctly high surface area to mass ratio (typically ranging from 40-100 m^2/g, compared to 0.05-10 m^2/g for micron sized spunbonded or melt blown non-wovens) which can be beneficial in a variety of applications. Electrospun fibers can have varied applications and have been used in areas like protective textiles, electronic sensors, scaffolds for tissue engineering, drug delivery substrates, air and water filtration etc[9].

The goal of this study is to fabricate a nanofibrous filter media which is capable of filtering out toxic pollutants from air and liquid media. Chitosan based nanofibrous filter media would take advantage of both physical and chemical mechanisms to effectively filter out toxic pollutants from air and liquid media, delivering the next generation of non-toxic, environmentally benign filter media made from naturally occurring biodegradable materials.

1.1 Literature Review

1.1.1. Chitosan – Structure, Properties and Applications.

Chitosan is obtained from chitin by the deacetylation of chitin or removal of the acetyl linkage using conc. NaOH. Figure 1.1 shows the structure of chitin and chitosan and process of deacetylation of chitin to form chitosan[10]. Chitosan is a copolymer of N-acetyl-D-glucosamine and D-glucosamine. The sugar backbone of chitosan consist of β-1, 4-linked D-glucosamine. In its structure, chitosan is very similar to cellulose, except for the amino group that replaces the hydroxyl group on the C-2 position[11]. The D-glucosamine content which affects the properties of chitosan is related to the degree of conversion or degree of deacetylation (DDA) of chitin to chitosan. A 100% DDA chitosan indicates 100% conversion of chitin to chitosan whereas a 0% DDA chitosan is essentially chitin. An 80% DDA chitosan would contain 20% N-acetyl-D-glucosamine and 80% D-glucosamine linkages.

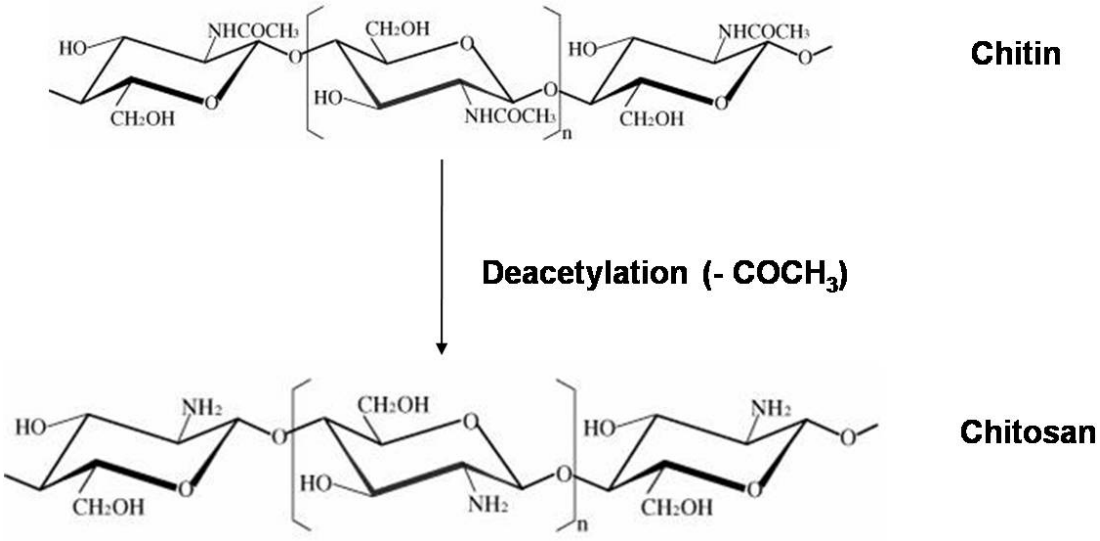

Figure 1.1 Structure of Chitin and Chitosan

Natural biopolymers like chitin have usually very high molecular weights (usually larger than one million Daltons)[12]. Molecular weight of chitosan varies and is dependent on the raw material sources, and method of preparation. At high temperature (> 280°C) chitosan begins to undergo thermal degradation. Typically pyrolysis of polysaccharides is accompanied by a random split of the glycosidic bonds and further decomposition leading to formation of acetic acid, butyric acid and other fatty acids [13]. Increased dissolved oxygen, shear degradation due to hydrodynamic forces can also contribute to the thermal degradation of chitosan[11]. Chitin is a highly crystalline hydrophobic polysaccharide and insoluble in most organic solvents; however chitosan is soluble in aqueous organic acids. Chitosan can be easily modified by utilizing the reactivity of the primary amino group and the primary (-OH) and secondary ($-CH_2OH$) hydroxyl groups. Some of the commonly synthesized and used derivatives of chitosan are quaternary chitosan salts, N-carboxyalkyl chitosan, N-Acylychitosan etc[14].

The major physical characteristics that affect the functional properties of chitosan are its molecular weight and crystallinity[15]. The crystallinity of chitosan is dependent on the source of chitin from which it is extracted and can be found in three forms i.e. α-chitin (shrimp and crab shells), β-chitin (squid pen) and γ-chitin (stomach cuticles of cephalopoda). The most commonly available chitin is α-chitin[16].With increase in molecular weight, crystallinity increases due to tighter packing of chains leading to increase in mechanical properties of chitosan films[17]. Stevens et.al[17] showed that films made from same molecular weight chitosan and varying DDA showed an increase in % crystallinity with increasing DDA.

Chitosan is protonated at pH < 6.5 and becomes positively charged polycation as shown in equation 1. The number of positively charged $-NH_3^+$ groups on the chitosan backbone is a function of the degree of deacetylation, and solution pH which is related to the pKa of the solution as shown in equation 1. A higher degree of deacetylation would lead to a larger number of positively charged groups on the chitosan backbone. At 50% protonation, pH=pKa. Sorlier et.al[18] have studied the effect of pH and degree of deacetylation (DDA) on chitosan solution pKa and found that for varying DDA from 5%-75%, pKa varies between 6.3 and 7.2.

$$H^+ + RNH_2 \leftrightarrow RNH_3^+, K_a$$

$$K_a = \frac{[H^+][RNH_2]}{[RNH_3^+]} \qquad (1)$$

$$pK_a = -\log K_H$$

$$pH = pK_a + \log\frac{[RNH_2]}{[RNH_3^+]}$$

Chitosan has been widely used as a metal chelating agent in industry and metal binding occurs due to the ionic bonding between the dissociated metal ion in solution and NH_3^+ ion on the chitosan fiber surface and also the available $–NH_2$ and –OH sites on chitosan backbone can serve as coordination sites for metal ions.[19] Numerous mechanisms have been proposed to explain the binding of metal ions by chitosan and it has been widely accepted that amine sites are the main reactive sites for interaction with metal ions[16]. Table 1.1 summarizes the metal binding capacity of chitosan for various heavy metal ions[20-22]. The interaction between chitosan and hexavalent chromium has been extensively studied and an adsorption capacity of 273 mg Cr/g chitosan was achieved for chitosan flakes. It was found that absorption capacity was strongly related to pH, at pH = 3 sorption was almost 90% and was reduced to 10% at pH = 7.0 with an initial chromium concentration of 5 mg/l[22]. The total number of amine sites in the chitosan molecule may not be available for metal sorption as some of them may be involved in forming inter and intra-molecular hydrogen bonds, and binding can also be influenced by the residual crystallinity of the polymer.

Table 1.1 Adsorption capacities (mg/g) of chitosan for various heavy metal ions

Material	Cr^{6+}	Ni^{2+}	Pb^{2+}	Hg^{2+}	Zn^{2+}	Cu^{2+}	Cd^{2+}	Pt^{6+}
Chitosan powder	273	2.4	16.36	815	75	222	5.93	
Non-crosslinked chitosan beads	80					85		
Crosslinked chitosan beads	50					60		280

The adsorption of metal ions by chitosan has been modeled and data has been fitted to various adsorption isotherms like Langmuir, Freundlich and Langmuir-Freundlich[16]. However since these models were "force fitted" they were valid only over a small concentration range. A simplified equilibrium model has been proposed by Juang et.al[23] who have modeled the absorption behavior based on the competing reaction between proton and metal ions (as shown in equation 2)[23] for the same amino acid binding groups. Protonation constant of chitosan was measured (log K_H) by studying the sorption of various metal ions like Cu^{2+}, Ni^{2+} and Zn^{2+} and found to be in accordance with literature which validated the model.

$$H^+ + RNH_2 \leftrightarrow RNH_3^+, K_H$$

$$M^{2+} + n_m RNH_2 \leftrightarrow M(RNH_2)_{n_m}^{2+}, K_M, \tag{2}$$

$$K_H = \frac{q_H}{C_H q_{NH_2}}$$

$$K_M = q_M / C_M (q_{NH_2})^{n_m}$$

where C and q are concentration of species in aqueous and solid phases respectively.

Cross linking chitosan using epichlorohydrin or glutaraldehyde improves the stability of chitosan at low pH. However, it leads to reduction in binding capacity compared to uncross linked chitosan validating the hypothesis that electrostatic attraction between amino sites and metal ions was the dominant mechanism for metal binding of chitosan[21] as cross linking leads to reduction in number of available $–NH_2$ available for binding. The adsorption of metal ions by chitosan is also affected by the physical properties of chitosan like its molecular weight and crystallinity[24]. Milot et.al[24] have studied the effect of crystallinity and molecular weight on the molybdate sorption by chitosan. They found that the sorption capacity decreased with increased crystallinity whereas there was no clear correlation between molecular weight and sorption

capacity. Increased crystallinity hinders the number of available amine sites due to the tight packing of the structure caused by increased inter and intra-chain hydrogen bonding between chitosan chains[25]. The metal binding capacity data shown in Table 1.1 also suggest a size effect. Chitosan flakes, which have a higher surface area to mass ratio compared to chitosan beads, exhibit higher binding capacities. The affinity of chitosan for heavy metal ions has been summarized in the literature to be Pd>Au>Hg>Pt>Cu>Ni >Zn>Mn>Pb>Co>Cr>Cd>Ag[26, 27].

The antibacterial properties of chitosan are also due to the interaction between the positively charged amide groups on the chitosan backbone and negatively charged components in the microbial cell membranes. Binding between chitosan and cell wall components alters the barrier properties and prevents entry of nutrients or causes leakage of intracellular components[28] both of which lead to death of the cell. The factors that affect the anti-microbial effectiveness of chitosan are similar to those that affect its metal binding capacity like degree of deacetylation, pH, molecular weight, crystallinity, and microbial buffer solution temperature[29]. Shimojoh et.al[30] have studied the effect of molecular weight (constant DDA) and test microorganism on the antibacterial activity of chitosan. They found that chitosan with MW 220,000 was most effective whereas chitosan with MW 10,000 was least effective in its bactericidal activities; however bactericidal activity of chitosan with MW 70,000 was better for some test bacteria compared to chitosan with MW 426,000. No clear correlation has been developed between molecular weight and antibacterial activity although it is generally accepted that increased molecular weight leads to improvement in antibacterial properties[29]. Liu et.al[31] studied the effect of molecular weight, degree of deacetylation and pH on the antibacterial activity of chitosan and carboxymethylated chitosan. They found that with increasing molecular weight up to 91,600 the activity increased however upon further increase of molecular weight it actually decreased due to increase in inter and intrachain hydrogen bonding in chitosan which reduces the amount of available $-NH_3^+$ sites. The antibacterial activity was directly proportional to degree of deacetylation and the antibacterial activity was highest at pH = 6.3 above which it was minimal due to poor solubility and de-protonation of chitosan in the medium. For pH < 6.3 the activity gradually decreased till pH = 4.0 and then increased[31]. The carboxymethylated chitosan showed higher antibacterial properties then chitosan. Liu et.al attribute that to the inter and intramolecular attraction between the carboxyl and amide groups leading to an increase in the number of $-NH_3^+$ sites. The temperature of the buffer medium also affects the antimicrobial activity as studied by Tsai et.al[32].

They found that at buffer solution temperatures between 25°C and 37°C the E-coli cells were completely killed within 5hr and 1hr respectively, however at low temperature (4°C and 15°C) the activity was lowered for 5hrs after which it stabilized indicating poor interaction between chitosan and E-coli at low temperatures[32].

Owing to its polycationic nature and excellent metal binding and antimicrobial properties chitosan has been used for a wide variety of applications ranging from the medical industry to cosmetics to the water purification industry[14]. Chitin/chitosan can be obtained in variety of shapes and forms like powders, flakes, fibers, hollow fibers, sponges and scaffolds[26]. Some of the key areas where the use of chitosan has matured are:

a. Biomedical Applications: Chitosan gels have been extensively used as a drug release substrate because it is easily degradable, nontoxic, and biocompatible. Various drugs like aspirin, diazepam, ibuprofen, insulin and diclofenac sodium have been incorporated in chitosan matrix of various shapes and forms like gel beads, coatings, spherical agglomerates, microspheres etc.[33] Chitosan has also found use in making artificial kidneys, wound healing dressings, making artificial skin, orthopedics, dentistry, cosmetics, ocular bandage lenses etc.[14, 33] Researchers at the British Textile Technology Group (BTTG) have patented a method to develop chitin based fibrous dressings; the chitin/chitosan used for this work was obtained from micro fungi instead of shrimp shells. The fibrous wound dressing were made using paper making wet laid technology[34].
b. Chromatographic Separations: The polycationic nature of chitosan makes it highly useful as a packing material in chromatography columns as it can interact with organic substances like proteins and also with transition metal ions to achieve desired seperations[35].
c. Food and Nutrition: Chitosan can also bind fat and has been used to make dietary weight loss tablets which are commercially available in Europe. Chitosan has also been widely used in food packaging industry as it is non-toxic, biodegradable, and good oxygen and water vapor permeability.
d. Water Engineering: One of the major applications of chitosan is in the purification of waste water. Chitin/chitosan has been widely used as a flocculating agent to remove heavy metal ions from waste water streams owing to its excellent metal adsorption capacity as discussed earlier.

e. Textile Industry: Textiles made from or coated with chitosan have been developed and used for their anti-microbial and metal chelating properties. Chitin/chitosan fibers have been made using wet spinning of polymer solutions in 2% acetic acid. Formation of chitin/chitosan fibers is limited by its poor solubility in most common organic solvents and its thermal degradation before melting making it difficult to process using conventional fiber forming methods like fiber spinning, melt blowing etc. Chitosan coated fabrics have been studied for their antimicrobial efficacy. Tseng et.al[36] studied the effect of chitosan-citric acid coating on wool fabrics and found that oxidized woolen fabrics formed crosslink's with chitosan and the coated fabrics did achieve bactericidal properties. The effect of chitosan coatings on cotton fabrics was studied by Hudson et.al[37] who have also observed the efficiency of these kind of antimicrobial coatings against both gram negative and gram positive bacteria. The absorption and release of silver and zinc ions on chitosan fibers has been studied for their anti-microbial and wound healing applications respectively[38]. Chitosan fibers were prepared by wet spinning process and were treated with different concentration solution of $AgNO_3$ and $ZnCl_2$. Results showed that absorption of Ag and Zn ions was a function of concentration of solutions and immersion time and the process was reversible i.e. if the fibers were place in saline solutions the ions would be desorbed. Chitosan fibers showed a 77% reduction in E-coli whereas chitosan fibers with Ag particles showed 100% reduction in E-coli[38].

1.1.2. Electrospinning

Electrospinning of polymers has grown to be a field of keen interest with various research groups taking advantage of this relatively easy and inexpensive method of fabricating fibers in the micro to nano meter range. It is a process by which sub-micron sized polymer fibers can be produced using an electrostatically driven jet of polymer solution[8]. The fibers are collected as a non-woven mat. Electrospun nanofiber mats offer a distinctly high surface area to mass ratio (typically ranging from 40-100 m^2/g) which can be beneficial in filtration applications. Figure 1.2 shows plot of surface area to mass ratio v/s fiber diameter of textile materials[39].

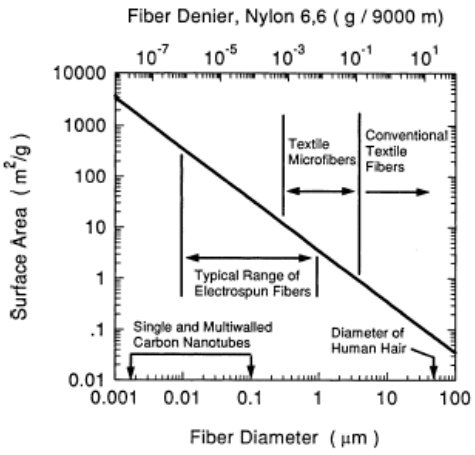

Figure 1.2 Surface area to mass ratio of electrospun fibers vs. fiber diameter.

The fundamental principle underlying the process of electrospinning is that a spherically charged droplet of a low molecular weight conducting liquid under vacuum is under the influence of two forces, 1) the disintegrative electrostatic repulsive force and 2) the surface tension acting on the droplets which tends to hold the droplet in spherical shape. Under equilibrium conditions the two forces balance each other as depicted in Figure 1.3a. However when the charge acting on the droplet is increased the electrostatic repulsive force acting on the droplet overcomes the forces of surface tension and the droplet breaks up into smaller particles (Figure 1.3b). This phenomenon is called as electrospraying and has been used for spray painting and coating technologies. Envisioning the same effects on a high molecular weight polymer solution that has sufficiently high number of chain entanglements the breakage of the charged droplet under the right conditions of applied electric field and solution viscosity could lead to formation of a steady jet which would ultimately form into a fiber. For any polymer solvent system to be successfully electrospun, it should be able to form a charged polymer fluid jet[40], which is formed when the viscous forces acting on the polymer droplet are high enough to overcome the forces of surface tension. The formed charged polymer fluid jet after travelling a certain distance (~3 mm) undergoes a bending instability followed by a complex chaotic whipping motion[41] wherein the solvent evaporates and polymeric fibers are formed and collected on the grounded target.

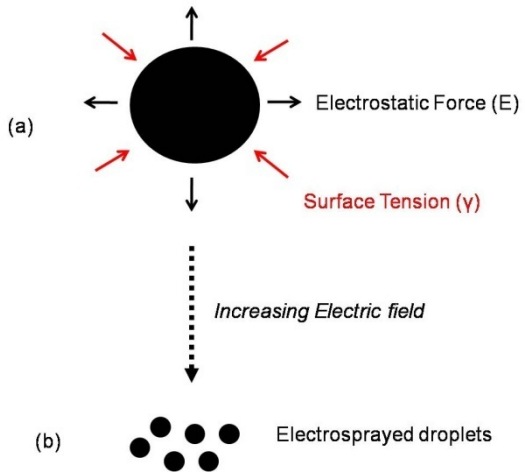

Figure 1.3 Effect of increased electric field on charged particle (a) Particle under equilibrium (b) Electrospraying

For electrospinning, the viscosity of the solution (which is a direct result of the concentration of polymer in solvent and its molecular weight) is the most critical parameter. If polymer concentration is lower than the critical chain overlap concentration c* the charged polymer jet breaks into droplets or electrospraying occurs. As the concentration is increased above c* formation of fibers with bead like defects is observed and ultimately at the entanglement limit (c>>c*), uniform beadless nanofibers are obtained[42] as shown in Figure 1.4. The critical chain overlap concentration is inversely proportional to the intrinsic viscosity[42] i.e. $c^* \sim [\eta]^{-1}$. Shenoy et.al have developed a relationship wherein prior knowledge of the entanglement and weight average molecular weight (Me,Mw) of a polymer could help in predicting the requisite polymer concentration for fiber formation in a polymer-good solvent system[43]. They calculated the entanglement number (n_e) which is ratio of weight average molecular weight and entanglement molecular weight of polymer in good solvent. Knowing the entanglement number and performing series of experiments for different polymer solvent systems they have been able to understand and predict the effect Me on fiber formation. According to their model when $n_e < 2$ only beads are formed, if $2 < n_e < 4$ we get bead + fiber formation and when $n_e > 4$ only fibers are formed.

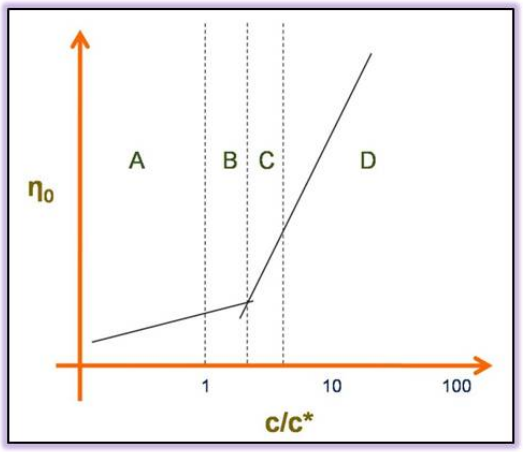

For electrospinning of PMMA

A. **(c/c*)< 1, dilute region, formation of droplets**
B. **1<(c/c*)<3, semi dilute un entangled region, formation of droplets along with few beaded fibers**
C. **3<(c/c*)<4, semi dilute entangled region, formation of beaded fibers**
D. **(c/c*)>6, formation of uniform fibers without bead defects**

Figure 1.4 Effect of concentration on viscosity and spinnability of PMMA-DMF systems.[42]

The effect of electric charge on liquid droplets has been studied historically dating back to the 19th century. In 1882 Lord Raleigh studied the instability of electrically charged liquid droplets and showed that the electrostatic force overcomes the surface tension which tends to act in the opposite direction when the droplet is sufficiently charged[44]. Taylor[45] studied the disintegration of water drops, and he theoretically demonstrated that a conical interface between two fluids could exist in equilibrium in an electric field. The droplets were found to have elongated at the onset of instability and its end formed into a conical shape which has semi-vertical angles close to 49.3 degrees, thus the first suggestions to the development of a Taylor cone which has been discussed by later researchers as the key to fiber formation during electrospinning.

In 1934 Anton Formhals patented an invention[46] related to a process and apparatus that was designed for the production of artificial filaments by the use of an electrical field on liquids, which contain dissolved solid materials like cellulose acetate. The solutions are passed into an electric field formed between electrodes in a thin stream or in drops in order to separate them into a plurality of threads. In 1971 the first polymer fibers by electrospinning were produced by Bumgarten et.al[47] , he studied the formation of micro fibers of acrylic by electrospinning. He determined the limits of spin-ability of polyacrylonitrile in dimethylformamide solvent and also

observed a relationship between fiber diameter and solution viscosity. In 1981 Larrondo and Manley performed similar work on polymer melts and they observed that the fiber diameter decreased with increasing melt temperature. Given the relationship between melt temperature and viscosity they were able to draw a qualitative correlation between diameter and viscosity[48].

In the last decade, science and technology has seen the advent of nanotechnology and nanosystems wherein the requirements are to fabricate smaller and smaller devices. This era of nanotechnology has helped to regain interest in the field of electrospinning with researchers across the globe trying to spin various polymer systems. In 1995 Doshi et.al[8] published the electrospinning of polyethylene oxide and described the electrospinning process and its effects on the fiber morphology and possible applications of the fibers. They found that viscosity below 800 cp polymer solution was too dilute to form a stable jet and the jet broke, at a viscosity of higher then 4000 cp it was too difficult to form fibers due to the drying of the solution at the tip. Fong et.al[49] studied the influence of polymer concentration, solvents used, tip-target distance, and flow rate on the formation of beaded fibers during the electrospinning of PEO. They found that the viscoelasticity of the solution, charge carried by the jet and surface tension of the solution were the key factors that influenced the formation of beads during electrospinning. Deitzel et.al[50] have evaluated systematically the effects of two important processing parameters, spinning voltage and solution concentration on the fibers formed. They found that spinning voltage strongly correlated with the formation of bead defects in the fibers, and their measurements can be used to signal the onset of the processing voltage at which the bead defect density increases substantially. Solution concentration has also been found to most strongly affect the fiber size, with fiber diameter increasing with increasing solution concentration according to a power law relationship. In another study by Deitzel et.al[51] they tried to control the deposition area of the electrospun PEO fibers by using multiple field electrospinning apparatus which was used by applying a secondary external electric field of the same polarity as the surface charge on the jet. This mechanism allows for greater control over the deposition of the electrospun fiber on a surface and for collection of the electrospun fibers in other forms than non-woven mats. A novel hybrid methodology which combines traditional polymer processing techniques like twin screw extrusion with electrospinning has been proposed by Wang et.al[52]. They have made electrospun nanofibers of polycaprolactone containing uniformly dispersed β-tricalcium phosphate nanoparticles. The twin screw extruder is used to facilitate uniform mixing

of the nanoparticles with the electrospinning polymer solution and results showed that the particles were uniformly dispersed in the fibers whose size ranged from 200-2000 nm[52]. This unique method can be advantageous for making composite nanofibers incorporated with nanoclay, carbon nanotubes, and drugs with uniform mixing. Recently researchers in Germany have reported an unexpected result of forming nanoscaled fibers up to 25 nm from a polymer solution during standard spin coating process. They explained the fiber formation relied on the Raleigh-Taylor instability of the spin coated liquid film that arose due to a competition of the centrifugal force and the Laplace force induced by the curvature of the rotating chuck[53].

Both electrostatic and fluid dynamic instabilities can contribute to the basic operation of the process. The bending instabilities that occur during electrospinning have been studied and mathematically modeled by Reneker et.al[40]. After the jet travels, straightforward unsteadiness appears in the form of loops. The jet does not bend but it also forms lateral excursions that grow into spiraling loop. New bending instabilities arise when the jet is thin enough and stress relaxation of the viscoelastic stress has taken place indicating splitting and splaying of the fibers and formation of a Taylor cone. Another group led by Rutledge also studied electrospinning with regards to electrically forced jet and instabilities and proposed a stability theory for electrified fluid jets[54, 55]. A series of papers demonstrates that an essential mechanism of electrospinning is a rapidly whipping fluid jet. This whipping action of the fluid jet was shown well by Reneker et.al [41] in their paper on electrospun nanogarlands of polycaprolactone. They found that electrically driven bending instability in the electrospinning of polycaprolactone results in the contact and merging of segments in different loops of the electrospinning jet while the jet is in flight. These contacts limit the lateral expansion of the jet path suggesting that no splitting and splaying from a single jet occurs during electrospinning and only a single jet of fibers undergoes a whipping action as it approaches the target (Figure 1.5).

Several attempts have been made to model and predict the phenomena of electrospinning. Spivak and Dzenis[56] modeled and predicted the radius and motion of a weakly conductive viscous jet accelerated by an external electric field taking into account the inertial, hydrostatic, viscous, electrical and surface tension forces. The polymer fluid was described by a non-linear rheological constitutive equation (Ostwald-deWaele law) and a one-dimensional equation for jet radius was derived and analyzed. The model predictions were found to be in agreement with experimental observations.

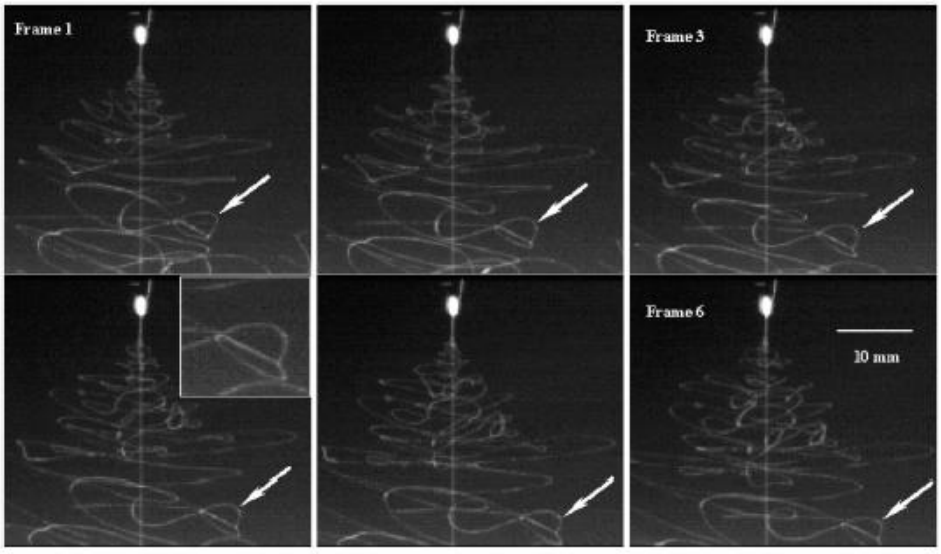

Figure 1.5 Whipping action of electrospun fibers of polycaprolactone captured by a fast shutter speed digital camera, observed that no splitting and splaying of the jet occurs[41].

Yarin et.al[40] have studied and explained the formation of the charged electrical jet after exiting the syringe and formation of bending instabilities during its complex motion between the syringe and target. Initially the jet travels in a straight line but as the motion of the jet is affected by the lateral forces acting on the jet a bending instability developed and grew. The jet was being continuously stretched as it travelled further due to repulsive forces between charges carried with the jet, however instead of continuing in a straight line the jet began to loop and the loops grew larger in diameter as the jet travelled further and became thinner. Creation of these multiple loops occurred within a finite region as the jet travels. The cycle of bending instabilities repeated itself until all the solvent had been evaporated and the jet dried out. They concluded that electrostatic interactions between individual charge elements in the jet and between charge elements and the macroscopic electric field were primarily responsible for initiation and perpetuation of the bending instability.

To control the spread of the Taylor cone and diameter of the bending instabilities Deitzel et.al[51] created an electrospinning apparatus which had charged circular copper rings placed in between the solution ejecting syringe and the fiber collection target as shown in Figure 1.6.

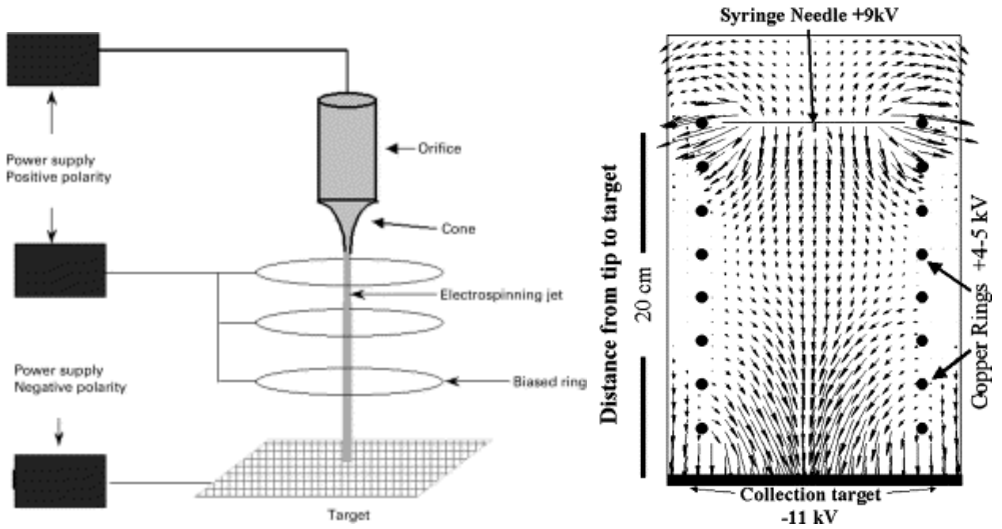

Figure 1.6 Schematic of multiple field line electrospinning apparatus (left), simulated electric field distribution in a multiple feed set-up (right)[51].

It can be seen that the charged copper rings referred to as an 'electrostatic lens' helped converge the charged electric jet along the center of the applied electric field hence controlling the spread of the fibers. Several other researchers[54, 55] have also modeled the electrospinning phenomenon and tried to explain it using various theories like electrohydrodynamics of electrified fluid jets[57, 58]. They came up with a number of predictive phase diagrams which could predict the onset of bending instability or whipping motion as function of the applied electric field and solution conductivity.

Most of the research carried out in electrospinning in the past decade or more has focused primarily on electrospinning of different types of synthetic and biopolymer systems, and scale up of the process for mass production of the fibers and has been well summarized in many review papers published on electrospinning[9, 59-65]. Electrospinning process conditions and effect of above mentioned process parameters has been widely studied and optimized to form nanometer sized uniform fibers of most commonly used synthetic polymers like polycarbonate[66], polystyrene[67],nylon-6[65, 68], poly(vinyl alcohol)[69], polyaniline[70], poly(methymethacrylate)[71], polyacrylamide[72, 73] etc.. From the above it can be deduced that the principle factors that govern fiber formation during electrospinning of any polymer-solvent system are:

a) Physical properties of polymer and solvent i.e. molecular weight, solubility etc:

One of the earliest and highly cited works that studied the effect of solution parameters (conductivity, surface tension, and viscosity) and applied electric field on fiber formation summarized that with increase in viscosity, solution conductivity, applied electric field and reduction in surface tension beadless fiber formation was favored [49]. Increasing the solution conductivity by adding NaCl led to an increase in net charge density and formation of thinner beadless fibers[49]. Addition of ethanol to PEO/water system increased the volatility of the solvent reducing the surface tension and improving the spinnability[49].

b) Applied electric field:

Fong et.al[49] found that a certain critical voltage was required to charge and elongate the polymer droplet and onset of the bending instabilities, voltages higher than the critical voltage led to further extension and thinning of the charged jet and formation of thin bead less fibers. Using a biased AC or "AC-DC" electric supply highly aligned electrospun nanofiber mats can be obtained[74].

c) Distance between charged syringe and collecting target:

The distance between the syringe and the target also plays a critical role in fiber formation. A greater distance gives more time for solvent evaporation and leads to formation of thinner beadless fibers[75].

d) Flow rate of polymer solution:

The solution flow rate also affects fiber formation, if the solution flow rate is faster than the rate at which it can be charged it leads to formation of large beads and an instability in the system[75].

e) Ambient parameters like humidity during electrospinning:

Stephens et.al[67] studied the effect of moisture on surface microstructure of electrospun fibers, they observed that as the humidity of the electrospinning environment was increased microspheres or surface pores were being formed on electrospun polystyrene fiber surface. The size shape and number of pores could be controlled by the solvent and relative humidity of the electrospinning chamber. The mechanism of pore formation was attributed to formation of breath figures on surface of electrospinning jet. As the solvent is evaporating water molecules are condensing on the jet surface and when the jet dries and solidifies to form fiber it leaves behind a cup shaped pore on the surface of the fiber[67].

f) Motion and design of electrospinning target:

The mechanical and molecular alignment of electrospun fibers can be controlled by modifying the target used to collect the fibers. The use of a rotating drum as a target leads to formation of mechanically and molecularly aligned electrospun polyacrylonitrile fibers[76, 77].

g) Spinning solution temperature:

Another way of varying or reducing the solution viscosity of electrospinning polymer solutions which has proven to be useful in electrospinning naturally occurring high molecular weight biopolymers is heating the polymer solution during electrospinning. Researchers have investigated the effect of blowing hot air around the needle carrying the polymer solution. This modified electrospinning process has been termed as "electroblowing" by Um et.al[78]. The hot air heats the solution which reduces the viscosity and aids in fiber formation. The blown air also helps to further stretch the polymer jet and increase the spin-draw ratio. Hyaluronic acid which is a naturally occurring biopolymer and relatively difficult to spin because of its high molecular weight, inter/intra chain hydrogen bonding, and high solution viscosity was easily electrospun using this hot air modified apparatus using aqueous hydrochloric acid as a solvent[78, 79]. The modified electrospinning apparatus used in this study by Um et.al[78] is as shown Figure 1.7. They measured the temperature of the hot air using a thermocouple at three points marked (A) point where air came out of the air tube, (B) point where air came out of the gap near the spinneret and (C) point where solution droplet came out around the spinneret. Experiment trials showed that point C was the most accurate prediction of actual temperature of electrospinning solution; hence temperature read by thermocouple C was recorded.

Lu et.al[80] studied the electrospinning of polyacrylonitrile using DMF as a solvent at elevated temperatures using an apparatus as shown in figure 1.8, they used a jacket type heat exchanger around the syringe to heat the electrospinning solution. The solution temperature was measured at the needle end using a thermocouple as they observed a temperature gradient along the length of the needle due to its "one dimensional fin" geometry. During the spinning process they encountered problems with maintaining a stable jet and formation of a Taylor cone. A high temperature saturated DMF vapor is introduced around the jet which helps prevent the drying of the jet as the temperature at the end of the needle reaches the boiling point of the solvent. Effect of needle length was also studied on the fiber formation during electrospinning.

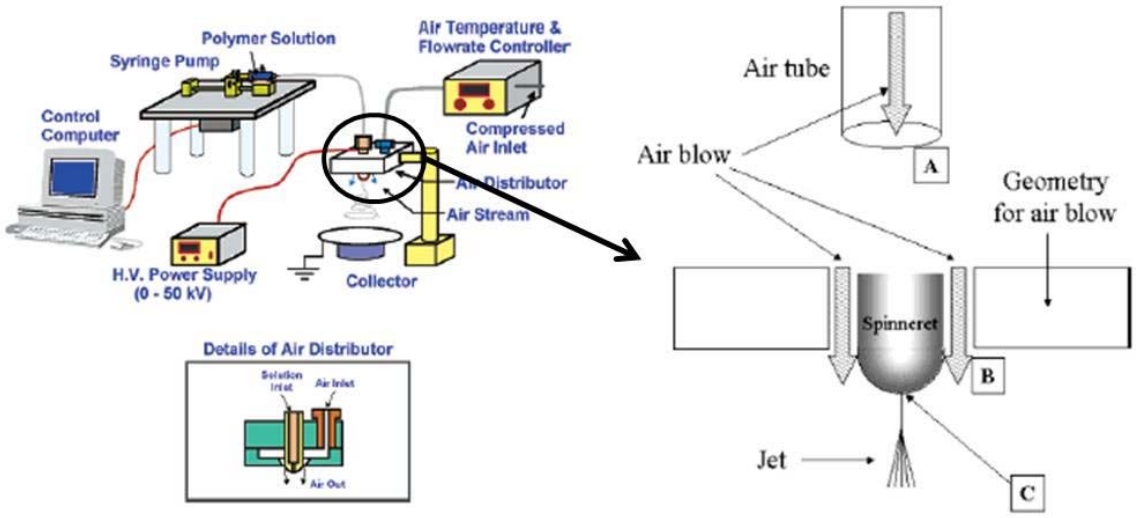

Figure 1.7 Schematic of heated electrospinning unit design by Um et.al[78] to electrospin Hyaluronic acid.

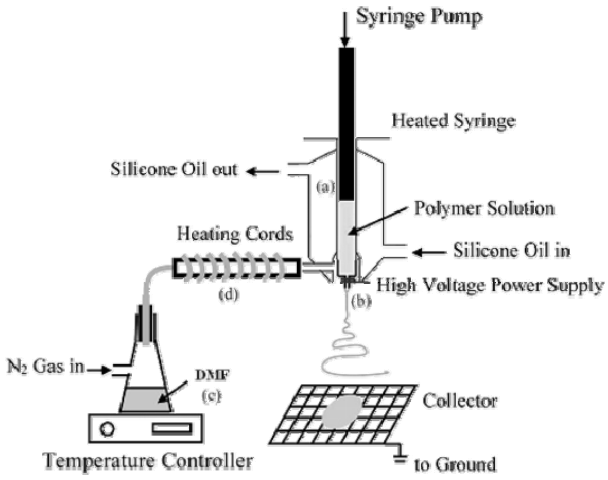

Figure 1.8 Schematic set-up of high temperature electrospinning unit by Lu et.al[80].

With an increase in needle diameter an increase in size of Taylor cone and electrified jet were observed, along with an increase in fiber diameter from 256 to 502 nm (needle diameter increased from 0.57 to 2.77 mm) and lower drawability and lessbirefringence. They found that high temperature spinning was an alternate way of modifying solution properties to form thinner fibers with lower crystalline order but with higher chain orientation. With increased temperature the viscosity and surface tension of solution decreased with increase in

conductivity. Also, at higher temperatures a strong viscosity dependence of fiber diameter was observed (@ 32.2°C $d_f = \eta_0^{0.74}$; @ 88.7°C $d_f = \eta_0^{0.52}$)

Electrospinning is a truly versatile process and can be modified to produce fibers with different size, shape and components. Polymer blends can also be electrospun to produce polymer fibers with desired morphology like bi-component fibers or core-sheath fibers or co-continuous fibers. Bi-component fibers of poly(vinyl chloride)/Estane and poly(vinyl chloride)/poly (vinylidiene fluoride) have been successfully fabricated as described by Gupta et.al[81]. Fibers produced by this method were a mixture of both polymers, however a single fiber was not a blend of both polymers as in the experimental set-up used, the two polymer solutions came into contact only at the tip of the needle. Polymer blend solutions have also been widely electrospun. Feng[82] studied the phase morphology of blend solutions of polycarbonate/poly(vinyl chloride), he did not find any phase separation in the formed fibers and attributed it to dominance of kinetic effects (rapid solution evaporation) over thermodynamic factors (time of mixing, molecular weight difference) which favor phase separation. Wei et.al[83] studied numerous polymeric blend systems and found that the right combination of solubility parameter difference, polymer molecular weight, and blend molecular weight ratios which facilitate higher chain mobility would lead to formation of core-sheath structures. Nanofibers of blends of polybutadiene/polycarbonate (25:75) spun using tetrahydrofuran as solvent showed core sheath morphology[83]. Polymers difficult to electrospin by themselves can also be spun by blending them with easily electrospinnable polymers like poly(ethylene oxide) (PEO). Fibers of 1 μm diameter have been fabricated by blending PEO and poly-3-dodecylthiophene (P3DDT, an electronic polymer used for sensors etc.)[84]. The formed fibers were characterized for their phase morphology using fluorescence imaging as P3DDT shows an emission signal of fluorescence, which revealed presence of P3DDT core surrounded by PEO. The PEO sheath was then removed by washing the fibers with acetonitrile which selectively dissolves PEO leaving behind structurally intact P3DDT fibers[84].

Lim et.al[85] studied the effect of crystalline morphology on the tensile properties of electrospun nanofibers. Fibers were electrospun from 10, 12 and 14 wt% polycaprolactone in a solvent mixture of dichloromethane and N-N-dimethylformamide. Nanofibers formed from

polymer solutions of lower concentration have higher degree of molecular orientation and crystallinity, and have superior strength and stiffness.

Nanofibers having anti-bacterial properties have been fabricated by electrospinning of polyelectrolytes. Electrospinning of polyelectrolytes like poly(2-(dimethylamino)ethyl methacrylate hydrochloride)(PDMAEMA.HCL) has been studied and ultrathin fibers with diameter 2-3 orders of magnitude less then neutral polymers were obtained[86]. Fiber formation was correlated to the rheological properties of these polyelectrolyte solutions and it was observed that addition of NaCl reduced the concentration required to form fibers[86].These polyelectrolyte fibers can be used for protective clothing as they have anti-bacterial properties[86]. Polyurethane cationomers (PUC) containing different amounts of quaternary ammonium groups have been synthesized by Youk et.al[87] and successfully electrospun into nanofiber mats. The PUC nanofibers showed greater than 99.9% reduction in colonies when tested against Staphylococcus aureus and Escherichia Coli microorganisms[87]. Antimicrobial nanofibers with up to 5 log reduction in activity (after 120 mins of contact) have been fabricated using photo-cross-linked poly (vinyl pyrolidone) and poly(ethylene oxide) nanofibers containing complex bound iodine[88]. SEM images of these nanofibrous membranes showed that no bacteria were attached to the surface of the fibers and it was concluded that bacteria were killed as soon as they came in contact with iodine vapors[88]. Electrospun nylon-6 nanofibers containing N-halamine additives have shown up to 8 log reduction in Staphylococcus aureus and Escherichia Coli micro organisms in a short period of contact time (40 mins). N-halamine was directly added to nylon-6/formic acid solutions and fibers obtained showed uniform distribution of N-halamine on surface of fiber[65].

1.1.3. Electrospinning of Biopolymers

As this study involves the electrospinning of a biopolymer chitosan, detailed review of electrospinning of biopolymers is presented herewith. Biopolymers can be defined as macromolecules which are obtained from natural sources. They include polysaccharides (cellulose, chitin, chitosan, dextran, alginate), proteins (collagen, gelatin, fibrinogen, elastin, silk), DNA etc. Electrospinning of biodegradable polymers and biopolymers has generated a lot of interest[89-92] in recent years. Electrospun biopolymer based nanofibrous structures meet the essential design criteria of an ideal tissue engineered design scaffold based upon its structure

which acts as an excellent substrate to support and guide cell growth[93-95]. Electrospun fibers made of different synthetic biodegradable and biocompatible polymers like polyurethane[96-99], poly (glycolic acid)[100], polycaprolactone[95] etc have been made using common organic solvents like chloroform, N,N-dimethylformamide, tetrahydrofuran etc. and demonstrated to be useful for wound cleansing, healing, cell growth, cell proliferation and scaffolds for tissue engineering.

Electrospinning of cellulose

Cellulose is the most abundant natural, renewable, biodegradable polymer. Cellulose and cellulose derivatives (cellulose acetate) have been widely electrospun with potential applications in biomedical industry, composites and filtration[62, 101-105]. Common solvents used for electrospinning cellulose are mixtures of N-methylmorpholine oxide (NMMO)/water or lithium chloride/N,N di-methylacetamide[106]. For both solvent systems it was necessary to apply a post processing step of coagulation with water to obtain sub-micron sized stable cellulosic fibers. Cellulose acetate has been electrospun using acetone, acetic acid and N,N-dimethylacetamide as solvent[105], and these have been deacetylated using NaOH to obtain sub-micron sized cellulose fibers. Rutledge et.al have fabricated bactericidal cellulose acetate fibers containing chlorhexidine. Bactericidal efficiency up to 99.9% was achieved against E.coli and S.epidermidis microorganisms[103]. Cellulose acetate nanofibers containing $AgNO_3$ when irradiated with UV light led to formation of Ag coated anti-microbial nanofibers. 99.9% reduction in both gram negative (E. coli,K. pneumoniae and P. aeruginosa) and gram-positive (S. aureus) test micro-organisms was observed when in contact for over 18 hrs with Ag coated cellulose acetate nanofibers[102].

Electrospinning of chitin/chitosan

Electrospinning of chitosan is limited by its poor solubility in most organic solvents. It is only practically soluble in aqueous acid solutions. Some success has been achieved in electrospinning of chitosan out of acetic acid[107] and using environmentally harmful and toxic solvent like trifluroacetic acid[62, 104] wherein fibers formed readily dissolved in aqueous solutions and had to be glutaraldehyde cross linked using amide linkages to preserve their structural integrity. Chitosan nanofibers have also been made from deacetylation of chitin fibers spun using 1,1,1,3,3,3-hexafluoro-2-propanol[108] (HFIP) as a solvent. Electrospun fibers made of structurally modified N-carboxyethylchitosan[109] and quartenized chitosan[110] have been made by blending chitosan with poly(vinyl alcohol) and poly(vinylpyrrolidone) and fibers formed have shown

antimicrobial activity against pathogenic microorganisms (98.8% reduction after 90 mins contact). Most of the other work in this area has been related to spinning chitosan blends with synthetic polymers like PEO and poly (vinyl alcohol) (PVA)[111, 112] ; wherein beaded fibers were obtained at (66:34) or lower loading of chitosan: synthetic polymer in blend solutions. Duan et.al[113] studied the electrospinning of chitosan/PEO blends and found that both microfibers and ultrafine fibers (fiber diameter 80-180 nm) were obtained with solutions containing higher ratio of PEO. XPS analysis of fiber surface showed that microfibers (fiber diameter in microns) had only PEO on the surface whereas the ultrafine fibers had both chitosan and PEO on the surface. Lou et.al[114] electrospun chitosan/PEO (60:40) blend fibers and studied the attachment of Osteosarcoma cells (MG63) on the fiber surface. Chitosan blend fibers did not exhibit cytotoxicity thus providing a favorable substrate for cell growth and proliferation. Table 1.2 summarizes the various known studies of electrospinning of chitosan and chitosan containing blends, most of these studies are targeted at potential use of chitosan nanofibers as tissue engineering scaffolds or other biomedical applications.

Electrospinning of other polysaccharides

Nanofibers of alginate/PEO blends have been successfully electrospun by Bhattarai et.al[123]. The nanofiber network has mechanical properties comparable to cartilage and demonstrated cellular compatibility with chondrocytes. Hyaluronic acid nanofibers have been electrospun as described earlier using a heat assisted electrospinning apparatus. It has varied applications as drug implants, ocular lens protective material etc. Another polysaccharide electrospun is dextran which is obtained from bacteria and has been used for delivery of drugs, proteins and imaging agents. It has been electrospun using mixture of water, dimethylformamide (DMF) and dimethyl sulfoxide (DMSO) as solvent. Proteins like Bovine Serum Albumin up to 10 wt% could be easily incorporated into electrospun dextran nanofibers[124].

Electrospinning of Collagen

Collagen is the main structural component of the extracellular matrix. Bowlin et.al[89] have electrospun type I and type III collagen using HFIP solvent. Cellular studies were conducted on these electrospun scaffolds and encouraging results demonstrated their use for the bioengineering of cartilage. Collagen/elastin blends have been electrospun and studied as materials for making vascular grafts[125]. Gelation a natural biopolymer obtained by the hydrolysis of collagen has been electrospun by blending with polycaprolactone using trifluoroethanol as solvent[126]. Collagen has

been blended with chitosan and nanofibers formed showed intermolecular interaction between blend fibers possibly producing new materials for biomedical applications[127].

Electrospinning of Silk

Silk, a material commonly used for textiles and obtained from silkworms, contains a fibrous protein termed fibroin which has attracted attention for biomedical applications as it has excellent mechanical properties, is anti-inflammatory, biocompatible and biodegradable[128]. Silk and silk/chitin blends have been electrospun using HFIP as a solvent[128, 129]. Fibers showed good cytocompatibility. Bowlin et.al[90] and Wnek et.al[69] have studied the feasibility of electrospinning fibrinogen for tissue engineering and wound dressing applications respectively. The solvent for electrospinning was HFIP and the nanofiber mats showed excellent mechanical integrity and strength. Elastic modulus of a 6*6 cm nanofiber mat of 0.7 mm thickness was found to be 80MPa with a peak stress of 2 MPa compared to a 110nm diameter poly(glycolic acid) electrospun nanofiber of similar dimensions which showed a modulus of 60 MPa and peak stress of 5 MPa[69].

Electrospinning of other proteins

Milk proteins like casein and other enzyme proteins which cannot be normally processed into fibrous forms have been easily fabricated into nanofibers by blending with synthetic polymers like PEO and PVA. Xie et.al[130] showed that ultrafine nanofibers of these enzyme containing proteins were prepared and showed enhanced catalytic activity towards hydrolyzing olive oil then cast films of same material, due to increase in surface area. Egg albumin a highly functional food protein has been electrospun by blending with PEO using formic acid as a solvent, fiber formation was a function of polymer blend ratios and fibers were formed with as little as 1:0.1 (Egg Albumin:PEO) blend ratio[131]. Zein is a prolamine, the major storage protein of corn, which comprises about 45–50% of its protein content. It has been widely used a coating material for food or tablets to protect foods from stomach acids. Recently electrospinning of Zein has been explored and nanofibers of zein and zein/Hyaluronic acid blends have been electrospun using alcohol and acetic acid as solvents[132, 133]. Other proteins explored for their electrospinnability are wheat protein[134] which is a polydisperse plant protein and has been used in the food industry to strengthen dough networks. It has been electrospun using HFIP as a solvent.

Table 1.2 Summary of known studies of electrospun chitosan/chitosan blends

Polymer (s)	Molecular Wt	Degree of deacetylation	Solvent	Electrospinning Conditions	Ref
Chitosan 10	3210kDa	78%	TFA/MC	15 kV, 15 cm	[104]
Chitosan 10	210kDa	78%	TFA	15 kV, 15 cm	[104]
Chitosan	70kDa 191-130kDa	74% 83%	TFA	26 kV, 6.4 cm, 1.2 ml/h	[62]
Chitosan	210kDa	91%	TFA/MC	25 kV, 15 cm, 2ml/h	[115]
Chitosan		95%	TFA/MC	25kV, 20 cm	[116]
Chitosan	106kDa	54%	aq. AA	3-5 kV/cm, 20 µl/min	[107]
Chitosan10/PVA Chitosan100/PVA	210kDa 1300kDa	78% 77%	aq. AA	15kV, 15cm	[104]
Chitosan/PVA	1600kDa	82.5%	aq.AA	18kV, 25cm	[112]
Chitosan/PVA	120kDa	82.5%	aq.Acrylic acid	22kV, 12cm	[117]
Chitosan/PEO			aq.AA	15 kV, 20 cm, 0.1 ml/h	[113]
Chitosan/PEO	190kDa	85%	aq.AA	20-25 kV,17-20 cm	[111]
Chitosan/UHMWPEO	190kDa /5000kDa	85%	aq.AA		[118]
Chitosan/Collagen	100kDa/1000kDa	85%	TFA/HFIP	20kV, 130cm, 0.8ml/h	[119]
Chitosan/Silk fibroin	220kDa	86%	FA	16kV, 8cm, 1 ml/h	[120]
Hexanoyl Chitosan	576kDa	88%	Chloroform	8-18kV,12cm	[121]
Carboxymethyl Chitosan	40-405kDa	84.7%	water	10-15kV, 17-20cm	[122]

(TFA-trifluoroacetic acid; MC-dichloromethane; AA-acetic acid; HFIP-hexafluoroisopropanol; PVA-poly(vinylalcohol); PEO-poly(ethyleneoxide; UHMW – ultrahighmolecularweight))

Electrospinning of Deoxyribonucleic Acid (DNA)

DNA, a nucleic acid which is known to contain genetic specificity of biological developments of all living organisms, has also been electrospun. Reneker et.al[135] first demonstrated the electrospinnability of DNA fibers using a 0.3 -1.5 % fibrous calf thymus Na-DNA (MW:10^9 g/mol) in a mixture of H_2O/ethanol (7:3) . Similar observations were found by Takahashi et.al who observed the spun DNA fibers using AFM[136]. Liu et.al have electrospun DNA fibers from mixtures of DNA/PEO[137]. Craighead et.al[138] also electrospun DNA/PEO blends and showed upon spinning, the DNA molecules were stretched and could be released from the fiber. Plasmidic DNA was incorporated in a PLA-bPEG-b-PLA block co-polymer and electrospun into nanofibers, and its release characteristics over 20 days was studied[139]. It was found that DNA released was structurally intact, capable of cellular transfection and successfully encoded the protein beta-galactosidase. DNA nanofibers can also be prepared by surface functionalization of nanofibers made from synthetic polymers. Polystyrene nanofibers have been functionalized using a layer-by-layer method with various substrates like polyelectrolytes, DNA and gold to form functionalized nanofibers with specific applications as biosensors, catalysis etc[140].

1.1.4. Nanofibrous Filter media

Nanofibrous non-woven media offer the distinct advantage of high surface area to volume ratio; they have low basis weight, high permeability and small pore size that make them suitable for wide range of air and water filtration applications. Using electrospinning to fabricate nanofibrous filter media we can easily control the fiber diameter, filter thickness and porosity. Barhate et.al[141] have shown that by optimizing the applied electric field, tip-target distance and fiber collection method the porosity, fiber size and thickness of electrospun poly(acrylonitrile) fiber mats can be controlled which in turn can control their filtration performance. The present use of nanofibrous filter media is limited to prefiltration, due to its small pore size and lack of self-supporting mechanical strength[1]. Figure 1.9[142] shows the size of the common particulate media, micro organisms and other pollutants. While particulates up to 0.3μm can be easily filtered using conventional micron size non-woven filter media made by conventional non-woven processing techniques like melt blowing, there is a need in industry for media which can trap particles of smaller sizes[143]. Nanofibrous filter media can play an important role in dealing

with these small contaminant sizes (< 0.3 µm) as they have high porosity, interconnected open pore size, high permeability for fluids and high specific surface area[1].

Nanofibers have been extensively used for air filtration in commercial, industrial and defense applications over the past two decades. Donaldson Company Inc. is one of the major companies which has pioneered the application of nanofibrous filter media for air purification. Pulse-clean cartridges incorporating micron sized cellulosic media, cellulosic/synthetic blend media and nanofibrous cellulosic media were tested and compared for filtration performance. The nanofibrous cellulosic media showed the lowest pressure drop[144]. As pore size and fiber size are reduced, the pressure drop is expected to increase, but due to interception and inertial impaction, nanofibers tend to exhibit better filtration efficiencies at same or lower pressure drops compared to micron sized filter media. For interaction of particulates with nanofibers the effect of slip flow at the fiber surface has to be considered[145].

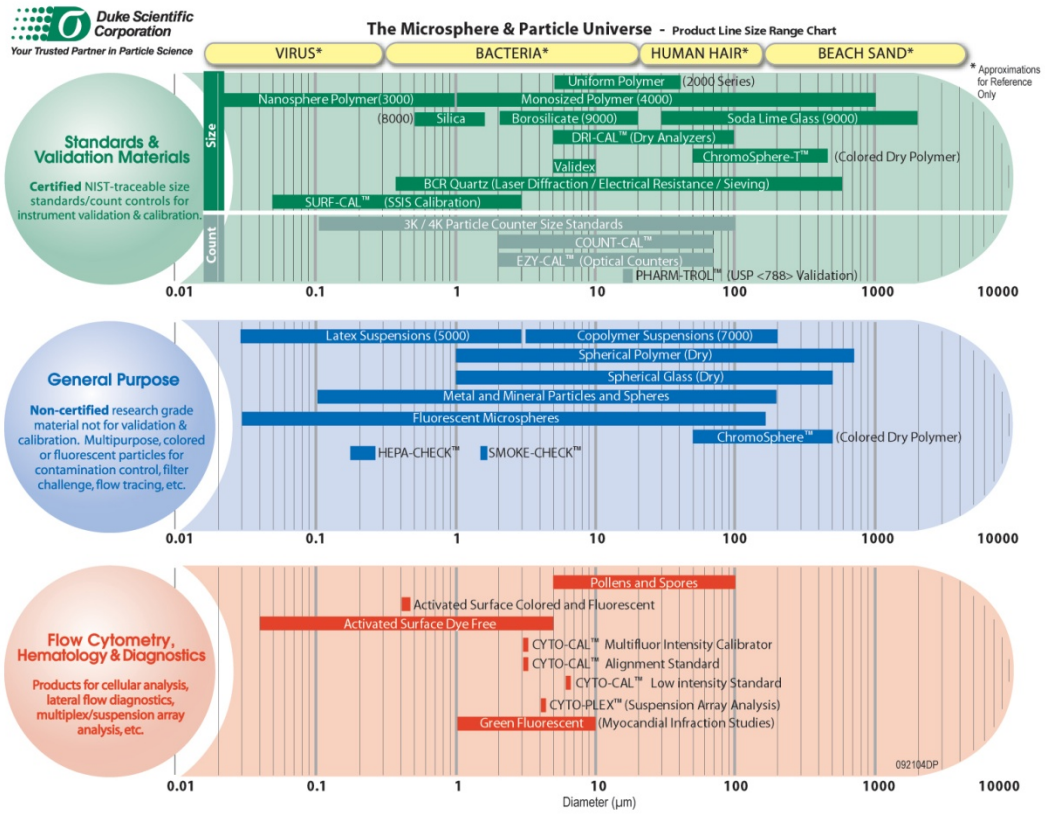

Figure 1.9 Size ranges of typical air and water borne pollutants

Filtration theory generally assumes that when a particulate media comes in contact with fiber surface "no-slip" condition occurs at point of contact between particle and fiber i.e. air velocity is zero at that point. However, Graham et.al.[145] have shown that as fiber size is reduced (< 0.5 microns) slip flow must be considered and diffusion of particles along with interception and inertial impaction lead to higher filtration efficiencies. At high face velocities impaction is the dominant filtration mechanism for nanofibers whereas at lower face velocities collection/filtration is by diffusion[146]. The Knudsen number (Kn) is used to describe the molecular movements of the fluid at the fiber surface, and is defined as the ratio of mean free path of the air ($\lambda = 0.0666 * 10^{-6}$ m) to the mean value of the radius of the fibers (Rf)[141]. Depending on Kn four different flow regimes can be defined around a fiber (1) Continuum regime ($Kn<10^{-3}$), (2) Slip flow regime ($10^{-3}<Kn<0.25$), (3) Free molecule regime ($Kn > 10$) and (4) transient region ($0.25 < Kn<10$)[147].

$$Kn = \frac{\lambda}{R_f}$$

Figure 1.10 shows the various interaction mechanisms dominating at different particulate sizes[143]. Hence nanofibrous filter media offer unique opportunity for physical (size based) and chemical (adsorption or diffusion) based separations.

As the electrospinning process has matured and different synthetic polymers have been electrospun researchers have started developing their products for varied applications such as for aerosol particulate filtering[39, 148], high efficiency particulate air filters (HEPA)[146], antimicrobial air filter[102, 149], coalescence oil filter[150] and catalytic filters for recycling and reusing highly specific catalysts like enzymes[39].

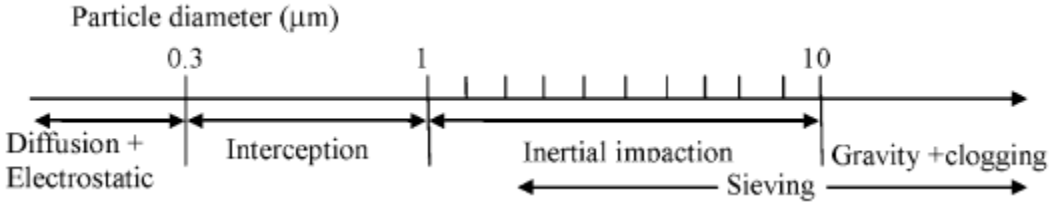

Figure 1.10 Operative particle size in various interaction mechanisms

Ahn et.al[146] tested electrospun Nylon-6 nanofibers for aerosol filtration against commercially available HEPA filters. The normal criteria for HEPA filter performance is they have efficiency of 99.97% to filter 0.3 μm particles at 5 cm/s face velocity. The electrospun Nylon-6 nanofibers had 99.993% efficiency which is superior filtration efficiency than HEPA filters. One drawback of the nanofibers was that they exhibited higher pressure drop than the HEPA filters. However, to achieve the same filtration performance, a substantially lower nanofiber basis weight was required (HEPA filter: basis weight = 78.2 g/m^2,thickness = 500 μm, pore size = 1.7 μm; Espun Nylon 6 filter: basis weight = 10.75 g/m^2, thickness = 100 μm, pore size = 0.24 μm)[146]. Wang et.al[151] studied the filtration performance of electrospun poly(vinylalcohol) nanofibers spun on top of a spunbonded and melt blown polypropylene. The filtration performance of these nanofibrous filter media was tested against 0.6 μm NaCl aerosol particles. The spun bond (fiber diameter = 13 μm, pore size = 41 μm) layer had a 6% filtration efficiency, whereas the melt blown layer (fiber diameter = 4 μm) had a 30% filtration efficiency. When a 0.5 g/m^2 electrospun layer (fiber diameter = 0.2 μm, pore size = 0.74 μm) was placed on top of spun bond layer the filtration performance improved from 6 to 20% and was 100% when weight of e-spun layer was 2.8 g/m^2. When the same e-spun fiber mat was place on top of the melt blown layer the performance ramped up from 13 % to 60% at 0.5 g/m^2 (e-spun fiber) to 100 % at 2.4 g/m^2 (e-spun fiber)[151]. Similar results were obtained by Harlin et.al[152] who studied the effect on filtration performance of an electrospun layer of polyamide-66 fibers on a spun bond substrate. They concluded that filtration efficiency increased with incorporation of as little as 0.02 g/m^2 nanofiber layer and was up to 90% with 0.5 g/m^2 nanofiber coating for sub-micron sized aerosol particles. However, a drawback of coating an electrospun layer is that it could be easily delaminated from the substrate and was mechanically weak hence a top protective layer of spun bond or melt blown material would impart mechanical strength to the composite filter[152]. Okuyama et.al[153] studied the filtration performance of electrospun poly(acrylonitrile) fibers (270-400 nm size range) against NaCl aerosol particles (< 80nm in size). Filter quality factor or figure of merit (Equation 3a) along with the single fiber collection efficiency was found to be independent of thickness of nanofiber mat and function of nanofiber diameter and packing density. Higher figure of merit or quality factor is indicative of better filter performance.

$$Q = -\frac{\ln(P)}{\Delta p} \ldots\ldots\ldots\ldots\ldots\ldots\ldots\ldots\ldots\ldots (3a)$$

where Q is the quality factor, P is penetration of aerosol particles through the filter and Δp is pressure drop across filter

Wang et.al[2] have also studied the effect of particulate size, nanofiber solidity and fiber diameter on the quality factor and filtration efficiency on a single nanofiber layer on a substrate. Fiber solidity is defined as shown by Equation 3b.

$$\alpha = \frac{\pi d_f}{4h} \ldots\ldots\ldots\ldots\ldots\ldots\ldots\ldots\ldots (3b)$$

where α is the nanofiber solidity, d_f is fiber diameter and h is distance between two nanofibers

Experimental results proved that with increasing fiber solidity filtration efficiency and pressure drop increased[2]. The figure of merit (which is a function of particle size and fiber diameter) decreases with increased solidity for small particles; whereas for particles near the penetrating size increasing solidity increases figure of merit. Nanofiber performance was compared against standard glass fiber media of 0.053 cm thickness, fiber diameter = 1.9 μm and 0.05 solidity, nanofibers had better figure of merit for particles larger than 100 nm compared to glass fiber filters.

The single fiber collector efficiency was modeled based on theory proposed Kirsh and results were in agreement with experimentally observed data[153]. Maze et.al[147] simulated the filtration performance of nanofiber webs at reduced pressures. The nanofibers were modeled as straight cylinders, assuming that fibers lie horizontally on the web and do not bend at cross over points, a complex 3-D web generation algorithm was developed to model the nanofibers taking into consideration the orientation distribution of the fibers. Figure 1.11 shows top view of the virtual electrospun fiber mats of varying diameters[147]. With increasing diameter the surface pore size increased.

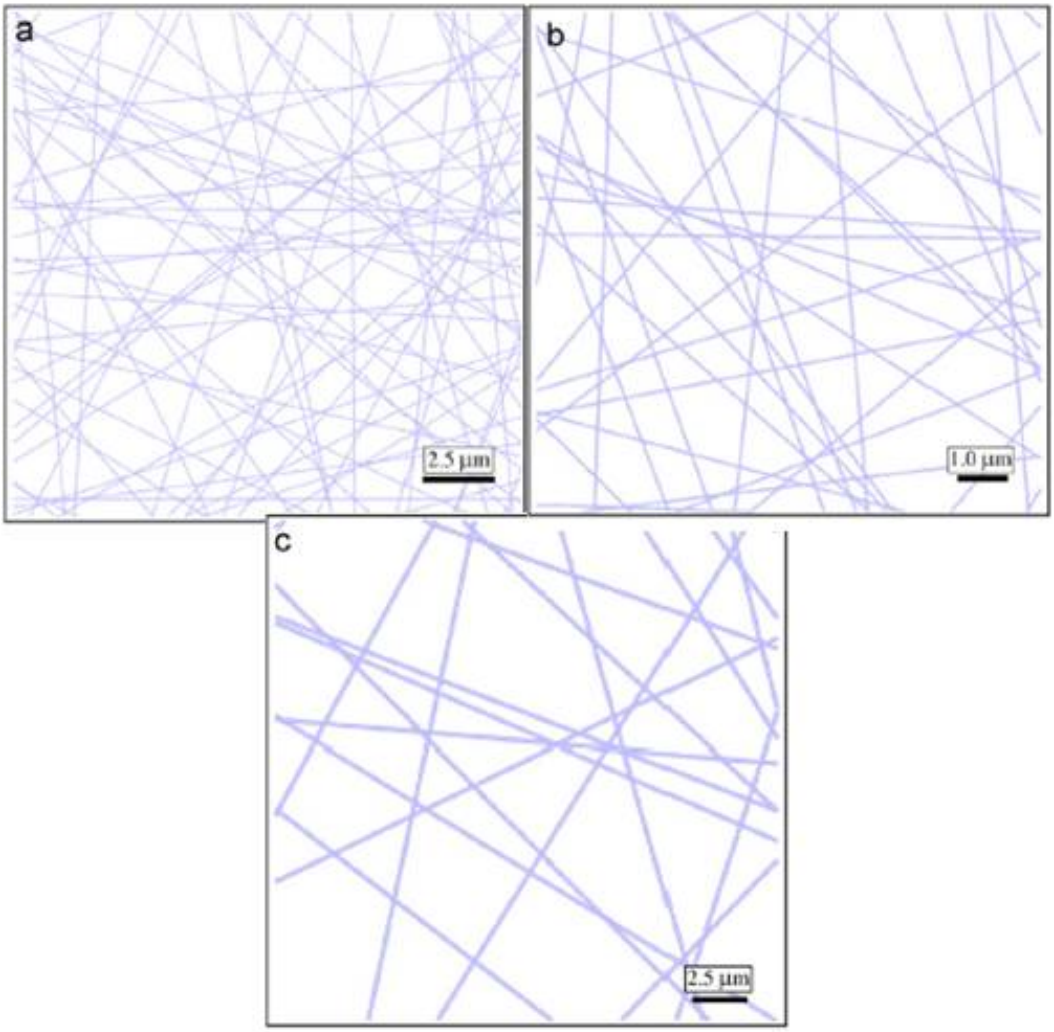

Figure 1.11 Top view of three virtual electrospun fiber-webs made of fibers with a diameter of (a) 50 nm, (b) 100 nm, and (c) 200 nm[147].

Filtration efficiency at const. pressure drop and thickness but varying fiber diameter was modeled. Reduction in fiber diameter led to increase in filtration efficiency. The effect of Brownian diffusion and interception mechanism on nanofiber of 100 nm diameter with varying particulate size was modeled and is as shown in Figure 1.12, with increasing particle diameter Brownian diffusion decreases whereas capture by interception increases[147].

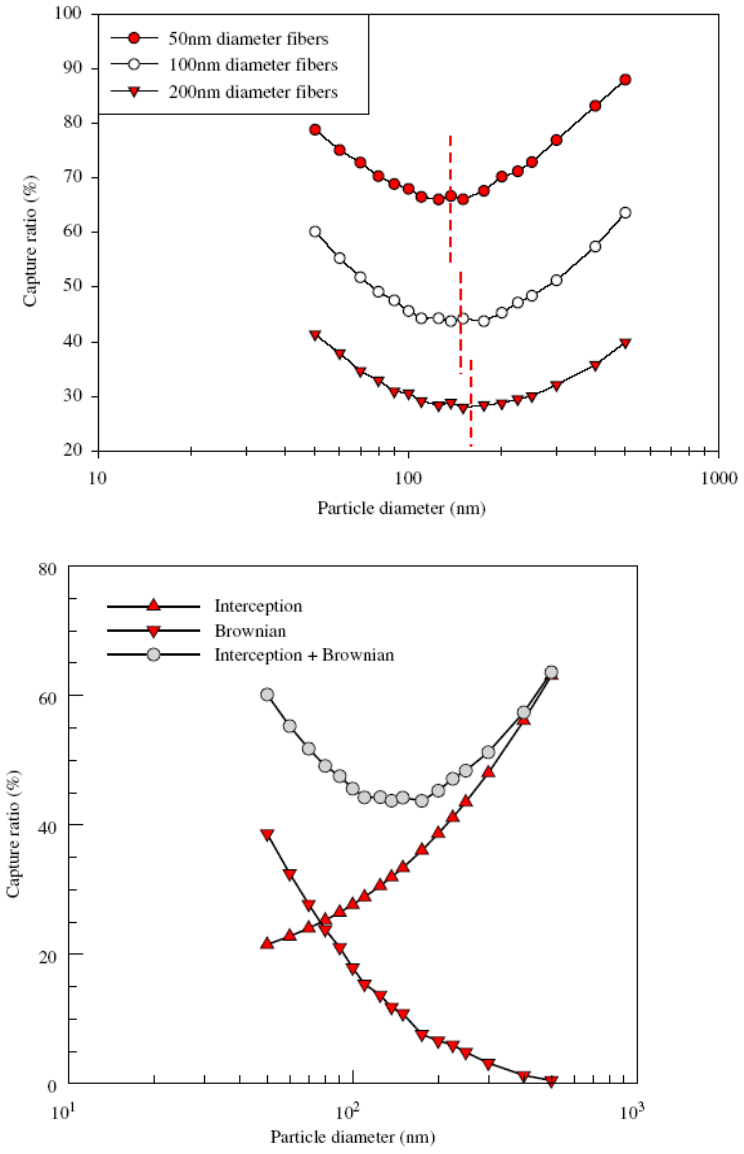

Figure 1.12 Collection efficiency of web of different diameter but constant pressure drop and thickness (top),The influence of capture due to Brownian diffusion is separated from that due to interception for the web of 100 nm (bottom)[147].

With increase in air temperature of the air/aerosol particulates the collection efficiency increased due to presence of a stronger Brownian diffusion at higher temperatures. Cake formation which is similar to membrane fouling was also studied and was found to be faster if larger sized challenge particles were used[147].

Recently, fabrication of chloridized PVC electrospun nanofiber membranes have been fabricated by Sang et.al.[154] which can bind up to 5mg/g fiber heavy metal ions like Cu^{2+},Cd^{2+} and Pb^{2+}. They also showed that use of Micellar-enhanced filtration (MEF) method to adsorb heavy metal ions from waste water streams by the nanofibrous membranes. In MEF the contaminant ions (size on order of 0.1 nm) which are normally permeable to filtration membranes can be made impermeable by forming their large size impermeable micelles by adding surfactants to the waste water stream[154].

Electrospun membranes using polyvinylidene fluoride were fabricated using a mixture of N,N-dimethylacetamide and acetone (1:1) as solvent and tested for their liquid filtration efficiencies against different sized polystyrene (PS) latex particles[155]. The formed nanofiber membranes had pore size in 10 – 4 micron size range, and a 91% separation was achieved for 5μm sized PS latex particles[155]. The same group also investigated the use of electrospun polysulfone membranes as pre-filter material prior to ultrafiltration. The electrospun polysulfone membranes could remove 99% of 10, 8 and 7 μm sized PS particles without fouling. Irreversible fouling occurred for particles < 2 μm, below 0.5 μm sized particles the filter behaved as a "cake filter"[156] and was clouded with PS particles. Electrospun fibers obtained from recycled polystyrene were mixed with conventional micron sized glass fiber filter media to separate water droplets from an emulsion of water in oil[150], separation efficiency increased from 60% to 91% with addition of 0.09 g electrospun polystyrene nanofiber layer. Conventional ultrafiltration or nanofiltration membranes for water filtration are based on porous membranes which exhibit a low flux rate, Yoon et.al.[157] have tested a composite electrospun nanofibrous filtration membrane which exhibited a magnitude higher in flux rate while achieving the same 99 % rejection. Their composite membrane composed of a base layer non-woven polyester substrate (fiber diameter = 10 μm), a two-layer with reducing fiber diameter electrospun PAN nanofiber mat (fiber diameter layer 1 = 100 nm, layer 2 = 800 nm), and a chitosan coating layer on top. The chitosan layer was added as it would allow water to permeate through the membrane and prevent fouling of the nanofibrous filter media[157]. Chitosan/poly(ethylene terephthalate) (PET) and chitin/PET nanofibrous mats (chitosan/chitin content = 10wt%) with fiber diameters in the order of 200 – 800 nm have been fabricated using electrospinning using aq.acetic acid solvent[158]. The two types of nanofiber mats were tested for bacterial inhibition of Staphylococcus aureus and Klebsiella pneumonia micro organism by soaking the fiber mats in known bacteria solution for 18 hrs.

PET/chitosan fibers exhibited the greatest growth inhibition (up to 90%) of the two bacteria, followed by the PET/chitin fibers (60%) and pure PET fibers which did not show any growth inhibition.

1.2 Project Goals

The objective of this research is to fabricate chitosan based nanofibrous filter media which can be used for air and water filtration. To achieve this goal the research will be divided into two parts:

1. **Controlled fabrication of nanometer sized non-woven fiber mats of chitosan using electrospinning – understanding of process – structure relationship**

In this part of the research, the goal is to identify and establish the processing conditions necessary for the fabrication of beadless chitosan nanofibers. After beadless nanofiber mats have been made they will be tested for their anti-microbial and metal binding properties. To assist in chitosan nanofiber formation blends of chitosan with other synthetic polymers like poly(ethylene oxide) (PEO) and poly(acryl amide)(PAAm) will be made. PEO was selected because it is soluble in water, has shown to produce ultrafine fibers using electrospinning[159], and has properties similar to many polysaccharides i.e. it has a linear structure and can form hydrogen bonds with other polymers. PAAm is another type of high molecular weight hydrophilic synthetic polymer which possesses $–NH_2$ similar to chitosan and cationic polyacrylamides. The latter have been investigated for their antimicrobial activity[160,161], but electrospinning of polyacrylamides has not been widely investigated[162]. Figure 1.13 shows the structure of PEO, and PAAm[46].

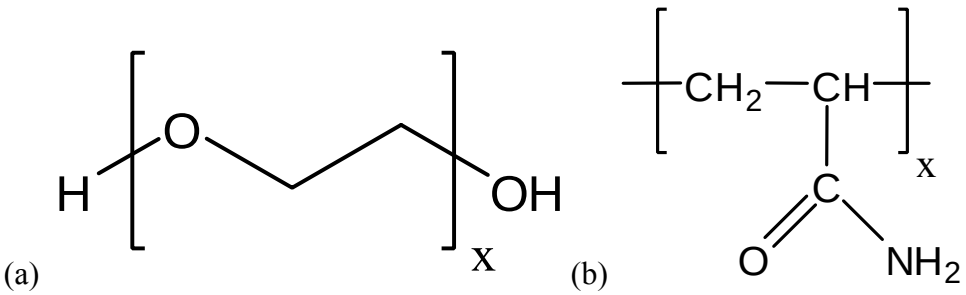

Figure 1.13 Structural formula of (a) PEO, (b) PAAm

The effect of the following material/process properties need to be studied and optimized for nanoscaled bead less fiber formation:

- Chitosan/Synthetic Polymer blend ratios.
- Chitosan and Synthetic Polymers Molecular Weight:
    - High Molecular Weight (HMW) Chitosan (Mv ~ 1400 kDa) with varying degree of deacetylation (DDA) (80%, 71%, 61%).
    - Low Molecular Weight (LMW) Chitosan (Mv ~ 100 kDa) with 70 – 80 % DDA.
    - HMW and LMW PEO (Mw – 900kDa, Mw – 300 kDa).
    - PAAm (Mw ~ 5000 kDa).
- Hot air flow-rate and temperature.

Effect of fiber structure and chemistry (chitosan content, fiber diameter, % DDA and varying blend polymer) on chromium (Cr(VI)) binding and anti-microbial properties will be studied. A model correlating the fiber structure and surface chemistry with (Cr(VI)) binding will be presented.

2. Fabrication and testing of nanofibrous filter media.

In this second and concluding part of the research, non-woven fiber mats produced and identified as potential candidates for filtration applications (based on structure, metal binding efficiency and anti-microbial efficiency) will be used to fabricate a chitosan based nanofiltration membrane. A two-layer nanofibrous filter media will be fabricated using a base layer of spun bonded polypropylene (PP) non-woven fiber mat, and an electrospun layer of chitosan nanofiber mat (produced in step 1). Spunbonded PP fiber mats are being chosen because it can effectively serve as a substrate for the thin electrospun nanofiber layer for filtration testing. Spunbonded PP would help provide mechanical integrity to the nanofiber layer. The fabricated nanofibrous filter media will be tested for its physical (based on size like aerosols, PS beads) and chemical (chromium, bacteria) filtration efficiencies. Figure 1.14 provides a flow-chart of the overall project objectives.

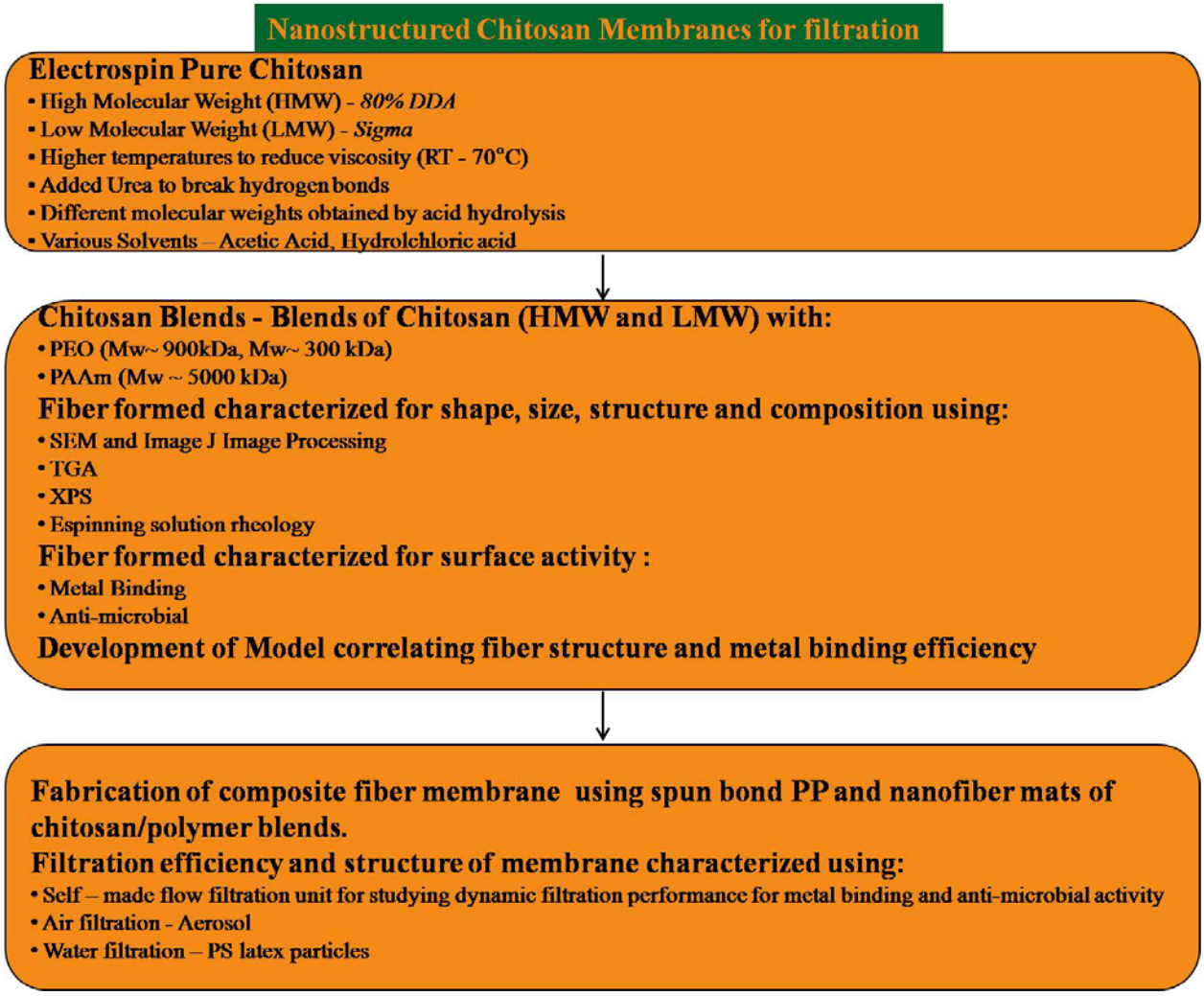

Figure 1.14 Summary of overall research plan.

2. Experimental Techniques

2.1 Filter Fabrication

2.1.1. Materials.

Chitosan with two different molecular weights was used. Chitosan of molecular weight Mv = 1400 kDa (HMW) with varying degree of deactylation (DDA) i.e. 80%DDA, 70% DDA, and 67% DDA was used as received from Primex Inc. Chitosan of lower molecular weight Mw = 100 kDa (LMW) and 83% degree of deactylation was used as received from Sigma. The DDA (HMW & LMW) and molecular weight (LMW) values of chitosan were obtained from the manufacturer and the molecular weight of HMW chitosan was determined by solution-viscosity method. Acid hydrolysis of chitosan was done to further reduce the molecular weight of HMW chitosan following a procedure similar to that of Liu et.al[163], and chitosan with varying molecular weights (300 kDa, 80 kDa, 20 kDa) was obtained. The basic procedure for acid hydrolysis for chitosan is (1) Dissolve 2% HMW Chitosan in conc. HCl @ 0°C for 4 hours, (2) Hydrolyze chitosan at room temperature for different times (1 hr, 3 hrs and 8 hrs) to get different MW chitosan, (3) The reaction was stopped by cooling solution to 0°C and adjusting solution pH to 4.5 with cold 12M NaOH. (4) Obtained solid chitosan mass was filtered and freeze dried to obtain chitosan powder. Figure 2.1 shows reduction in molecular weight of HMW chitosan with increasing hydrolysis time.

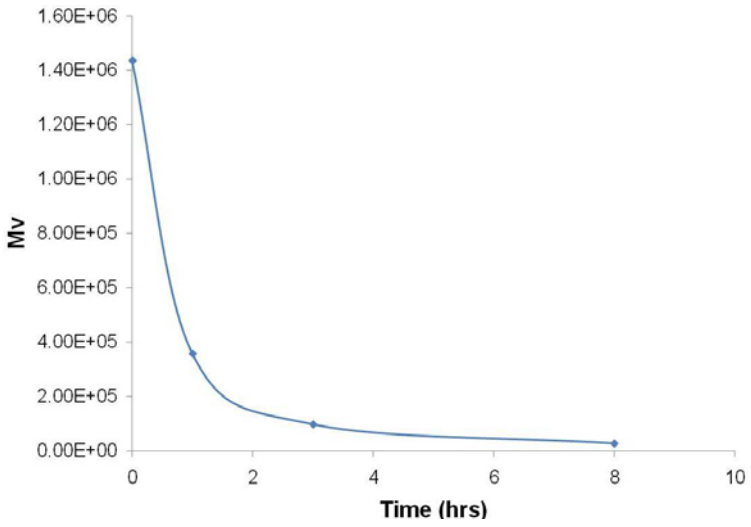

Figure 2.1 Viscosity average molecular weight (Mv) of HCl hydrolyzed chitosan

Two different molecular weights of polyethylene oxide (HMW Mw = 900 kDa and LMW Mw = 300kDa) were used as received from Scientific Polymer Inc. Polyacrylamide of molecular weight Mw = 5000 kDa was used as received from Scientific Polymer Inc. The solvents for electrospinning i.e. acetic acid (AA), hydrochloric acid (HCl) and trifluroacetic acid (TFA) were used as received from Sigma. Other chemical used in this study like urea, Brij-35 surfactant etc. were used as received from Sigma. To fabricate composite nanofibers, spun bonded polypropylene (PP) of 35 g/m^2 basis weight was used as received from The University of Tennessee Non-Woven Research Lab.

2.1.2. Electrospinning.

The electrospinning apparatus consisted of a metered flow pump (Harvard Apparatus Pump II), a high D.C voltage supply (Gamma High Voltage Research, Inc. Model HV ES 30P/DAM), and aluminum foils as targets for fiber collection. Figure 2.2 shows the schematic outline and the actual electrospinning set up used for this study. An air assisted heating unit was designed similar to one described by Chun and coworkers[78] to heat the polymer solution while it was being ejected through the needle by passing hot air around the needle at flow rates up to 75 ft^3/hr, and temperatures ranging from room temperature (25°C) to 70°C. The temperature of the heated air was controlled using a variac, while the flow rate was controlled using a rotameter. Temperature of the hot air was measured using a thermocouple at location as shown in Figure 2.2. The variac power required to attain desired air temperature was calibrated before beginning the experiments, and variac settings for different temperatures were established. During calibration the temperature of the hot air was also measured near the tip of the needle using another thermocouple, and compared with the reference temperature measured at location shown in Figure 2.2. Temperature at the end of the needle was slightly lower (~ 5°C) than at reference location. In this study, the polymer solutions were electrospun at hot air temperatures of 41°C and 70°C which corresponds to approximately 35°C and 61°C as measured at the end of the needle. Electrospinning solutions were prepared by dissolving the required polymers on wt% basis in the solvent and stirring the solutions for 24 hours to make a well mixed homogenous solution. While making electrospinning solutions, the strength of the acid solvent was adjusted to maximize solubility of polymer in solution. The solution was then ejected through a syringe

(Popper & Sons,7935) using a syringe flow pump at feed rate of 0.08 ml/min and applying a voltage of 30 kV and tip-target distance of 10 cm.

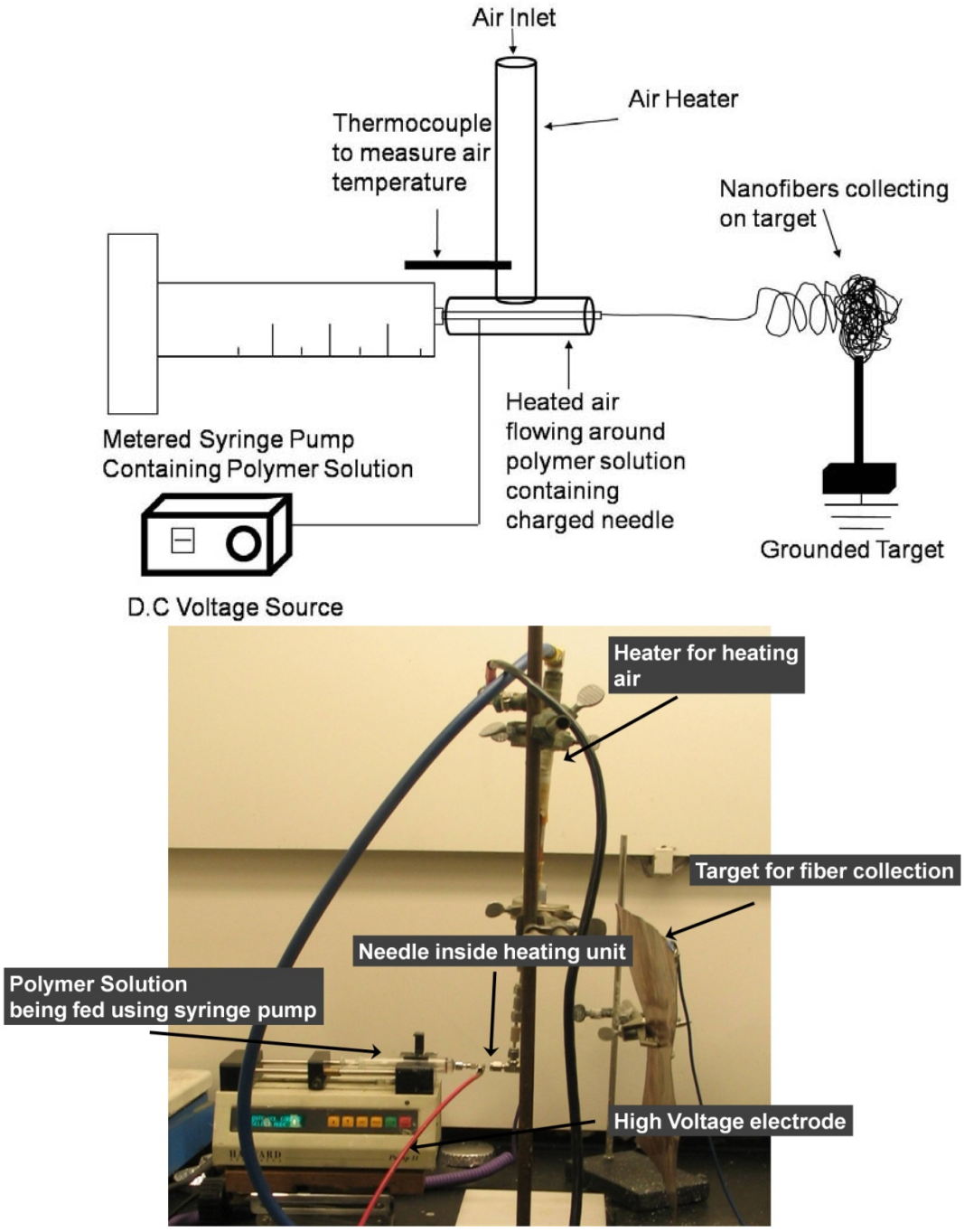

Figure 2.2 Schematic layout of electrospinning set-up (top), actual (bottom) electrospinning set-up.

2.1.3. Nanofibrous filter fabrication.

The nanofibrous filter media (Figure 2.3) was fabricated by electrospinning the chitosan solutions directly onto a spunbonded PP. Circular discs of 47 mm diameter were cut from these composite fibrous media for testing metal binding, anti-microbial filtration and polystyrene particle filtration efficiencies. For measuring aerosol filtration efficiency a mat size of 7 * 7 inches was required.

2.2 Structural Characterization

2.2.1 SEM/Image Processing

The electrospun fiber mat was characterized using a field emission scanning electron microscope (FESEM, LEO 1525) to study the fiber morphology. The SEM samples were sputter coated with gold to prevent charging during SEM imaging (Figure 2.4). Image processing software ImageJ (NIH) was used to measure the fiber diameter from the SEM micrographs. For each sample, fiber diameter was measured at 60 different points. The bead density of the fibers was also measured using the ImageJ image processing software using the SEM micrographs. Contrast between the beads and the fibers was sufficient to allow measurement of the fraction of area covered by beads using the analyze particle routine in the software. Measurements were done for three different images for each sample.

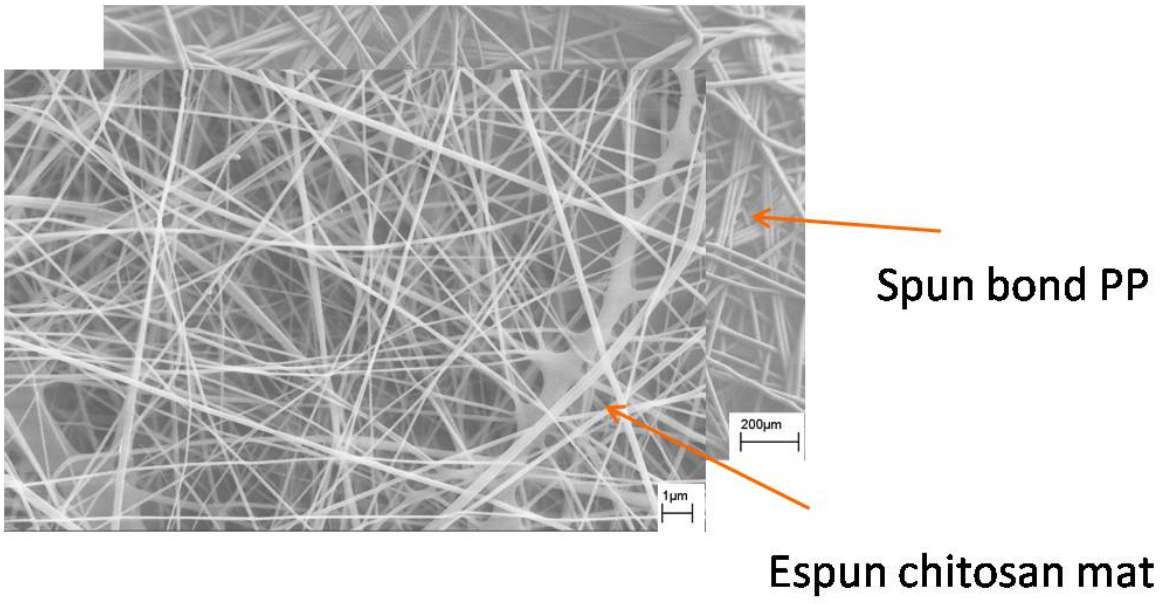

Figure 2.3 Schematic layout of electrospun nanofibrous filter membrane

Figure 2.4 FESEM - LEO 1525 (left), gold sputter coated electrospun fiber samples for SEM imaging (right).

2.2.2 Polymer Rheology

Shear viscosity of electrospinning solutions was measured using a TA instruments (AR 2000) rheometer. Solutions were subjected to a step shear rate of 0.01 sec^{-1} to 100 sec^{-1} and zero-shear viscosity (η_0) and rate index (n) of the solution was calculated by fitting the data to a Carreau model which describes relationship between viscosity and shear rate for psuedoplastic fluids[164].

$$\frac{\eta - \eta_\infty}{\eta_0 - \eta_\infty} = \frac{1}{((1 + (k * \dot{\gamma})^2)^{n/2})}$$

where η is the apparent viscosity, η_0 is the zero shear rate viscosity, η_∞ is the infinite shear rate viscosity, k is a time related to the terminal relaxation time, γ is the shear rate and n is the rate index.

The viscosity average molecular weight of HMW and acid hydrolyzed chitosan was measured using dilute solution viscosity measurements using a Canon-Fenske viscometer. A mixture of 0.1M CH_3COOH-0.2M NaCl was used as a solvent to prepare chitosan solutions with varying concentrations from $1*10^{-3}$ g/ml to $2.5*10^{-4}$ g/ml. The viscosity average molecular weight was determined using the Mark-Houwink equation[112]:

$$[\eta] = 1.81*10^{-3}M_v^{0.93}$$

2.2.3 Thermal Analysis – TGA

The compositional analysis of the fiber mats was done using a Mettler Toledo (TGA/SDTA 851^e) thermo gravimetric analyzer (TGA). Electrospun fiber mat samples were weighed (typical weights in range of 1-3mg) and heated at 10°C/min from 40°C to 500°C and weight loss for each polymer fraction in the fiber measured by taking first order derivative of the raw weight loss TGA curves obtained and then calculating area under the respective polymer degradation temperature peak.

2.3 Surface Properties Characterization

2.3.1. XPS

The surface chemistry of the electrospun fibers was characterized using a Thermo Scientific K-alpha X-ray photoelectron spectrophotometer (XPS). Electrospun fiber mat samples were stuck on the XPS sample holder using a double sided carbon tape. X-rays from an Al K-alpha (1480 eV) monochromatic source were used. A spot size of 400 microns (maximum allowable) was used to scan the surface of the samples so as to account for surface variations and get a better average of data. A surface scan of the sample was done to identify the chemical moieties on the sample surface, a high resolution scan for "C", "N" and "O" was done to identify the elemental peaks with changing % chitosan in blend fiber, varying chitosan DDA, varying fiber diameter, varying chitosan molecular weight, varying blend polymer and after metal binding of espun chitosan blend fibers (average of 30 scans). XPS data was analyzed using Thermo Avantage V 3.74 software to calculate atom % of various elements found on espun fiber sample surface. Peak fitting was done on the high resolution elemental scans (average of 10 scans) to obtain surface chemistry information. Reference scans of pure chitosan films cast from 1% HCl, pure PEO, PAAm films cast from water and pure PEO, PAAm electrospun fibers were also taken. The atom% values obtained from XPS were converted to weight fraction of chitosan present on fiber surface by using the ratio of atomic % "C" to atomic % "N" measured for the blend samples with the atomic fractions measured using the pure polymer samples. To correct for the surface charging effect, the C1s electron binding energy was shifted to characteristic value 285.0 eV[165] obtained from literature for all spectra and the flood gun was turned on.

2.3.2. Metal binding

The metal binding properties of the electrospun fiber mats were measured using the NIOSH manual of analytical methods (NMAM)[166]. Chromium solution (5 mg/L) was made by diluting the standard 1 mg/ml K_2CrO_4 solution purchased from Sigma. Weighed amounts of electrospun fibers were washed with acetone to remove presence of any residual acetic acid solvent to prevent the dissolution of the mat in aqueous solution. The washed mats were then soaked in 25 ml of 5 mg/L chromium solution and continuously shaken for 3 hours. Solutions containing chromium with no fibers were used as control. After 3 hours, 1 ml of fiber-soaked sample solution was taken and added to 7 ml of 0.5 N sulphuric acid (H_2SO_4). Diphenylcarbazide solution (0.5 ml) was added to above solution (as an indicator) and volume was adjusted to 25 ml by adding 0.5 N H_2SO_4. The chromium ion absorbance of these solutions was measured at 540 nm using a Shimadzu UV-Vis spectrophotometer (UV2102 PC,Shimadzu). Before each experiment, the spectrophotometer was calibrated and standard curves obtained by measuring absorbance for solutions prepared with known chromium concentrations (0 mg/L to 0.2 mg/L). For the electrospun fiber mats metal binding was determined by reading the chromium concentration at measured absorbance from the standard curves and then calculating the metal binding capacity on weight basis i.e. mg chromium/g chitosan. Measurements were done in triplicates. Figure 2.5 shows the effect of indicator on color change in chromium solutions (dark pink solutions indicate high chromium concentration).

Figure 2.5 The effect of indicator on color change in chromium solutions

2.3.3. Anti-Microbial

The antimicrobial properties of the electrospun fiber mats were determined using Escherichia coli K-12, as the test microorganism. Escherichia coli K-12 was grown in Brain Heart Infusion (BHI; Difco) broth for 48 hours at 35°C. Test fibers of known weight were then submerged into culture tubes containing 9 ml sterile phosphate buffer (0.05 M, pH=7.08) inoculated with ca. 10^6 CFU/ml bacteria, and mixed by vortexing and incubating for 6 hours at 25°C. Phosphate buffer with the same E. coli K-12 inoculum but with no fiber was used as positive control and phosphate buffer with fiber but no inoculum as the negative control. The survival of E. coli K-12 was determined using the pour-plate method on Trypticase Soy Agar (TSA) medium[167]. All measurements were performed with 3 replications. Figure 2.6 shows surviving E.coli K-12 on agar media after 24 hours of incubation. The reduction in E.coli count was reported as log reduction which is defined as:

$$\log reduction = \log(initial\ bacteria\ conc.) - \log(final\ bacteria\ conc.)$$

where, 1 log reduction is equivalent to 90% reduction in bacteria, 2 log is 99% reduction, 3 log is 99.9% reduction and so on.

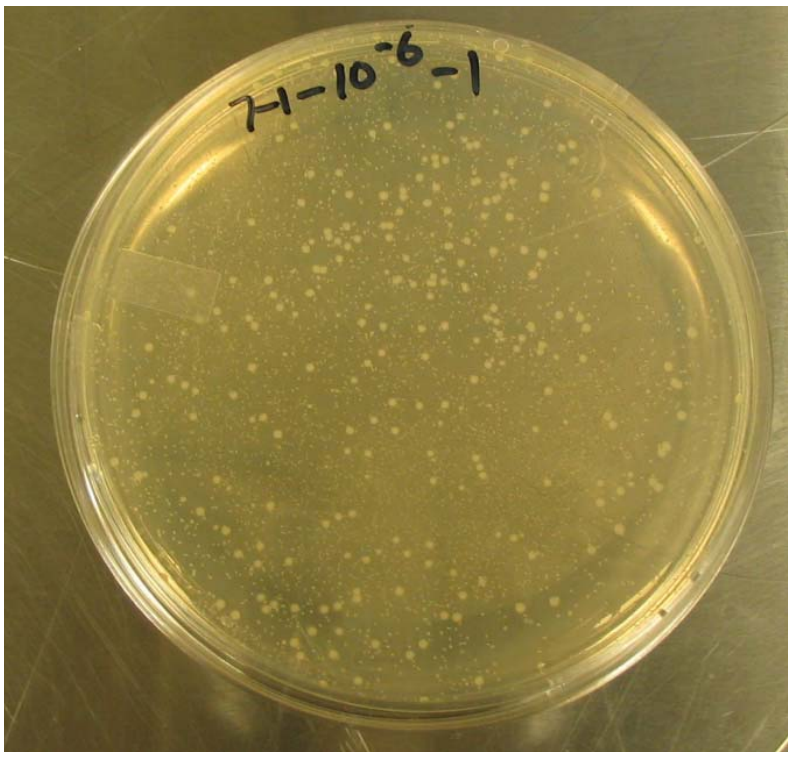

Figure 2.6 Surviving E.coli on agar media

2.4 Filter Media Characterization

To study the filtration performance of the electrospun chitosan fiber mats fabricated and characterized as mentioned above, a dynamic filtration efficiency study was performed as described below.

2.4.1 Filter Media Structural Characterization

The basis weight (g/m^2 or gsm) of the nanofibrous filter media was measured using ASTM standard D 3776-96. Basically a nanofiber mat of known area was weighed and the basis weight was calculated by taking ratio of mass over surface area.

The porosity of the nanofibrous filter media was measured using a PMI capillary flow porometer (Porous Materials Inc.), a wetting liquid Galwick^{TM} (Porous Materials Inc.) was used as a wetting liquid to spontaneously fill the pores in the nanofibrous membrane. The maximum pore detected was measured which is defined as the largest pore size detected as gas flow begins through a wetted sample at bubble point pressure. The complete pore analysis was difficult to achieve as the nanofibrous mat was delaminating even at low pressure.

The air permeability which can be another measure of the porosity of the nanofibrous membrane was measured according to ASTM D737-96 using a Textest FX 3300.

2.4.2 Metal Binding

A dynamic filtration test was set-up as shown in Figure 2.7. The set-up basically consisted of a filtration flask, filtration funnel and a fritted glass filter support of 47 mm diameter. The filtration unit was used as received from Millipore (Millipore 47mm All-Glass Vacuum Filter Holder, XX15 047 00). The composite fiber membranes fabricated as mentioned in section 2.1.3 were place on top of the filter support and the assembly was clamped. 100 ml of chromium solution (conc. = 5 mg/l) was passed through the filter membrane for ten consecutive times. After each pass of 100 ml chromium solution 1 ml of solution was removed from the sample and analyzed for chromium content using the method as described in section 2.3.2. A slight vacuum of ~ 1 mm Hg was applied to maintain a filtration time of 2 mins.

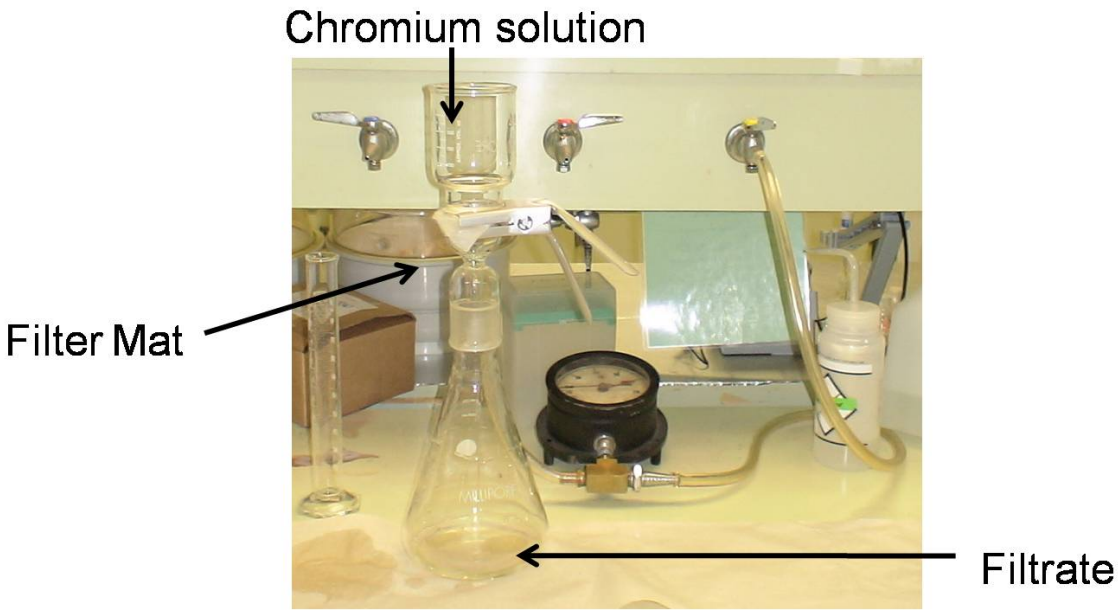

Figure 2.7 Set-up of the dynamic filtration test

2.4.3 Anti-Microbial

A dynamic filtration test was set-up similar to the one shown in Figure 2.7. Initially 100 ml of 7 log concentration of Escherichia coli K-12 test microorganism was passed through the filter membrane once. However the nanofiber membrane was overwhelmed by the high initial concentration of bacteria and was completely blocked and even after 3 hrs and applying high vacuum the solution could not filter through. Further tests were conducted by using lower concentration *i.e.* 4 log of Escherichia coli K-12 test microorganism. The anti-microbial efficacy of the filter membrane was determined in the same way as outlined in section 2.3.3.

2.4.4 Polystyrene latex beads

The liquid filtration efficiency of the nanofibrous filter media was assessed by passing 10 ml of 200 ppm 3 μm diameter polystyrene latex beads which were obtained from Sigma. The concentration of polystyrene latex beads in water was measured using a Shimadzu UV-Vis spectrophotometer (UV2102 PC, Shimadzu) at 490 nm wavelength. Stock solutions of varying ppm of PS latex beads were prepared and a master curve of concentration v/s absorbance was obtained using the UV-Vis. The concentration of the filtrate was calculated from the known

absorbance value obtained by UV-Vis measurements of the filtrate solution. Measurements were done in replicates of three.

2.4.5 Aerosol Filtration

The aerosol filtration efficiency was measured using a TSI Corp. model 8130 automated filtration testing unit at UTNRL. NaCl aerosol particles of 0.26 μm mean diameter, 0.075 μm count median diameter and concentration of 15 to 20 mg/m^3 were used. The penetration and pressure drop across the 7*7 inch chitosan based nanofibrous filter media was measured.

2.5 Statistical Data Analysis

Various data collected for structural and filtration performance of nanofibrous filter were analyzed using the one-way Anova Tukey-Kramer test to see if there was statistical difference in means between different sample groups using the JMP 6.0 statistical analysis software.

3. Fiber Formation – Results & Discussion

3.1 Pure Chitosan Electrospinning

3.1.1. Effect of Solvents and Spinning Solution temperature.

The solubility of chitosan in aqueous acids is very low; for the HMW chitosan the solution started to gel above 2 wt% and for the LMW chitosan the solution started to gel above 6 wt%. Formation of a gel is detrimental for electrospinning as the applied electrical force cannot overcome the high viscosity of the solution, and a stable jet required for the onset of electrospinning cannot form. The critical chain concentration of both the high and low molecular weight chitosan was calculated using the intrinsic viscosity values obtained. For HMW chitosan it was found to be 0.001 g/cc or 0.1 wt% (taking specific gravity of acetic acid to be 1.05 g/cc) and for LMW chitosan was 0.0116 g/cc or 1.2 wt%. Initial studies were done on electrospinning of pure chitosan using the 80% DDA HMW chitosan and LMW chitosan. Electrospinning of both these materials at varying concentrations in varying strengths of acetic acid (10% - 90%), hydrochloric acid (0.03N – 0.5N) and trifluroacetic acid (50%) did not result in fiber formation even when spun at higher temperatures (41°C,70°C) as shown in Figure 3.1. Amongst the three solvents tried initially, further studies were carried out with acetic acid as it was seen as the most promising candidate based on the shape of particles along with appearance of fibrils and the desire to stay away from more toxic solvents like TFA.

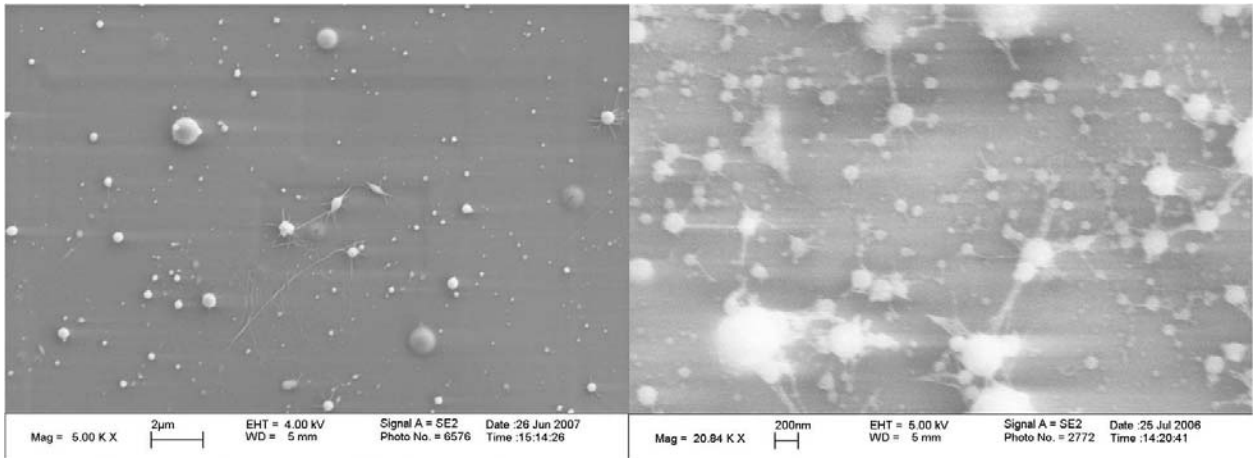

Figure 3.1 SEM images of the pure electrospun chitosan samples 1.4 wt% HMW chitosan spun from 50% acetic acid (left), 5 wt% LMW chitosan spun from 90% Acetic Acid (right).

3.1.2. Effect of molecular weight, addition of urea and salt .

Acid hydrolysis of chitosan was done to further reduce the molecular weight of HMW chitosan following a procedure similar to that of Liu et.al[163], and chitosan with varying molecular weights (300 kDa, 80 kDa, 20 kDa) was obtained. Electrospinning of these different molecular weights of chitosan also did not result in fiber formation. In order to reduce the amount of inter- and intra-chain hydrogen bonding in chitosan, urea was added which has been shown to disrupt hydrogen bonding in other polysaccharides[168]. Salt (NaCl) was also added to the electrospinning solution, as it is known that addition of salt helps increase solution conductivity and improve spinnability of polymer solutions[49, 86]. Figure 3.2 summarizes the effect of molecular weight, addition of urea and salt on the spinnability of chitosan solutions.

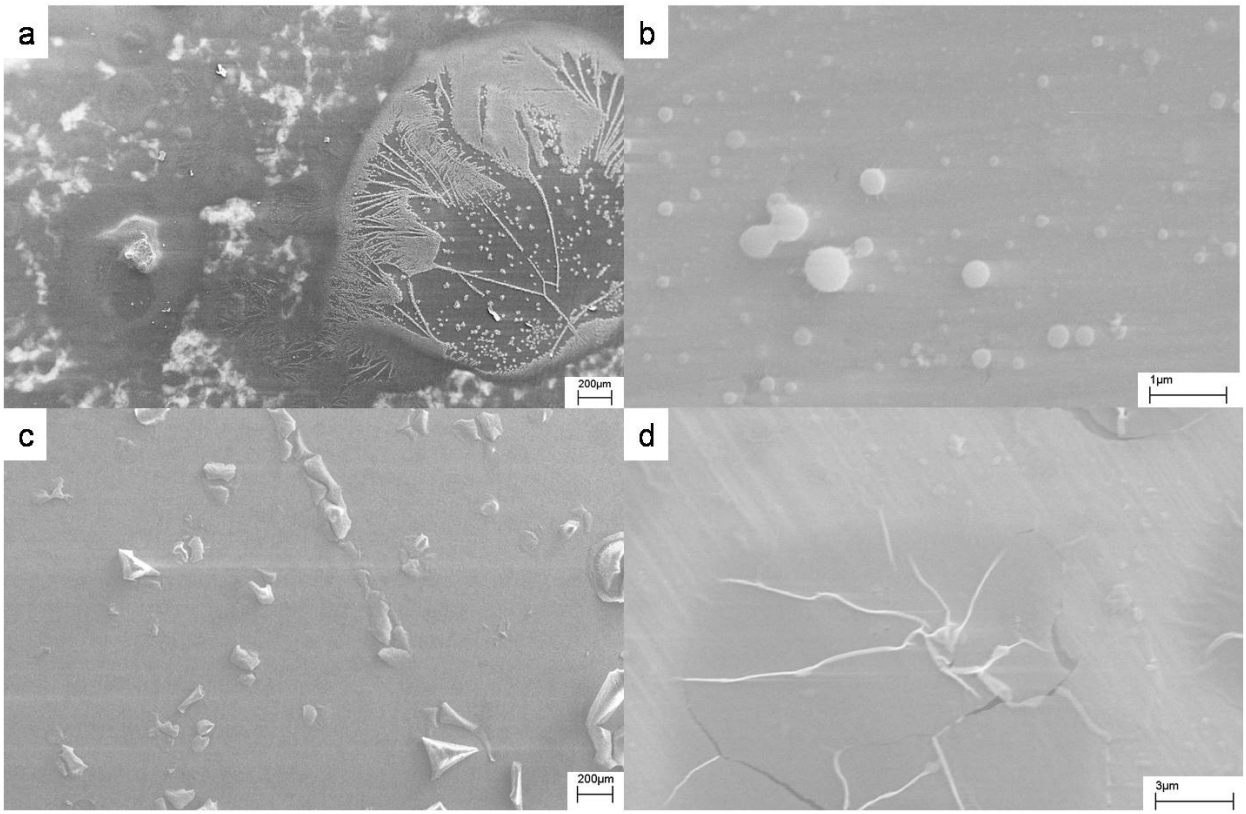

Figure 3.2 SEM images of the pure electrospun chitosan samples (a) 1.2 wt% HMW chitosan with 1.4 wt% Urea spun from 90% Acetic Acid (b) 6 wt% LMW chitosan + 0.3 wt% NaCl spun from 10% Acetic Acid(c) Hydrolyzed chitosan (Mv – 80 kDa) spun from 10% Acetic Acid (d) Hydrolyzed chitosan (Mv – 20 kDa) spun from 80% Acetic Acid

Table 3.1 Summary of processing condition for electrospinning of pure chitosan

Type of Chitosan (Molecular weight)	Solvent	Spinning Solution Temperature (°C)	Polymer Concentration
HMW Chitosan (Mv - 1400 kDa)	0.03N HCl	25, 40, 70	0.6 – 1.5 wt%
	0.1N HCl	25, 40, 70	0.1 - 2 wt%
	0.5N HCl	25, 40, 70	1.5 wt%
	50% TFA	25, 40, 70	1.5 wt%
	90% AA	25, 40, 70	1.2 wt% + 1.5 wt% Urea
	90% AA	25, 40, 70	1.5 wt%
LMW Chitosan (Mv - 100 kDa)	0.1N HCl	25, 40, 70	1.7 wt%
	90% AA	25, 40, 70	5 wt% with addition of salt
	30% AA	25, 40, 70	6 wt% with addition of salt
Hydrolyzed Chitosan (Mv – 300kDa)	80% AA	25	5 wt %
Hydrolyzed Chitosan (Mv – 80kDa)	90% AA	25	4 wt%
Hydrolyzed Chitosan (Mv – 20kDa)	80% AA	25	5 wt %, 6 wt%

Table 3.1 presents a summary of processing conditions that were studied, none of which resulted in fiber formation instead forming electrosprayed solution droplets. Hence, amongst the many challenges for electrospinning of chitosan is its limited solubility window in aqueous acids before gel formation, and strong inter and intra-chain hydrogen bonding between chains. To overcome the increased viscosity effect at higher concentrations the electrospinning apparatus was modified as described earlier to heat the solution during electrospinning with the goal of reducing solution viscosity at high chitosan concentrations and forming defect free fibers.

3.2 Electrospinning of Chitosan/PEO blends.

As electrospinning of chitosan did not result in the formation a non-woven fiber mat, PEO was added to the chitosan solutions. Blend solutions were prepared with varying weight fractions of PEO in the blend from 10% to 25%. PEO is partially soluble in acetic acid but completely soluble in water so as PEO content in blend solution increased, the strength of acid was reduced to enable complete dissolution of polymer. Chitosan/PEO blend fiber mats were produced by optimizing the effect of weight fraction PEO in the blend, molecular weight, and spinning solution temperature with the goal of forming nanoscale, beadless non-woven fiber mats with high chitosan content. All chitosan/PEO blend solutions discussed henceforth were electrospun at room temperature unless otherwise noted.

3.2.1 Effect of blend ratios and molecular weight.

Chitosan, when blended with as low as 10% PEO, resulted in the formation of non-woven mats of fibers. Figure 3.3 shows SEM images of HMW chitosan blended with HMW PEO with increasing % PEO in the blend. It can be seen with increasing % PEO, fiber diameter increases and number of bead defects is reduced. Figure 3.4 shows SEM images of LMW chitosan blended with varying % HMW PEO and a similar trend is seen. Figure 3.5 shows a plot of fiber diameter of electrospun fibers vs. % PEO in the blend solutions. From the fiber diameter data it can be seen that with increasing % PEO, fiber diameter increases which could be due to higher concentration of polymer in solution with increased PEO content. The concentration of polymers in solution was determined by studying solubility of polymer blends at different blend ratios and optimizing them so as to be able to form solutions which could form a stable jet which would lead to formation of fibers. At constant polymer concentration, viscosity of solution decreases with increased PEO content and reduced strength of acetic acid. Fibers formed using high molecular weight chitosan are thinner compared to those obtained using low molecular weight chitosan; this can be attributed to higher solution concentration of low molecular chitosan blends. The increased solution viscosity for LMW blends as seen in Table 3.2 is mainly a polymer concentration or solubility effect as LMW chitosan is more soluble then HMW chitosan. However it is difficult to establish any trend of fiber diameter v/s solution viscosity from the electrospinning solutions viscosity data because of difference in strength of solvents and polymer concentration amongst the various spinnable chitosan blends. Increasing the fraction of PEO in

the polymer blend also leads to reduction in number of bead defects because PEO helps in breaking down the inter- and intra-chain hydrogen bonding in chitosan by attaching itself onto the chitosan backbone by forming new hydrogen bonding between its –O– groups and water molecules and increasing solution chain entanglements[111]. The increase in chain entanglements is seen by decrease in rate index (n) with increasing PEO fraction in blend[169,170].

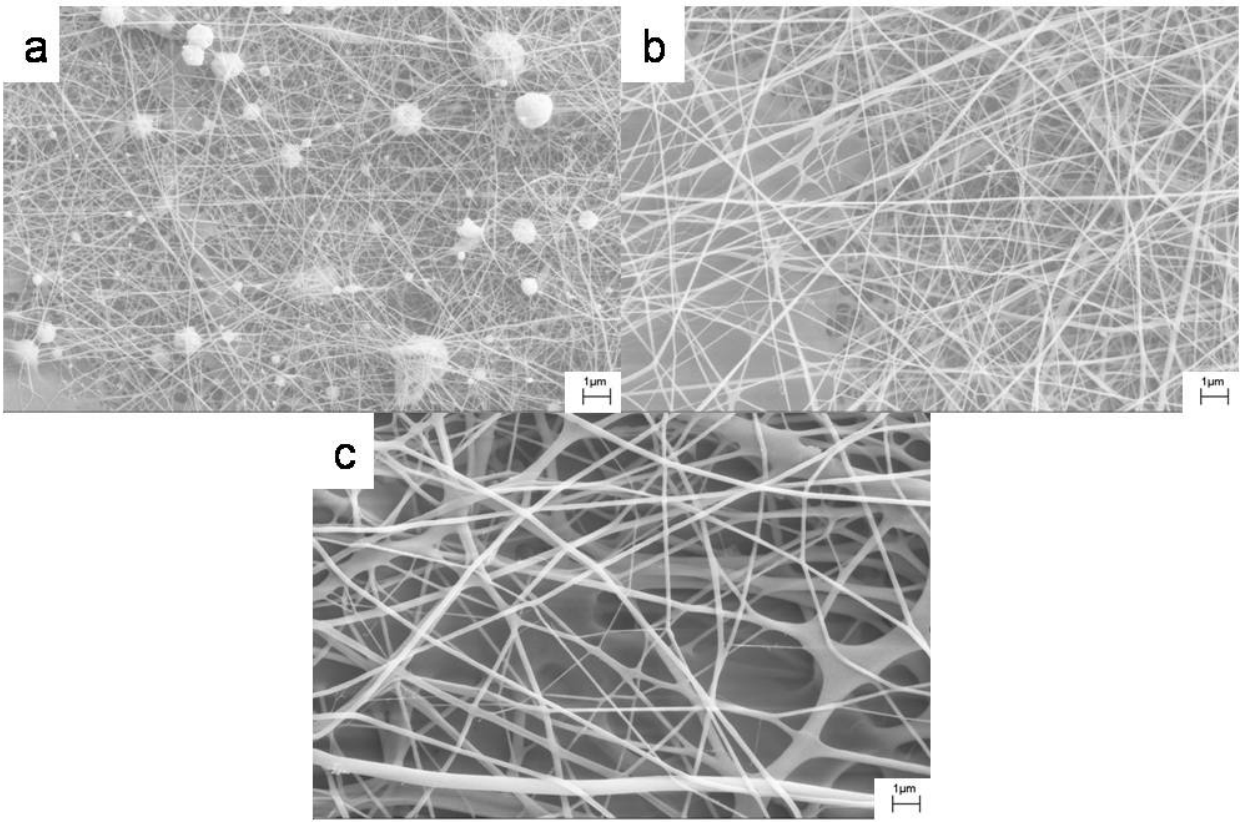

Figure 3.3 SEM images of HMW chitosan: HMW PEO blend fibers (a) 1.33 wt% HMW chitosan: HMW PEO (90:10) (b) 1.6 wt% HMW chitosan: HMW PEO (75:25) (c) 2.00 wt% HMW chitosan: HMW PEO (50:50).

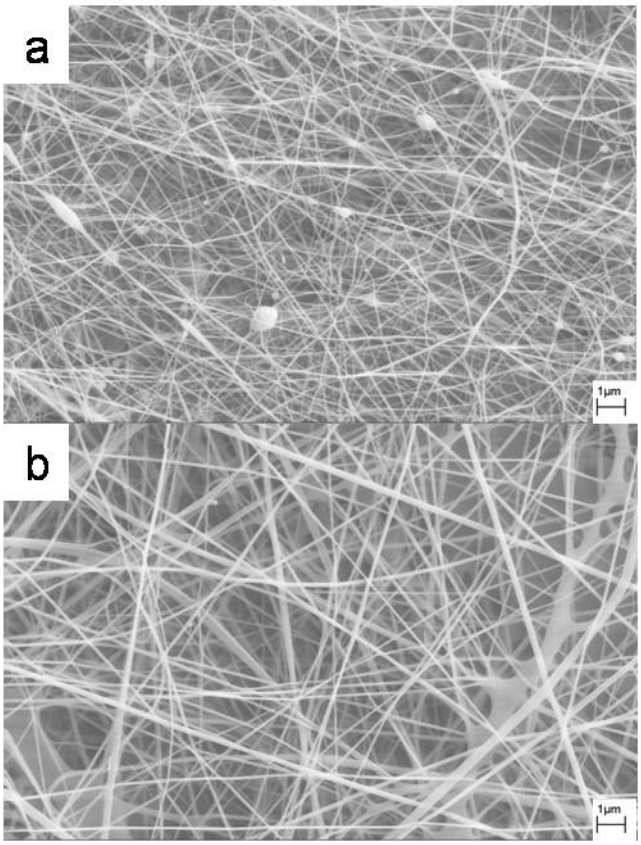

Figure 3.4 SEM images of LMW chitosan: HMW PEO blend fibers (a)4.5 wt% LMW chitosan: HMW PEO (90:10) (b) 4.5 wt% LMW chitosan: HMW PEO (75:25).

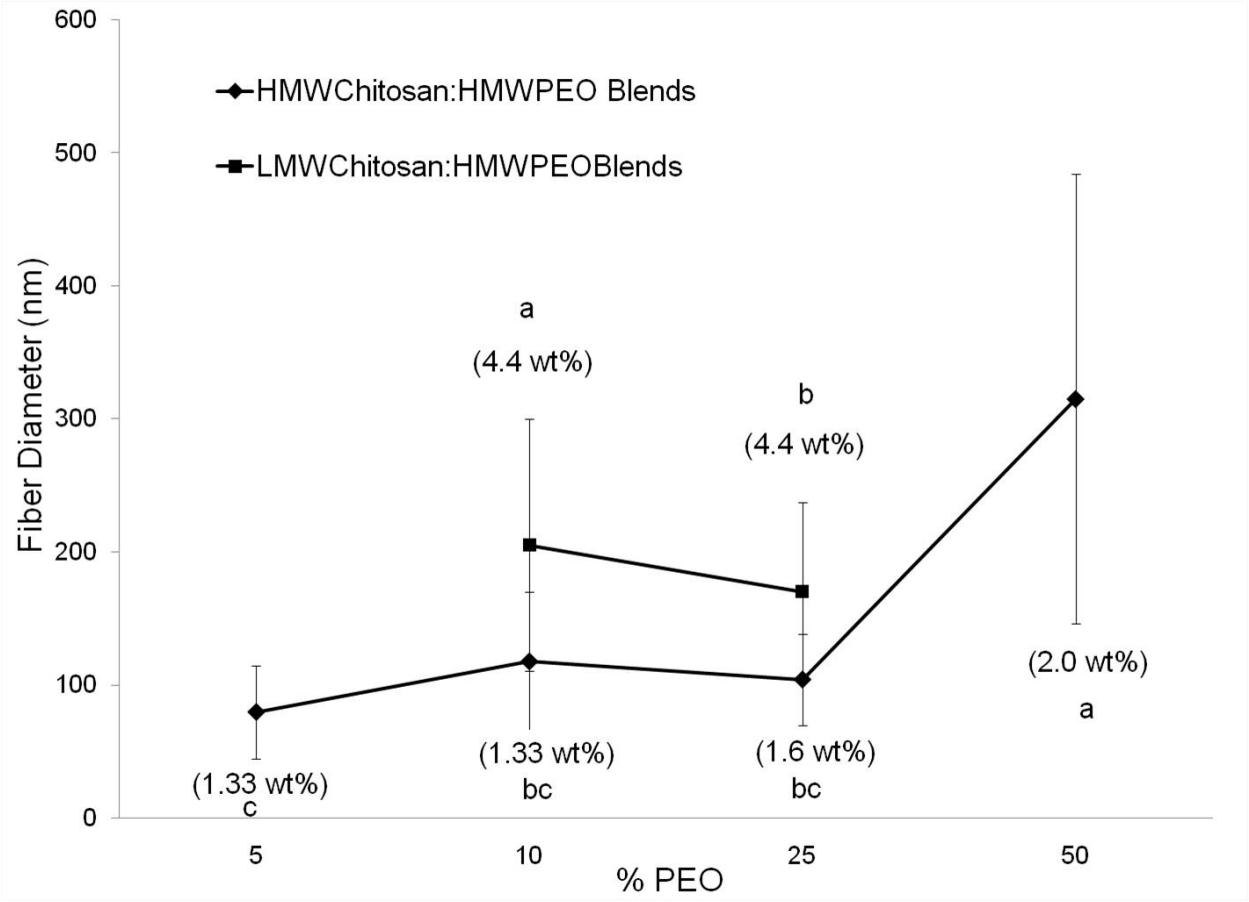

Figure 3.5 Fiber Diameter v/s % PEO (Error bars represent standard deviation (n=60), letters indicate significant difference at $p<0.05$, wt% in parentheses indicate total polymer wt% in solution)

Table 3.2 Zero-Shear (η_0) Viscosity of Chitosan/PEO blends

Sample	η_0 (Pa-s)	n (rate index)
1.33 wt% Pure HMW Chitosan in 75% AA	3.709	0.386
1.33 wt% HMW Chitosan: HMW PEO (90:10) in 75% AA	3.230	0.347
1.6wt% HMW Chitosan: HMW PEO (75:25) in 90% AA	5.986	0.394
4.5wt% LMW Chitosan: HMW PEO (90:10) in 50% AA	29.44	0.405
4.5wt% LMW Chitosab: HMW PEO (75:25) in 60% AA	21.36	0.383

Figure 3.6 shows SEM images of HMW chitosan blended with HMW PEO and LMW PEO. Average fiber diameter (n=60) for HMW chitosan: HMW PEO blends was 117 nm (±52nm) and for HMW chitosan: LMW PEO blends was 91 nm (±39 nm). Fibers are formed with as low as 10% PEO for HMW Chitosan/PEO blends. Spinning of solutions with ≤ 1 wt% total polymer concentration leads to electrospraying and above 2 wt% the solution is too viscous. Similarly for LMW chitosan blends, spinning solutions with ≤ 4 wt% total polymer concentration result in electrospraying and above 5 wt%, high viscosity prevents stable electrospinning. Hence it can be seen that the spinnability window for chitosan solutions is very narrow and dependent on % PEO in the blend and total concentration of polymer in solution.

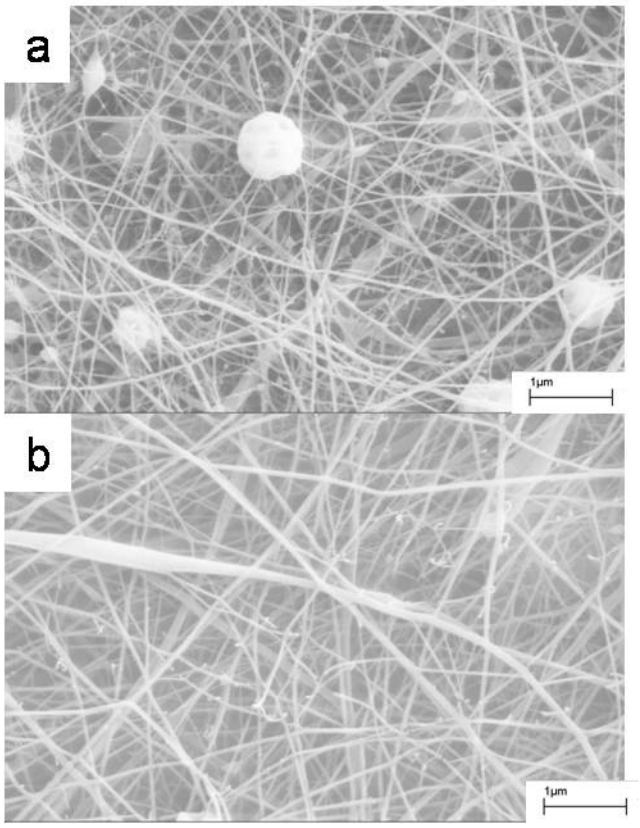

Figure 3.6 SEM images of (a) 1.33 wt% HMW chitosan: HMW PEO (90:10) blend fibers (b) 2.00wt% HMW chitosan: LMW PEO (90:10)

3.2.2 Effect of spinning solution temperature.

Solutions were electrospun at higher temperatures by blowing hot air around the feed needle. Figure 3.7 shows SEM micrographs of electrospun fibers of 1.33wt% HMW Chitosan: HMW PEO (95:5) electrospun by blowing air at 25 ft^3/hr at room temperature (25°C), 40°C and 71°C. It can be seen that as temperature increases, less defective fibers are obtained as indicated by lower bead density values at higher temperatures as shown in Figure 3.8. The increased temperature reduces the solution viscosity and the flowing air helps increase the spin-draw ratio, both of which together lead to further stretching of the unstable polymer jet during the whipping motion and aiding in the formation of beadless fibers. As air flow and temperature (71°C) are increased, there would be faster evaporation of solvent which would lead to increase in concentration of polymer solution exiting the syringe and formation of slightly thicker fibers. The effect of air flow rate on fiber formation was also studied, and as shown in SEM images of Figure 3.9 changing air flow from 25 ft^3/hr to 75 ft^3/hr did not have a significant effect on bead density compared to air temperature but increased air flow at higher temperatures led to a slight increase in fiber diameter.

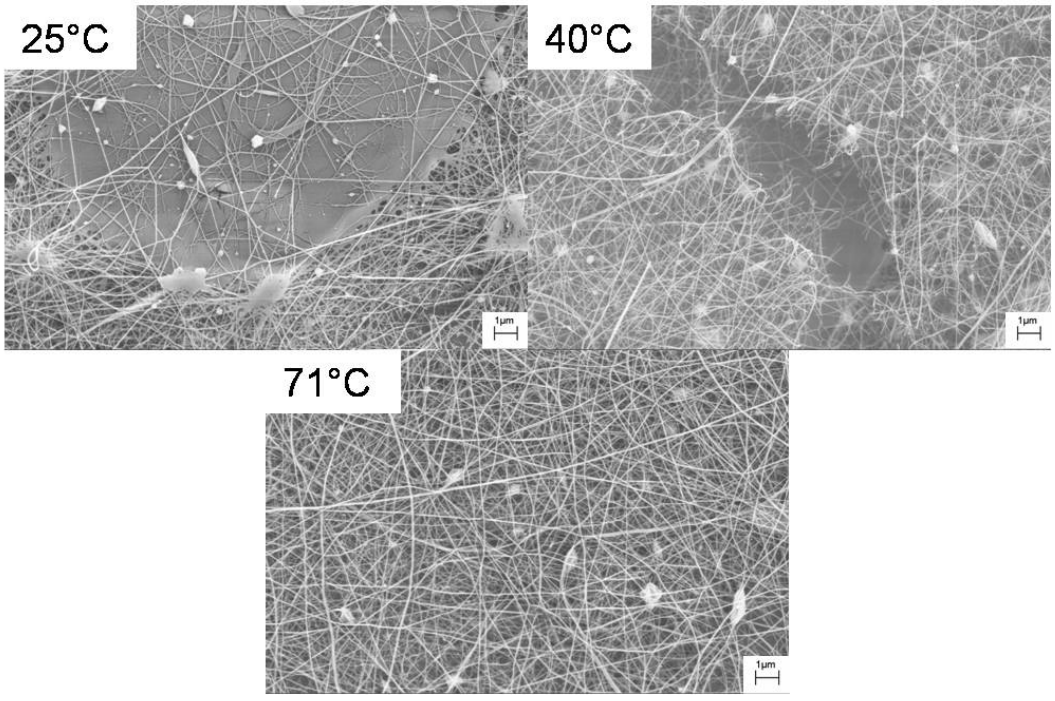

Figure 3.7 SEM images of 1.33 wt% HMW chitosan: HMW PEO (95:5) blend fibers at different spinning solution temperature and constant air flow rate of 25 ft^3/hr

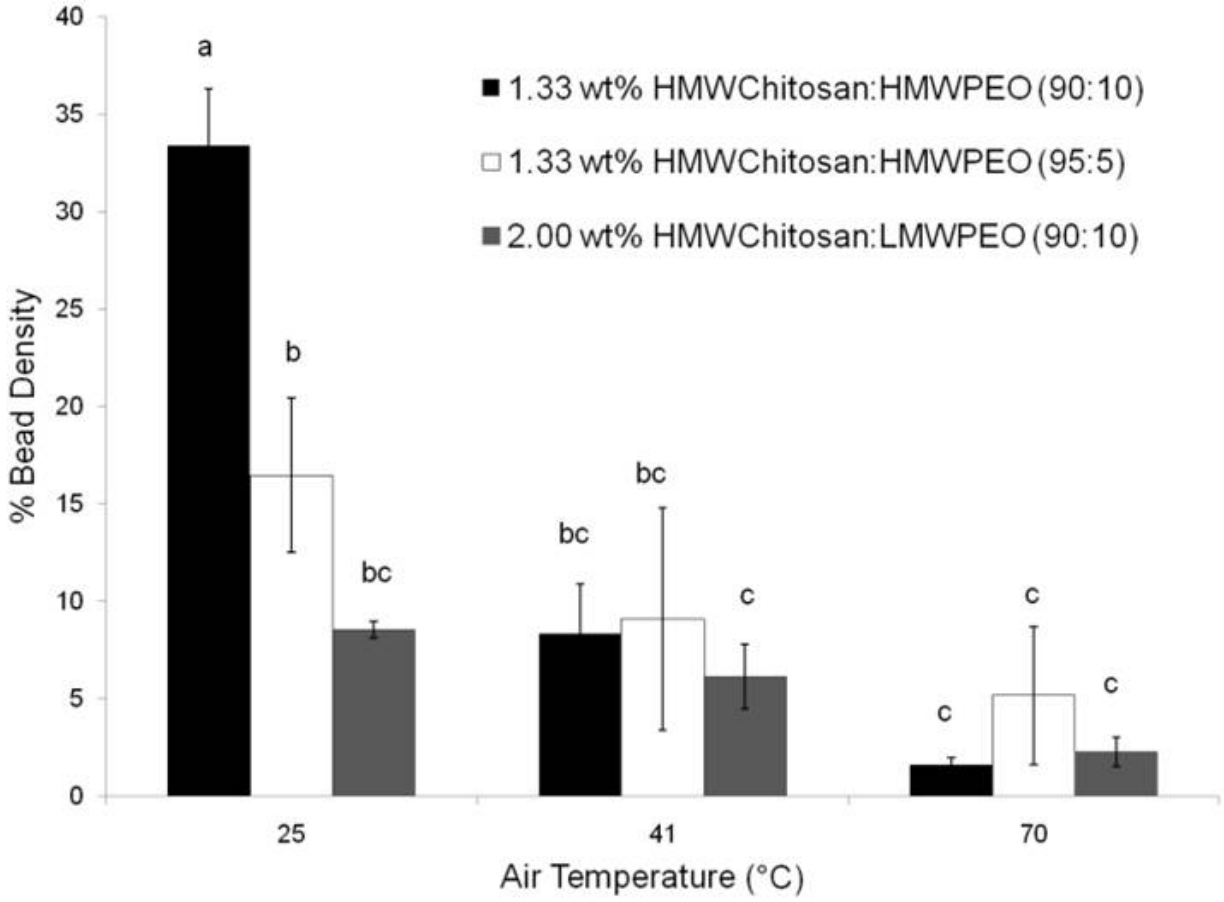

Figure 3.8 Bead density of various HMW chitosan: HMW PEO blend fibers at different spinning solution temperature and constant air flow of 25 ft^3/hr (Error bars represent standard deviation (n=3), letters indicate significant difference at $p<0.05$)

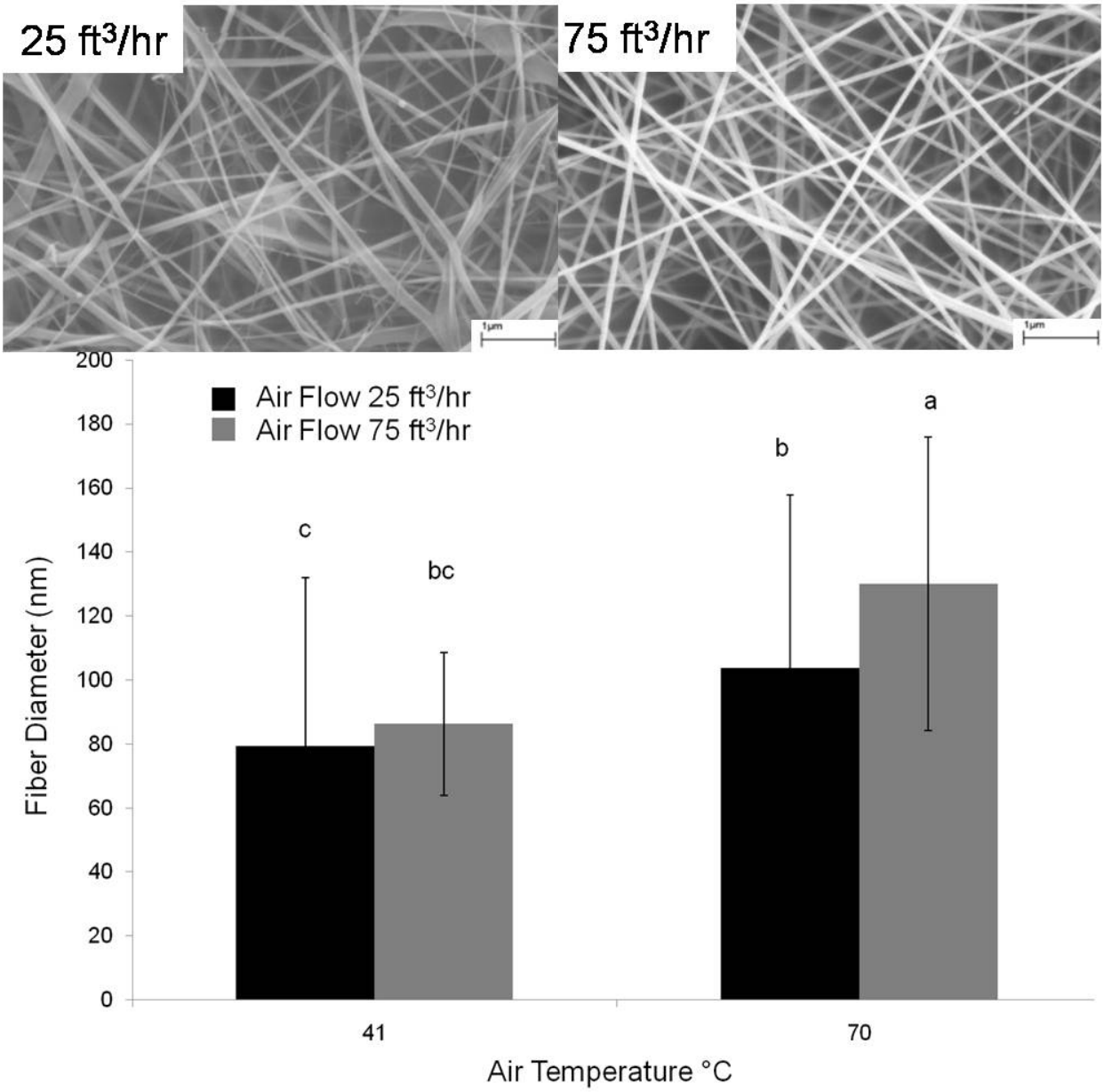

Figure 3.9 SEM images of 1.33 wt% HMW chitosan: HMW PEO (90:10) blend fibers at different air flow rates and 41°C air temperature (top)and fiber diameter of 1.33 wt% HMW chitosan: HMW PEO (90:10) blend fibers at different air flow rates and air temperature (bottom). (Error bars represent standard deviation (n=60), letters indicate significant difference at $p<0.05$)

3.2.3 Compositional analyses of electrospun chitosan/PEO blend fibers.

TGA analysis of the blend fibers confirmed the presence of both polymer fractions in the blend. Pure chitosan was found to thermally decompose at ~ 240°C and pure PEO at ~ 305°C. The thermal decomposition curves for the blend fibers showed distinct peaks for degradation temperatures of the two blend polymers as shown in Figure 3.10. In case of chitosan however complete weight loss is not achieved and there is residual polymer present (~ 45%) as can be seen in the raw weight loss curves of Figure 3.10a. Hence, only a fraction of the total chitosan in the fiber is obtained while measuring area under the chitosan peak and remaining unburnt material has to be added to this fraction to get total chitosan content in fiber. The estimated polymer fractions from the TGA scans are close to blend polymer ratios in solution as shown in Table 3.3.

Table 3.3 Calculated blend ratios in Chitosan/PEO blend fibers from TGA

Sample	% Chitosan in Solution	% Chitosan in fiber
HMW Chitosan : HMW PEO	95	97
HMW Chitosan : HMW PEO	90	97
HMW Chitosan : HMW PEO	75	73
HMW Chitosan : HMW PEO	50	45
LMW Chitosan : HMW PEO	90	98
LMW Chitosan : HMW PEO	75	69

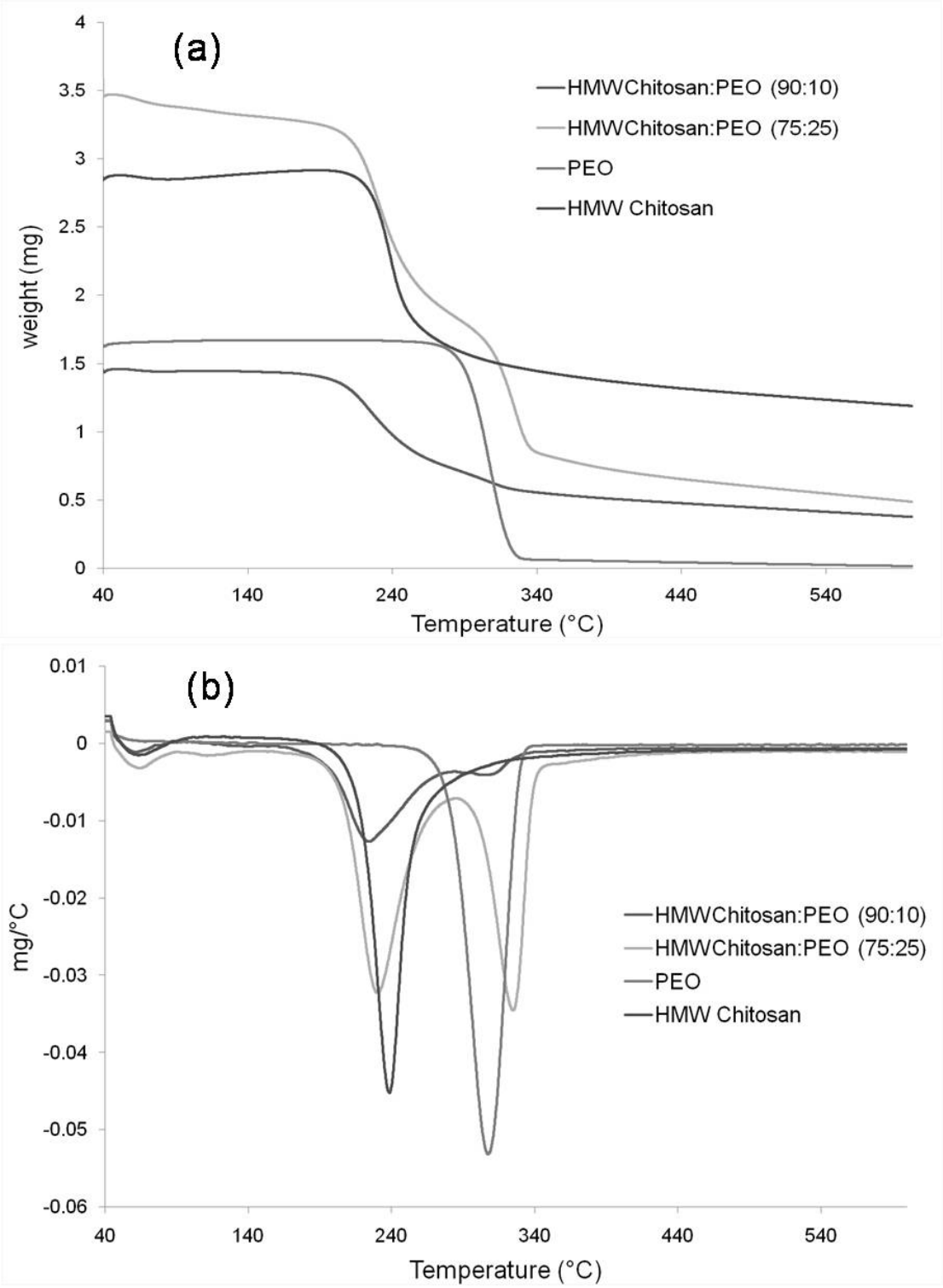

Figure 3.10 TGA analysis of chitosan/PEO fibers (a) Raw TGA scans showing presence of unburnt chitosan (b) First order derivative of TGA scans (blend ratios shown in paranthesis).

3.3 Electrospinning of Chitosan/PAAm blends

Chitosan/PAAm blend solutions were prepared with the goal of forming fibers with maximum chitosan content in the blend. Blend solutions were prepared by dissolving both polymer fractions in dilute acetic acid solutions.

3.3.1 Effect of molecular weight.

Initial studies at room temperature showed that both high and low molecular weight chitosan/PAAm blend fibers were formed with 75 % chitosan content, but higher chitosan % did not lead to uniform fiber formation due to an unstable jet. As shown in Figure 3.11, fibers obtained with LMWChitosan/PAAm blends were thicker (421 nm ± 153) compared to HMW chitosan/PAAm blends (132 nm ± 55) due to higher solution concentration resulting in higher viscosity (η_0 for HMWChitosan/PAAm (75:25) blends = 7.503 Pa.s; η_0 for LMWChitosan/PAAm (75:25) blends = 15.58 Pa.s) . To produce fibers with increased chitosan content, hot air was blown around the charged needle at various temperatures. Blowing of hot air helps reduce solution viscosity and increase evaporation rate of the solvent.[79] If temperature is increased closer to the boiling points of the solvent, drying of the jet could cause a large localized increase in viscosity at the tip of the needle. For this reason, we limited the maximum air temperature to 70°C in this study. The air-blowing rate helps improve fiber formation as it improves the spin-draw ratio allowing further stretching of the charged polymer jet during the whipping process.[78]

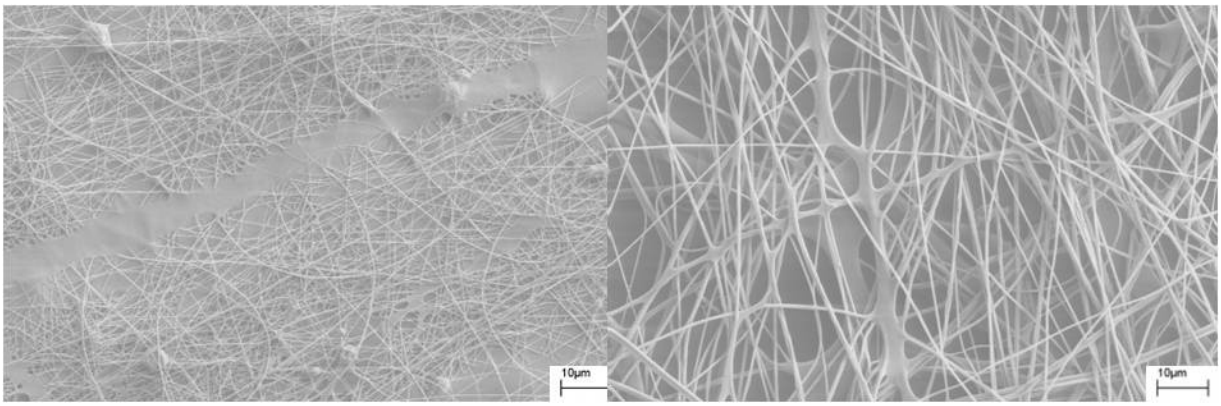

Figure 3.11: SEM images of (left)1.4 wt% HMWChitosan:PAAm (75:25) (right) 2.85 wt% LMW Chitosan:PAAm (75:25) blends.

3.3.2 Effect of polymer blend ratios and spinning solution temperature.

Blend solutions were prepared with reducing weight fractions of chitosan in blend starting with 95% chitosan and ranging down to that required for formation of nanometer sized, uniform, beadless fibers. Figure 3.12 summarizes the effect of blend ratios and spinning solution temperature on fiber formation. It can be seen that with increasing temperature, the fiber diameter increases slightly and the bead density decreases. SEM images of electrospun solutions containing 95% chitosan (Figures 3.12a) show poor fiber formation at room temperature, and very few fibers are collected on the target. As the temperature is increased (Figures 3.12bc) fiber formation is improved with bead less fibers formed at 70°C. When chitosan content was reduced to 90% (Figures 3.12def) with increasing spinning temperature, the transformation from beaded fibers to uniform bead free fibers is seen. Further reduction to 75% chitosan in the blend leads to formation of bead free fibers at room temperature (Figure 3.12g). As spinning temperature is increased (Figures 3.12hi), an increase in fiber diameter is seen. At higher temperature there is a faster evaporation of solvent leading to faster drying of the charged jet and increased chain entanglements which is validated by the reduction in rate index of solutions at constant blend ratio with increasing temperature as shown in Table 3.4.[170] Table 3.4 also details the zero-shear viscosity data of chitosan/PAAm blend solutions at different processing conditions. Renekar et.al have observed that spinning highly volatile polymer solutions leads to formation of polymer skin on the outside of the jet, subsequently leading to formation of a flat ribbon like structure.[171] SEM images of the Chitosan/PAAm fibers formed at high temperature also show some flat ribbon shaped fibers which would contribute to the apparent increase in fiber diameter at higher temperatures. The chitosan molecule is rigid in nature due to its high inter and intra-chain hydrogen bonding. Addition of a synthetic polymer helps break down some of these by forming new hydrogen bonds between chitosan and the synthetic polymer, and with reduced chitosan content fiber formation is improved.[111] With increasing solution temperature (for constant chitosan %), the overall viscosity of the solution decreases which along with the blown air helps in formation of uniform defect free fibers as the charged jet upon exiting the needle is further stretched, elongated and stabilized during the chaotic whipping motion that occurs as the jet travels to the target. There is no discernable trend in viscosity as a function of chitosan % at constant solution temperature, due to competing effects of higher molecular weight of PAAm compared to chitosan and hydrogen bonding between chitosan and PAAm chains. Air flow rate

was kept constant at 25ft^3/hr as it has been previously seen (section 3.2.2) that increasing it to 70ft^3/hr did not have significant effect on fiber formation.[172] Figure 3.13 and Figure 3.14 shows quantitatively the fiber diameter and bead density data, respectively, of electrospun chitosan/PAAm solutions at different blend ratios and increasing spinning solution temperatures.

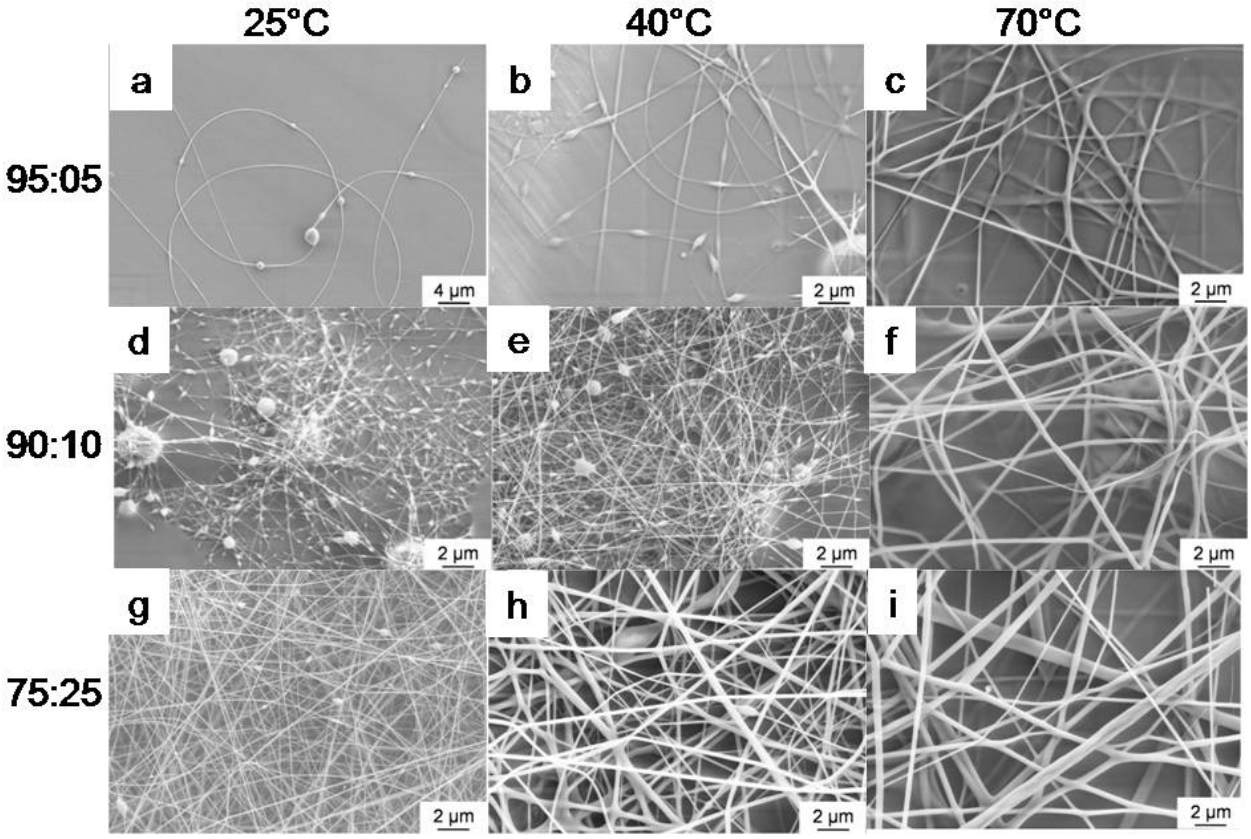

Figure 3.12 SEM images of 1.4 wt% HMWChitosan: PAAm blends at different blend ratios and hot air blown at 25ft^3/hr at different temperatures (fig 3.12a,3.12b,3.12c are HMWChitosan: PAAm (95:05) blend ratio, 3.12d,3.12e,3.12f are HMWChitosan: PAAm (90:10) blend ratio, and 3.12g,3.12h,3.12i are HMWChitosan: PAAm (75:25) blend ratio fibers)

Table 3.4 Zero-Shear Viscosity (η_0) of Chitosan/PAAm blends

Sample	Solution Temperature (°C)	η_0 (Pa-s)	n
1.4 wt% HMW Chitosan:PAAm(95:5) in 50% AA	25	3.208	0.3561
	40	1.539	0.3089
	70	0.611	0.2229
1.4 wt% HMW Chitosan:PAAm(90:10) in 50% AA	25	4.325	0.3691
	40	2.486	0.2961
	70	0.780	0.2589
1.4 wt% HMW Chitosan:PAAm(75:25) in 50% AA	25	3.446	0.895
	40	2.082	0.3208
	70	0.6863	0.2476

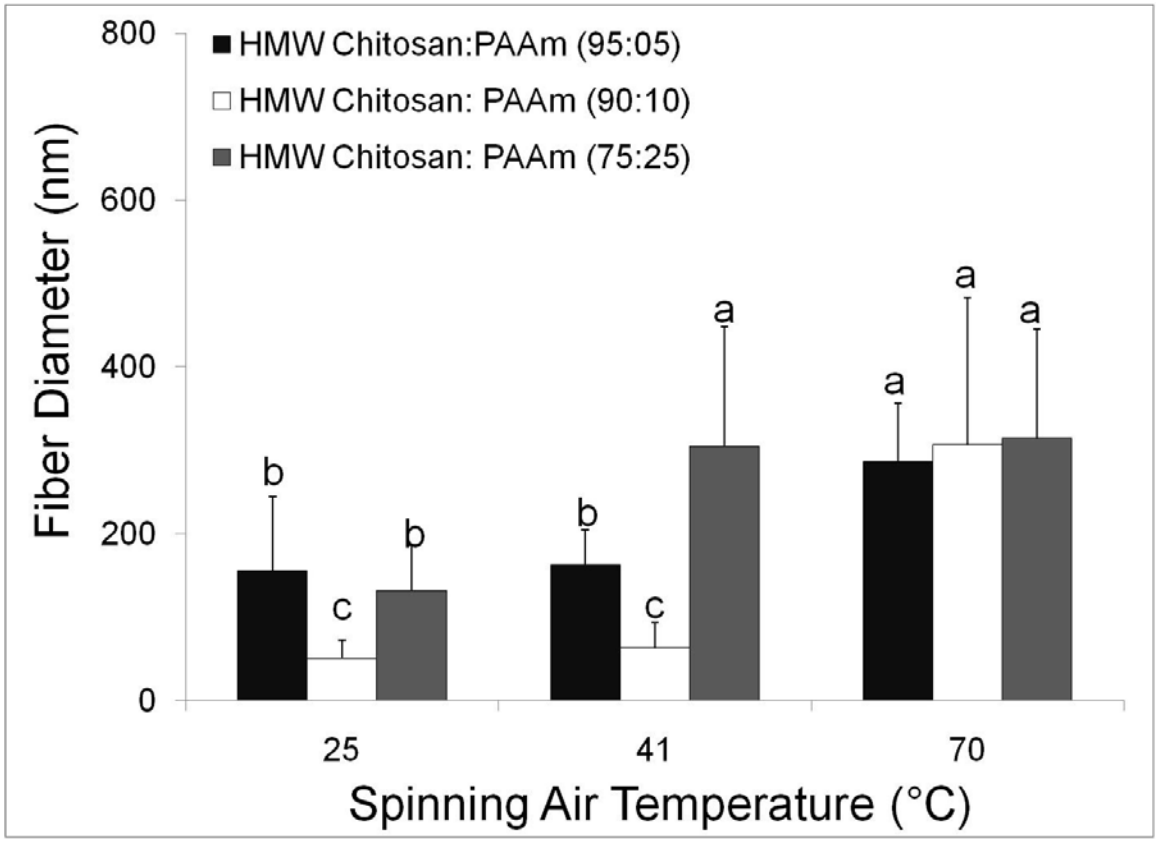

Figure 3.13 Fiber diameter of 1.4 wt% HMW chitosan: HMW PAAm blend fibers at different air temperature. (Error bars represent standard deviation (n=60), letters indicate significant difference at $p<0.05$)

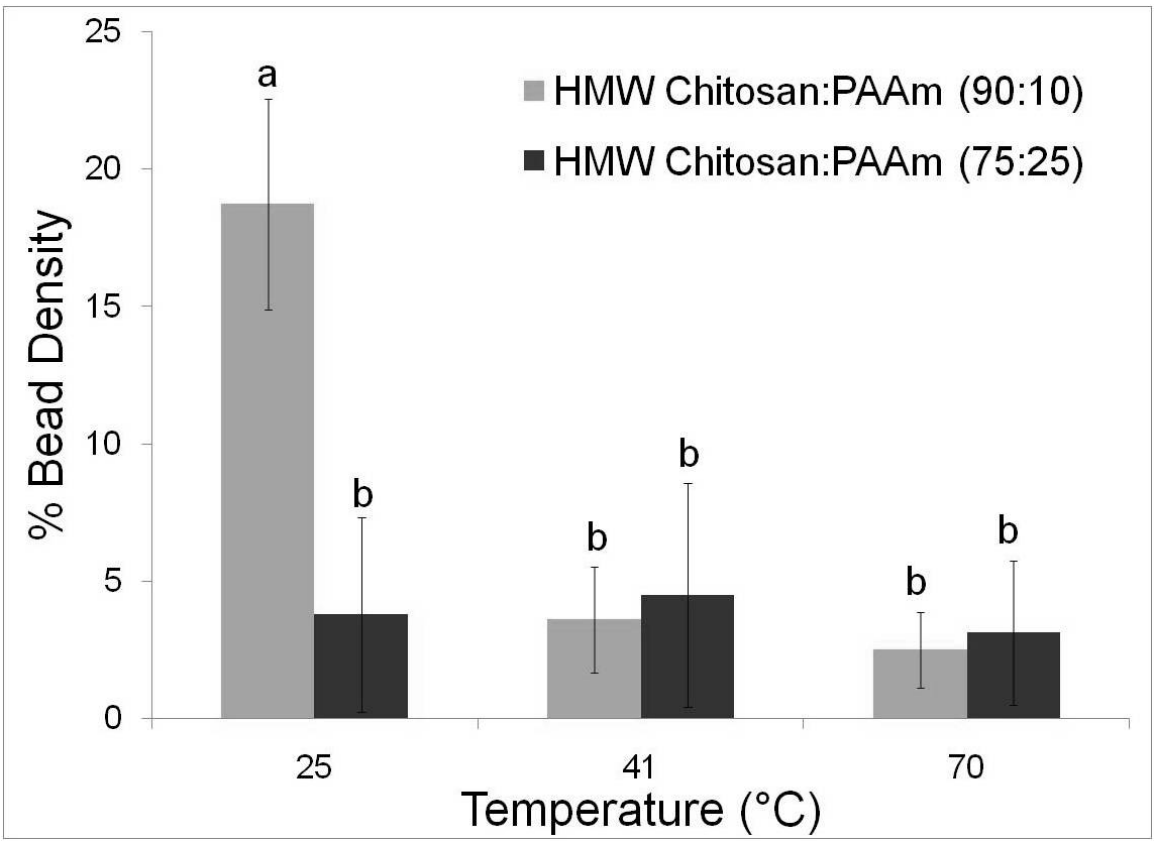

Figure 3.14 Bead density of 1.4 wt% HMW chitosan: HMW PAAm blend fibers at different air temperature. (Error bars represent standard deviation (n=3), letters indicate significant difference at $p<0.05$)

3.3.3 Compositional analyses of chitosan/PAAm blend fibers.

TGA analysis of the blend fibers confirmed the presence of both polymer fractions in the blend (Figure 3.15). Pure chitosan was found to thermally decompose at ~ 240°C and pure PAAm shows two degradation peaks one at ~ 240°C (due to melting of polymer chains and onset of degradation) and other broad peak at 350°C (due to further polymer degradation).[173] For both pure chitosan and PAAm the raw TGA curve shows presence of unburnt material residue. It is difficult to quantify the exact fractions of both polymers in fiber due to overlapping peaks (~ 240°C) of both polymers. The TGA curve for the 90% and 75% chitosan blend fibers showed absence or very small PAAm peak at 350°C. This suggests that there is possibly a low PAAm and higher chitosan content in the electrospun fibers (compared to the spinning solutions), and

our previous work (Section 3.2.3) quantifies that the fraction of polymers in fibers and blend solutions is not significantly altered during electrospinning.[172]

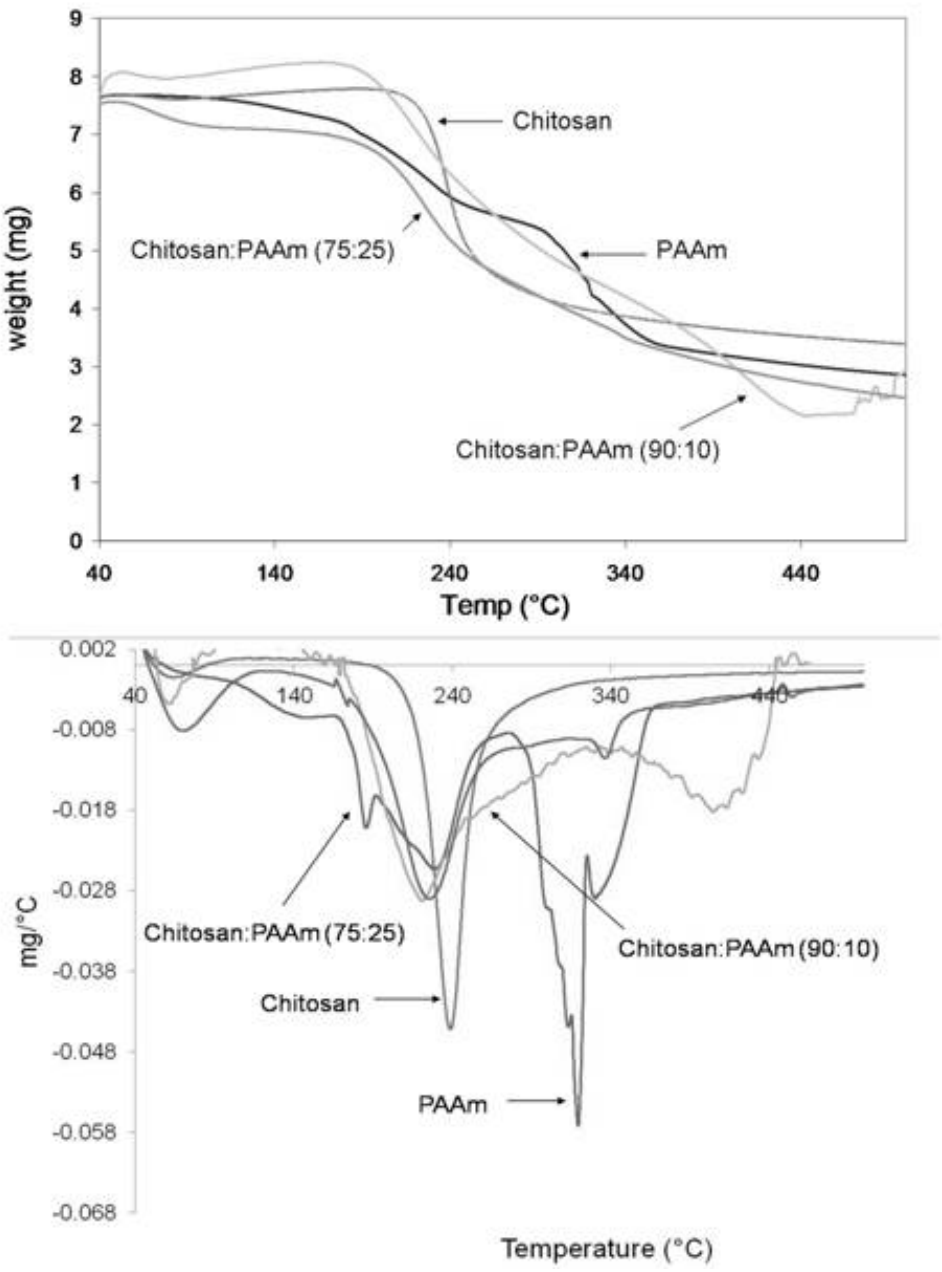

Figure 3.15 TGA analysis of Chitosan: PAAm blend fibers (a) raw TGA scans showing presence of unburnt polymer (b) first order derivative of TGA scans.

4. Surface Characterization – Results & Discussion

4.1 Proposed model correlating fiber surface area with surface amide content.

The advantage of using chitosan based nanofibrous filter media for metal binding and anti-microbial applications is that they offer high surface area to mass ratio, essentially offering higher filtration efficiencies at lower material loadings. As binding is mainly a surface phenomenon, the maximum binding efficiency of chromium by the electrospun nanofibers would be dependent on the physical shape and size of the fiber and its surface chemistry. To correlate the fiber size, surface chemistry with its maximum binding capacity a model has been developed. The model can serve as a tool to predict the chromium (VI) binding capacity of chitosan or chitosan/blend nanofibers as a function of fiber size, % chitosan in blend fiber, and degree of deacetylation of chitosan. To develop the model the following assumptions and data from literature were used:

- In the chitosan used in this study the degree of protonation of chitosan is 50% and solution pH ~ 6.5 (as has also been experimentally validated) *i.e.* 50% of the amide groups on the chitosan fiber surface are protonated.
- At pH = 6.5 and 5 mg/L concentration, K_2CrO_4 dissociates forming chromate ion (CrO_4^{-2}) as quoted in literature and shown in Figure 4.1[22].

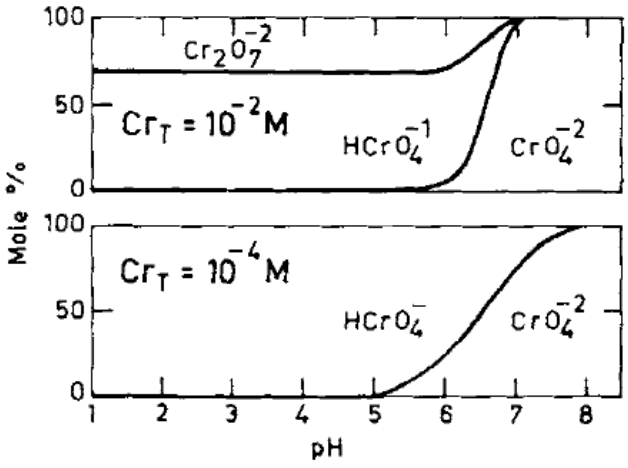

Figure 4.1 Distribution of hexavalent chromium species as a function of pH.[22]

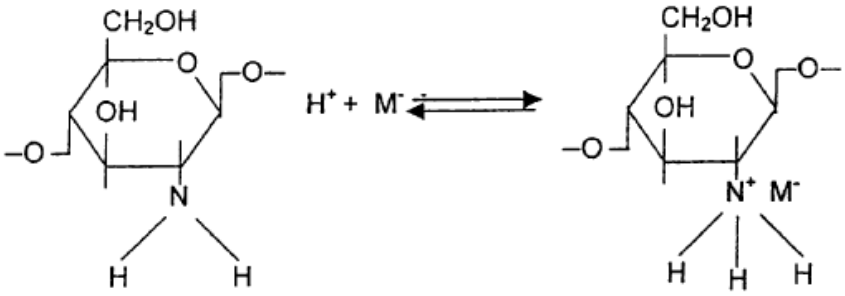

Figure 4.2 Interaction between Cr (VI) and protonated amine in chitosan.[174]

- Binding between positively charged amide group and negatively charged chromate ion takes place as shown in Figure 4.2.[174] *i.e.* one protonated amine is linked to one chromate ion.
- At equilibrium *i.e.* when reaction reaches steady state and maximum number of chromate ions that can be bound are bound by the chitosan, 96.4% chromium is bound by chitosan at pH = 4 whereas after 3 hrs it is 93% and after 20 mins (for dynamic filtration studies 10 passes of 2 mins each) binding is ~ 36% as shown in Figure 4.3.[22] Our binding experiments were done at pH = 7 at which the binding kinetics should be similar, however binding capacity will be different because of different degree of protonation.

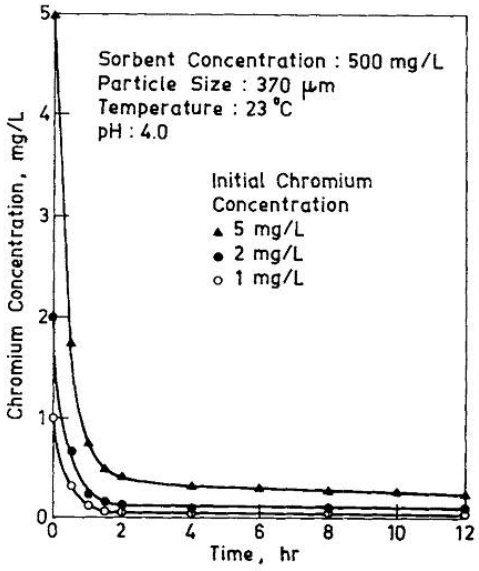

Figure 4.3 Reaction kinetics of Cr(VI) binding[22]

- Chitosan chains crystallize in an orthorhombic unit cell with dimensions a = 0.828 nm, b = 0.865 nm and c = 1.043 nm (fiber axis) as shown in Figure 4.4.[175] Each unit cell contains 4 glucosamine units with two $-NH_2$ groups facing outward (towards fiber surface) and two inward (*i.e.* amino groups arranged alternately in the 2 and 4 position). As 50 % amino groups are protonated there is one protonated amine per 0.865*1.043 nm^2 area of chitosan crystal *i.e.* one protonated amine per 0.8991 nm^2. The crystals are packed in a way as shown in Figure 4.5 with fiber length parallel to the c direction.

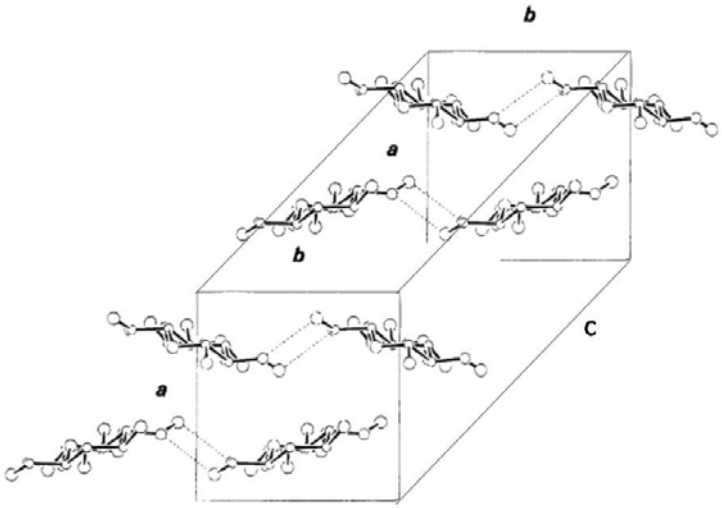

Figure 4.4 Orthorhombic chitosan unit cell.[175]

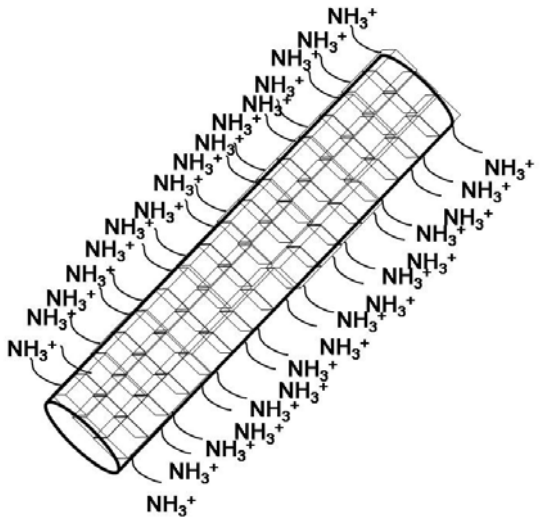

Figure 4.5 Packing of chitosan unit cell in fiber.

- The actual surface density of protonated amines is lower because chitosan is semi-crystalline or amorphous in nature. Theoretical density of 80% DDA chitosan is 1.51 g/cc, whereas the theoretical density of 100% amorphous chitosan is 1.5 g/cc. While calculating the # of protonated amines per square cm on fiber surface the percent difference between theoretical density and amorphous density of chitosan has to be accounted. The chitosan used for this study is nearly 100% amorphous as measured by our coworkers Li et.al.[176]

Model

Surface area to mass ratio of electrospun fiber is given by the equation:

$$\frac{Surface\ area}{mass\ of\ chitosan} = \frac{surface\ area\ of\ fiber}{(density\ of\ chitosan)(volume\ of\ fiber)}$$

$$\frac{Surface\ area}{mass\ of\ chitosan} = \frac{(2\pi rh)}{\rho\pi r^2 h}$$

$$\frac{Surface\ area}{mass\ of\ chitosan} = \frac{2}{\rho r}$$

where ρ is density of chitosan in g/cc and r is radius of fiber in cm.

We know there is one protonated amine per 8.991E-15 cm^2 for a 100% DDA, 100% crystalline chitosan. Therefore, for an electrospun fiber with known radius, % DDA and % chitosan in blend fiber.

$$\#\ of\ protonated\ amines\ (N_{NH3+}) = \frac{1}{2\rho_{theo.}r}\left(\frac{1}{8.991 * 10^{-15}}\right)(\%DDA)(\%\ Chitosan\ in\ blend)$$

where $\rho_{theo.}$ is the theoretical density or density of 100 % crystalline chitosan calculated for chitosan with varying degree of deacetylation(from appendix 1).

Knowing that our chitosan is highly amorphous the actual number of protonated amines per square centimeter should be lower than that calculated using the above equation. Hence, a correction for the density has to be done.

$$\#\ of\ N_{NH3+actual} = \left(N_{NH3+cryst}\left(\frac{\rho_{amor.}}{\rho_{(theo)}}\right)^{2/3}\right)$$

Since, one chromate ion is bound by one protonated amine and considering "x" is extent of reaction after known time ("x" value can be obtained from Figure 4.3)

# of bound chromate ions = (x)(# of protonated amines).

Therefore mg chromium bound per gram chitosan will be:

$$\frac{mg\ chromium}{g\ chitosan} = (x)(\#\ of\ N_{NH3+actual})\frac{(amu\ of\ CrO_4^{-2})}{(Avogadros\ Number)}$$

$$\frac{mg\ chromium}{g\ chitosan} = (x)(\#\ of\ N_{NH3+actual})\frac{(111.9961)}{(6.023 * 10^{23})}$$

Figure 4.6 and 4.7 show the effects of % chitosan in blend fiber (80% DDA chitosan) and % DDA (at 90% chitosan in blend fiber) on the Cr (VI) binding capacity respectively. (Calculations are shown in appendix 2&3). It can be seen that in both cases with varying % chitosan and % DDA as fiber diameter increases (> 400 nm) the effect of fiber diameter on binding capacity plateaus off *i.e.* fabricated electrospun fibers should have fiber diameter < 400 nm to effectively serve their purpose for metal binding. Results from this developed model will be compared with experimental data in chapters 5 and 6 for the electrospun chitosan/PEO and chitosan/PAAm nanofiber mats.

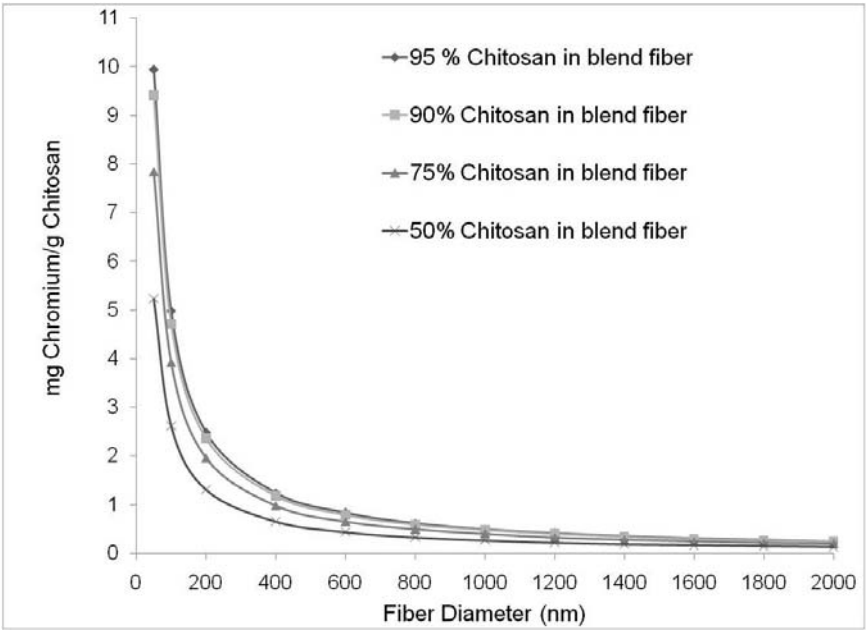

Figure 4.6 Effect of % Chitosan in blend fiber on Cr (VI) binding capacity.

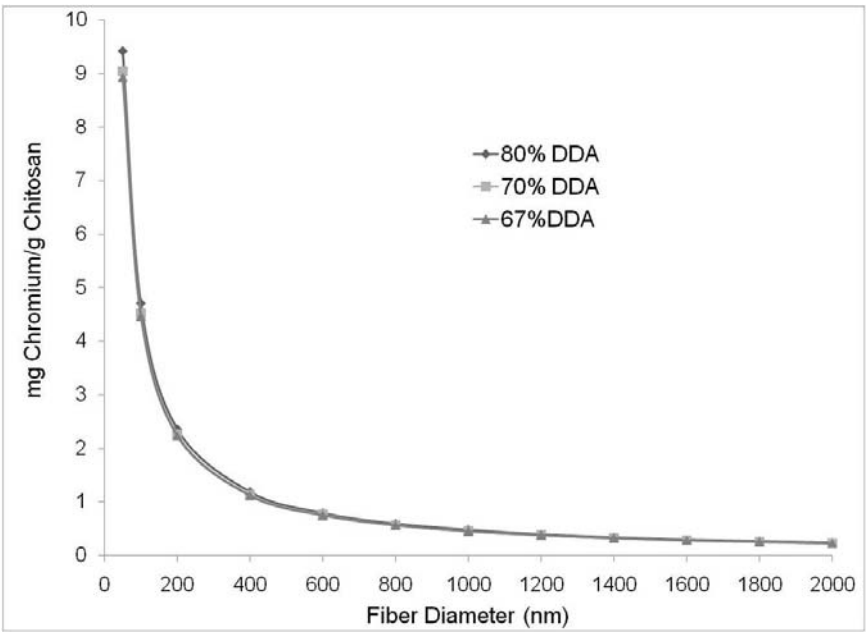

Figure 4.7 Effect of % DDA (90% chitosan in blend fiber) on Cr (VI) binding capacity.

4.2 XPS results

To understand the surface composition of electrospun fibers fabricated from chitosan/PEO and chitosan/PAAm polymer blend solutions, x-ray photoelectron spectroscopy (XPS) analysis of surface of electrospun fiber mats was done using procedure as described in section 2.3.1. XPS analysis of pure 80%DDA HMW chitosan films solvent cast from 1% HCl, pure PEO solvent cast from water, and pure PAAm solvent cast from water were used as standards for the three different polymers. Apart from the XPS scans of pure film samples for PEO and PAAm, XPS analysis was done of electrospun fiber samples of pure PEO and pure PAAm and compared to the film samples to study effect of film vs. fiber morphology on XPS results. Atomic % of the three main elemental peaks *i.e.* carbon, hydrogen and oxygen obtained from the XPS analysis of blend fibers was compared to those that can be derived theoretically knowing the chemical structure of the repeating unit of the individual polymers to calculate the weight fraction of chitosan present on fiber surface (detailed calculations are shown in Appendix 4). Figure 4.8 shows the survey scan of chitosan, PEO and PAAm for pure polymer films. The survey scan shows the expected C, N, O peaks for chitosan, PAAm and C,O peaks for PEO. The atomic % values are shown in Table 4.1. It can be seen from the data in Table 4.1 that the surface elemental composition as obtained from XPS for the pure polymers is in close agreement with

those obtained theoretically from the structure of their repeat units. The concentration of C1s peak is higher than the theoretical value and this could be because of surface contaminants, similar results have been obtained for surface analysis of the three polymers in literature[177-179]. The increase in C1s concentration for chitosan fiber samples could also be because of residual acetic acid present on the fibers. If we assume that for every chitosan repeat unit there is a half molecule of CH_3COO^- which is weakly associated with the fiber surface then the theoretical "C/N" ratio would increase from 6.4 to 7.4. The aluminum peak in the electrospun PAAm fiber sample is from the aluminum pan substrate on which the fibers were spun. The huge difference in surface composition in PEO fibers and films is because PEO fibers were spun on PP substrate and as the espun fiber layer is very open and may not have uniformly covered the PP layer the majority signal came from the underlying PP substrate (XPS of pure PP non-woven shows 90.54 atom% C and 9.46 atom % O[180]).

Figure 4.9 shows the "C", "N", and "O" elemental scans for the pure chitosan film. The elemental scans are in agreement with those obtained by Matienzo et.al[177]. Peak fitting of the carbon curve shows presence of four different signals. A rule of thumb for identifying the C1s peak is that the more electronegative the carbon atom is the higher its binding energy[181]. The structure of chitosan is very complex and Matienzo et.al have correlated each of the four different carbon signals with structure of glucosamine and N-acetyl glucosamine units that make up chitosan. The carbons at C2, C6 from glucosamine along with the C2,C6, and C8 from N-acetyl glucosamine make up one carbon environment (30.08%, 285.0 eV) consisting of C-C or C-H linkages. The carbons at C3, C4 and C5 of both glucosamine and N-acetyl glucosamine make up a second carbon environment (51.37%, 286.66 eV) consisting of C-OH, C-O linkages. The carbons at C1 "O-C-O" makes up the third environment (16.32%, 288.25 eV) whereas the carbons at C7 (H_2N-C=O) in the N-acetyl glucosamine makes up the fourth environment (2.2%,289.43 eV). The nitrogen curve also shows two peaks corresponding to the 58.48% protonated amine (400.3 eV) and 41.52% unprotonated amine (398.3 eV).[177] The oxygen curve shows presence of three regions contributed by the carbonyl groups, ether linkage and hydroxyl groups present in chitosan. The elemental scans for the other two polymers PEO and PAAm also show expected peaks as shown in Figure 4.10 and 4.11 respectively. The C1s peak from PEO shows three different regions at 283.4, 284.97 and 287.22 eV. The peak at 284.97 eV and 287.22 eV can be attributed to the C-C, and C-O linkages present in PEO respectively. In insulating

samples a small peak is seen at lower binding energies (~283 eV) and this is not attributed to any chemical group in the structure but to charging effects on the sample surface[182]. The O1s peak in PEO shows a single peak at 531.0 eV. [179]The C1s peak from PAAm shows two distinct regions at 285 eV and 288.1 eV the former corresponding to the C-C,C-H linkages and latter to the acetyl amine linkage. The N1s peak in PAAm shows a very small protonated peak (8.19%). The O1s peak is also as seen in literature at 531 eV.[178].

Table 4.1 Surface atomic composition of pure polymers obtained from their structure and XPS analysis.

Sample		Atom %					"C/N" ratio
		C1s	N1s	O1s	Cl2p	Al	
80% DDA HMW chitosan	theoretical	56.14	8.77	35.08			6.4
	from XPS (film)	61.11	5.6	28.18	5.11		10.92
Pure PEO	theoretical	66.67		33.33			∞
	from XPS (film)	66.77		32.39	0.11		∞
	from XPS (fiber)	96.26		3.74			∞
Pure PAAm	theoretical	60	20	20			3
	from XPS (film)	67.17	13.73	18.56	0.54		4.89
	from XPS (fiber)	61.24	12.48	22.68	0.45	3.14	4.91

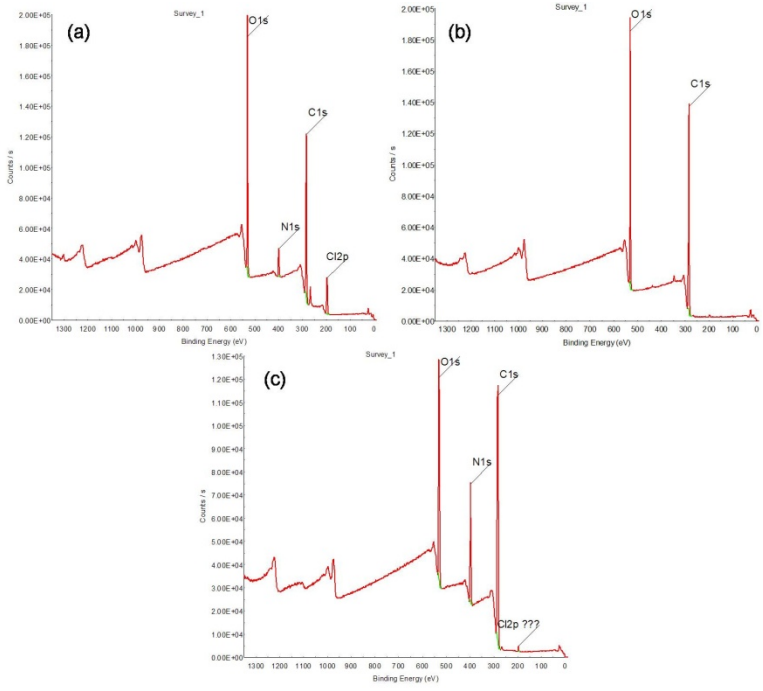

Figure 4.8 Survey XPS spectra of (a) pure chitosan, (b) pure PEO, and (c) pure PAAm film.

XPS scans of chitosan/PEO and chitosan/PAAm blend fibers were done with goal of understanding the effect of the following variables on surface chitosan content:

- % chitosan in blend solution.
- Chitosan % DDA at constant % chitosan in blend solution.
- Fiber diameter of electrospun fiber at constant chitosan % in solution.
- Chitosan molecular weight.
- XPS scans were also taken on samples after metal binding to compare surface chemistry before and after Cr(VI) binding experiments.

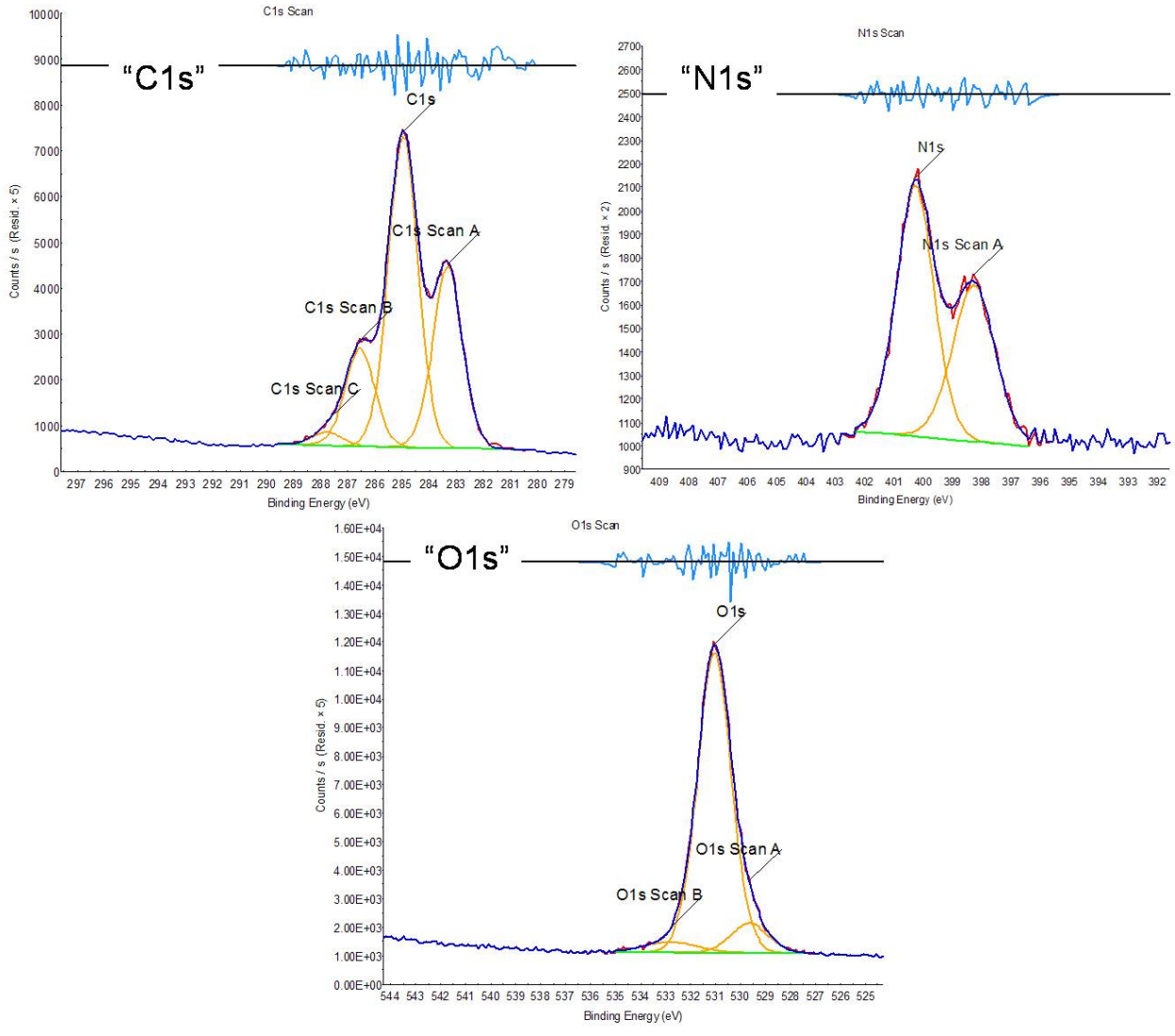

Figure 4.9 High resolution "C","N","O" elemental scans

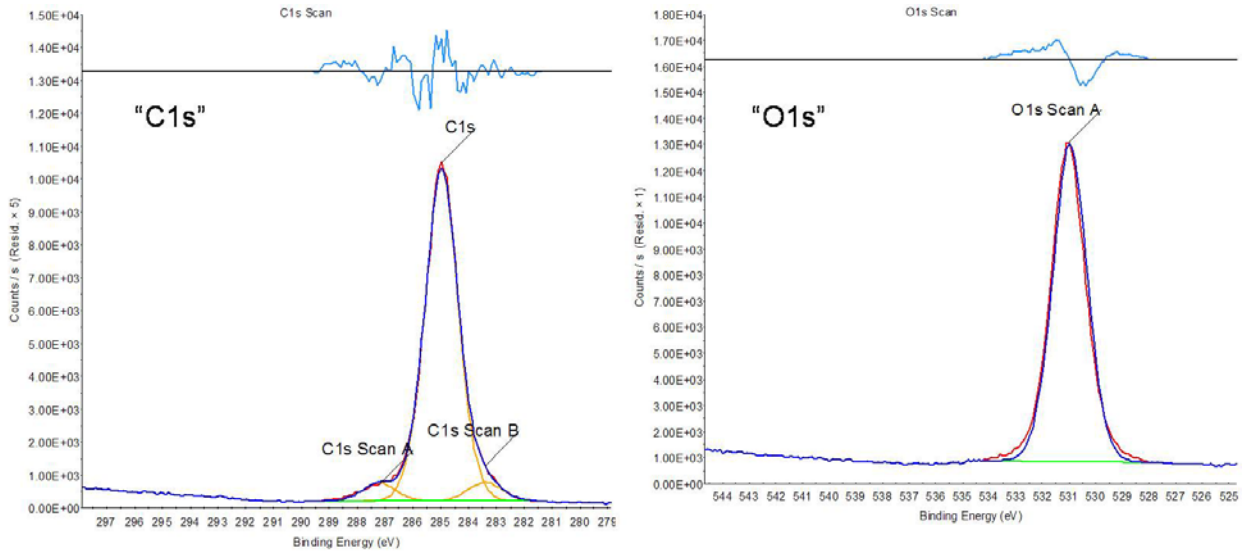

Figure 4.10 Elemental "C" and "O" scans of pure PEO films

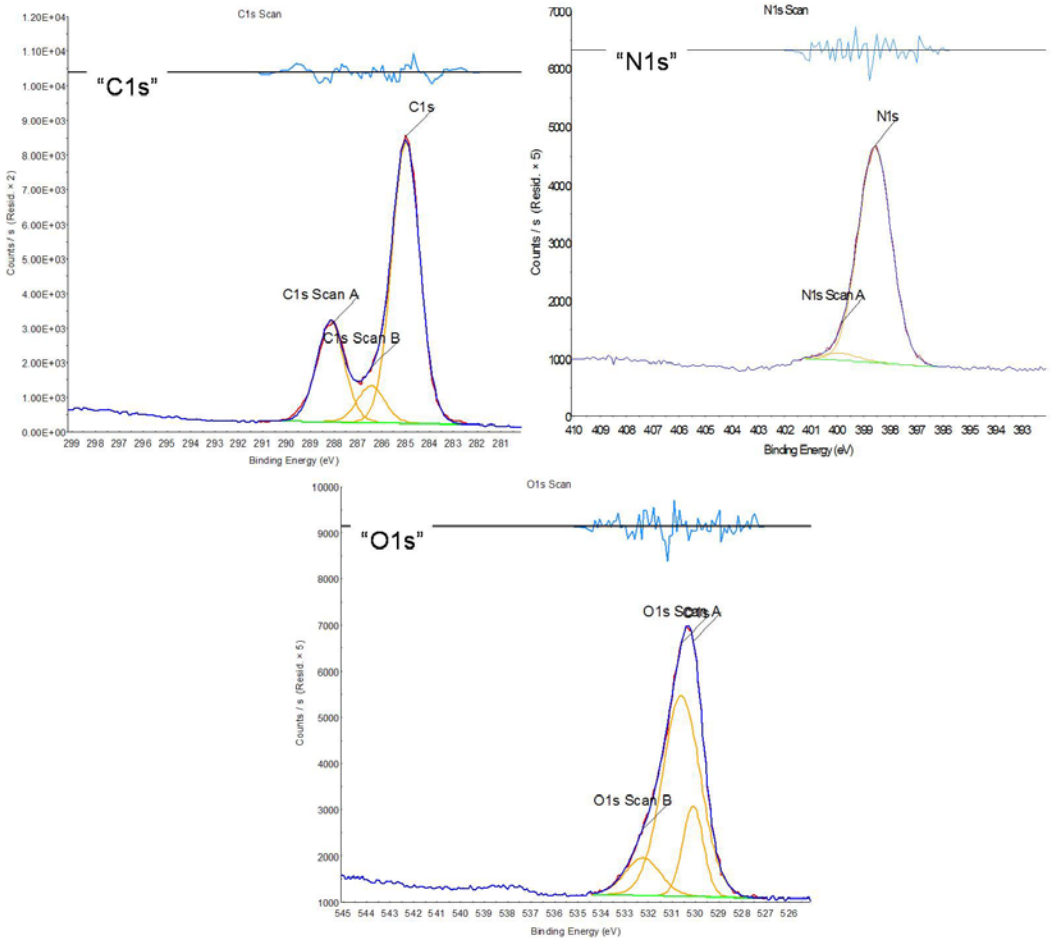

Figure 4.11 Elemental "C","N","O" scans of pure PAAm film

4.2.1 XPS – Chitosan/PEO blends.

Table 4.2 shows the atom% data as function of increasing PEO content in both HMW and LMW chitosan: PEO blend fibers. Figure 4.12 shows a plot of the surface nitrogen composition (atom %) as obtained from XPS vs. the chitosan concentration (wt %) in solution. It can be seen that with decreasing chitosan content the atom % N is decreasing or surface content of chitosan is decreasing. Also it can be seen that blend solutions made using higher molecular weight (HMW) chitosan have higher surface nitrogen content then low molecular weight chitosan blends for same blend ratios. Figure 4.13 shows the C1s and N1s elemental XPS scans. The pure chitosan has broad peak which by curve fitting (discussed earlier Figure 4.9) shows presence of four different types of carbon bonds in chitosan. As % chitosan in blend solution decreases the chitosan peak starts to lose its characteristic shape and evolves in to a broad peak which begins to narrow as concentration approaches that of pure PEO (which has a narrower C1s peak, Figure 4.10) in blend solution. As the peak at higher binding energies are attributed to the (H_2N-C=O) linkage in chitosan with decreasing chitosan content this peak disappears and peak begin to narrow. The N1s peak for pure chitosan shows two peaks but for the blend samples the protonated peak is not self evident and decreasing in size.

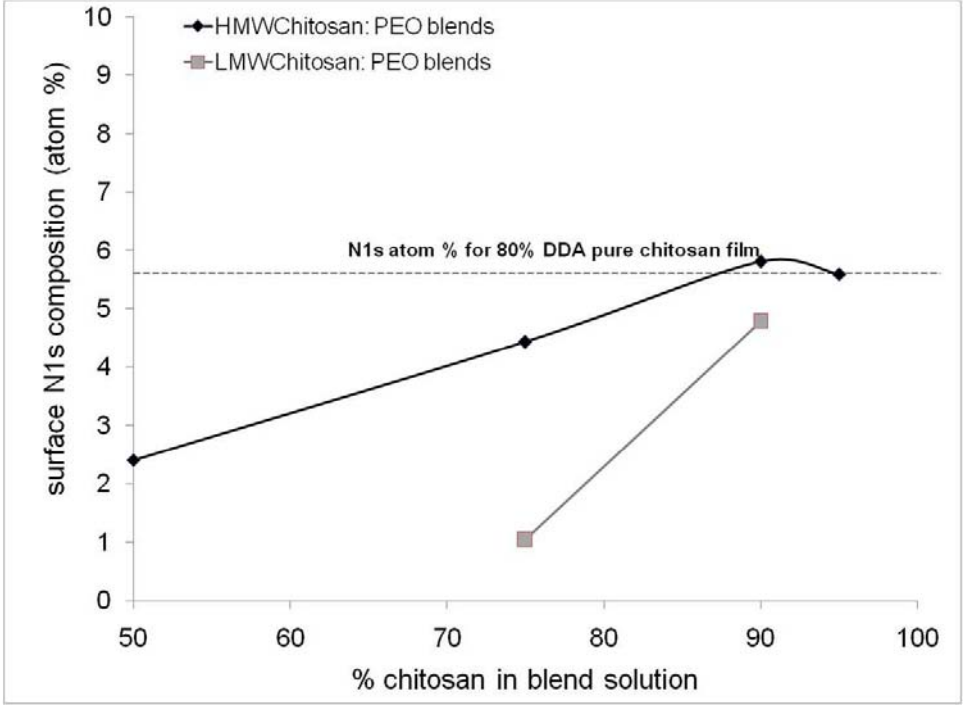

Figure 4.12 Surface nitrogen (atom %) vs. chitosan wt % in blend solution.

Table 4.2 Surface atomic composition of chitosan/PEO blends.

Sample	% Chitosan	Atom%			C/N ratio
		C1s	N1s	O1s	
HMWChitosanPEO blends	95	63.13	5.81	31.06	10.87
	90	65.58	4.44	29.97	14.77
	75	66.48	2.41	31.11	27.59
	50	70.05	0.39	29.55	179.62
LMWChitosanPEO blends	90	61.54	4.79	33.67	12.85
	75	66.97	1.04	31.99	64.39

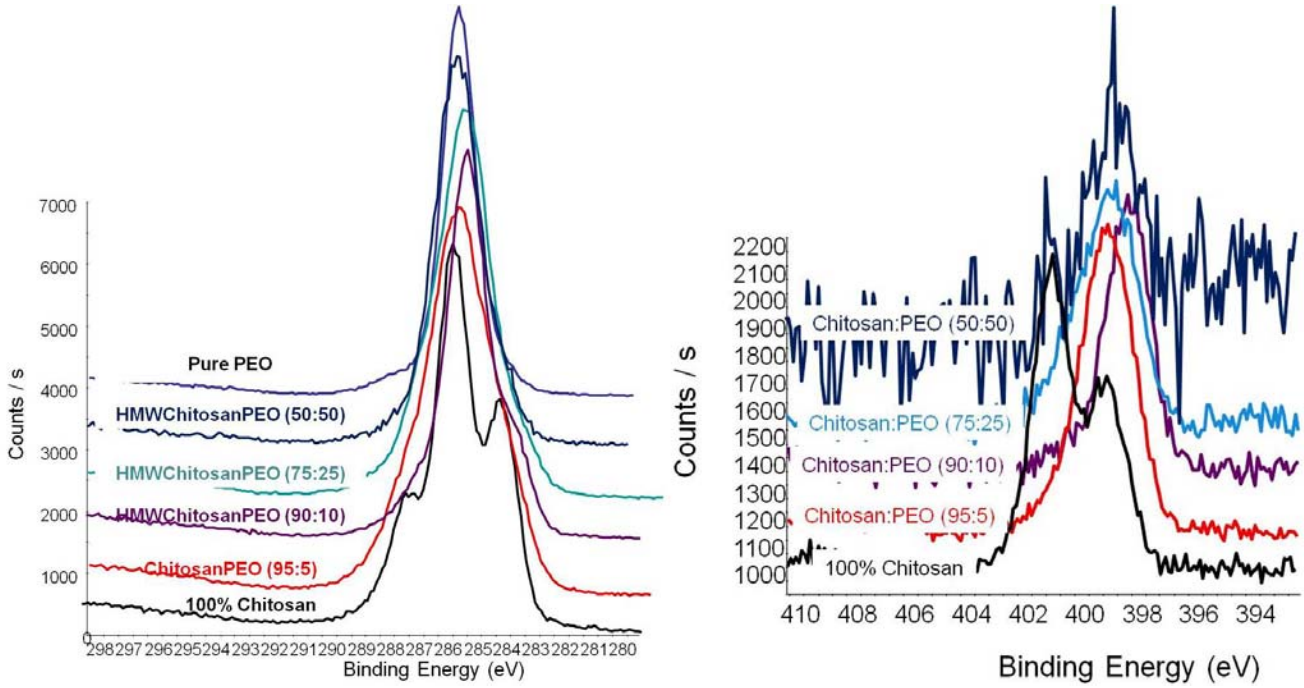

Figure 4.13 C1s (left) and N1s (right) elemental scans of chitosan/PEO blend fibers with decreasing % chitosan in blend fiber.

Calculation of surface chitosan wt%

From the structure of the chitosan and PEO repeat units it is known for pure 80% DDA chitosan theoretically there are 6.4 atoms of carbon and 1 atom of nitrogen per chitosan repeat unit, and for each PEO repeat unit there are 2 atoms of carbon and 0 atoms of nitrogen.

Let Nn be number of nitrogen atoms and Nc be number of carbon atoms in chitosan/PEO blend fibers and the C/N (carbon/nitrogen) ratio is Nc/Nn or "r". From XPS we know "r" and knowing that theoretically for each chitosan repeat unit there 6.4 atoms of carbon and 1 atom of nitrogen, and for each PEO repeat unit there are 2 atoms of carbon and 0 atoms of nitrogen we

can obtain surface chitosan concentration in weight basis. Surface chitosan wt% calculated using this hypothesis will be referred to as "calculations based on theoretical # of C".

$$Nc = \frac{Wt\ of\ chitosan}{mol.wt\ of\ chitosan\ rpt\ unit}(\#of\ C\ atoms\ perchitosan\ rpt\ unit\ ) + \frac{Wt\ of\ PEO}{mol.wt\ of\ PEO\ rpt\ unit}(\#of\ C\ atoms\ perPEO\ rpt\ unit\ )$$

$$Nn = \frac{Wt\ of\ chitosan}{mol.wt\ of\ chitosan\ rpt\ unit}(\#of\ N\ atoms\ perchitosan\ rpt\ unit\ ) + \frac{Wt\ of\ PEO}{mol.wt\ of\ PEO\ rpt\ unit}(\#of\ N\ atoms\ perPEO\ rpt\ unit\ )$$

$$Nc = \frac{Wt\ of\ chitosan}{169.4}(6.4\ ) + \frac{Wt\ of\ PEO}{44}(2\ )$$

$$Nn = \frac{Wt\ of\ chitosan}{169.4}(1\ )$$

$$\frac{Nc}{Nn} = \frac{\frac{Wt\ of\ chitosan}{169.4}(6.4\ ) + \frac{(1 - Wt\ of\ chitosan)}{44}(2\ )}{\frac{Wt\ of\ chitosan}{169.4}}$$

$$Wt\ of\ chitosan = \frac{0.045}{\left(\frac{1}{169.4} * \frac{Nc}{Nn}\right) + 7.67E - 3}$$

However as seen from XPS results of pure chitosan films the "C/N" ratio for 80% DDA pure chitosan film is 10.91 compared to theoretical value of 6.4. As the XPS detects excess carbon peaks due to surface contamination the above equations will not be able to accurately predict surface chitosan wt% of the blend fibers. To get a better estimate of surface chitosan wt% instead of using theoretical values of # of C and N atoms we use the values of obtained from the atom %

values from XPS for pure chitosan and PEO. Hence, # of C atoms per chitosan repeat unit is 6.96 and # of C atoms per PEO repeat unit is 2.0. Therefore using the data from XPS surface analysis the surface weight % of chitosan is given by the following equation. Surface chitosan wt% calculated using this hypothesis will be referred to as "calculations based on experimental # of C".

$$Nc = \frac{Wt\ of\ chitosan}{169.4}(6.96\ ) + \frac{Wt\ of\ PEO}{44}(2\ )$$

$$Nn = \frac{Wt\ of\ chitosan}{169.4}(0.64\ )$$

$$\frac{Nc}{Nn} = \frac{\frac{Wt\ of\ chitosan}{169.4}(6.96\ ) + \frac{(1 - Wt\ of\ chitosan)}{44}(2\ )}{\frac{Wt\ of\ chitosan}{169.4}(0.64)}$$

$$Wt\ of\ chitosan = \frac{0.045}{\left(0.00378 * \frac{Nc}{Nn}\right) + 0.0043}$$

Figure 4.14 shows the calculated surface chitosan wt% (calculated both by theoretical and experimental # of C) vs. the wt % of chitosan in blend solution. It is safe to say that the real surface chitosan wt % would lie between the calculated values using the experiment # of C and theoretical # of C i.e. for 95 wt % chitosan in blend solution surface chitosan composition would be between 63 and 100 wt% and for 50 wt% chitosan in blend solution surface chitosan composition would be between 4 and 7 wt% (calculations shown in Appendix 4).

As PEO content in blend solution increases, the amount of chitosan decreases non-linearly indicating possibly some kind of phase separation taking place during the spinning process. Ming et.al[83] have extensively studied the morphology development in electrospun fibers made using polymer blends. They have concluded that phase morphology of blend solutions is strongly dependant on the molecular weights of the two blend polymers, their viscosity differences, the solubility parameter difference between the components, and the interfacial tension between the two components. While studying the electrospinning of polybutadiene (PB,

Mw = 420 kDa) and polycarbonate (PC, Mw = 20 kDa) blend solutions they found that at PB concentrations up to 50% very fine co-continuous phase morphologies were observed on fiber surface i.e. there wasn't sufficient time for phase separation because of the domination of the higher molecular weight PB chains in the mixture. As the concentration of PC increased > 75% the more mobile PC chains moved outward and the higher molecular weight less mobile PB chains stayed in the center forming a core-sheath structure. Looking at the XPS results and change in surface wt% of chitosan at 50% chitosan in blend solution (for 50 wt% HMWchitosan in solution surface chitosan content is between 4-7 wt%) there could be phase separation and formation of core-sheath structure with formation of chitosan core (Mv of HMW chitosan is 1400 kDa) and PEO (Mw = 900 kDa) sheath. For the LMW chitosan (Mw = 100 kDa) PEO blends this effect appears to start at 75 wt% chitosan in solution (for 75 wt% LMW chitosan in solution surface chitosan content is between 12-20 wt%) because chitosan is more viscous then PEO but PEO molecular weight is higher and the competing kinetic and thermodynamic effects could lead to formation of a core sheath morphology on fiber surface.[83] Another indication that there is a phase morphology difference between HMW and LMW chitosan/PEO blends is that for LMW blends the surface nitrogen concentration is always lower for same blend compositions. This suggests that the molecular weight of blend mixtures influences the phase morphology of the fibers. The solubility parameter of chitosan, PEO, acetic acid and water was calculated using the group-contribution method as described by Hoftyzer and Van Krevelen[183]. This method takes into account the contribution of dispersive forces (Fdi), polar forces (Fpi) and hydrogen bonding (Ehi) in determining the solubility parameter (δt) which is given by the following equation.

$$\partial t = \left(\frac{\sum Fdi}{V} + \frac{(\sum Fpi^2)^{1/2}}{V} + \left(\frac{\sum Ehi}{V} \right)^{1/2} \right)^{1/2}$$

The solubility parameter for chitosan, PEO, acetic acid and water are 45.6, 22.86, 21.4 and 47.8 $J^{1/2}/cm^{3/2}$ respectively. The large difference in solubility parameter between PEO and chitosan further suggests the possibility of phase seperation in fibers with higher PEO content.

Table 4.3 shows the atom% data of HMWchitosan: PEO (90:10) blend fibers with increasing fiber diameter before and after metal binding. Figure 4.15 and 4.16 shows the surface

nitrogen content and calculated surface chitosan wt% with increasing fiber diameter. It can be seen that at constant blend ratio with increasing fiber diameter there is no clear trend in surface nitrogen content and surface chitosan concentration. Fibers of varying fiber diameter were obtained by addition of non-ionic surfactant Brij-35 or varying strength of acetic acid solution (explained in detail in Chapter 6, section 6.1). Our collaborators at University of Massachusetts, Amherst have observed that for fibers fabricated using 2mM Brij-35 surfactant the fiber chitosan content was reduced by more than half compared to fibers without addition of Brij-35.[184] This reduction in chitosan wt% in fiber by addition of Brij-35 (fiber diameter = 130 nm) would lead to decrease in surface chitosan or nitrogen content as seen Figure 4.15 and 4.16. After binding experiments, the surface nitrogen content is decreasing due to the electrostatic interaction of nitrogen with chromate; however it was surprising not to see any chromium peak in the XPS scans of samples after binding. Looking at the "C/O" (carbon/oxygen) ratio before and after metal binding it is seen that the C/O ratio increases after binding experiments. The C/O ratio for pure chitosan is 1.6 and pure PEO is 2. This increase in C/O ratio after binding suggests that upon binding the surface of fibers is rich in PEO. During the experiment PEO could be dissolving from the fibers and forming a film-like layer on fiber surface up on drying of the mats prior to XPS measurements. This could be a possibility why the chromium peak is not seen in the samples after metal binding samples. Dambies et.al[181] also have studied the surface chemistry of chitosan beads before and after metal binding. They studied three types of samples; native chitosan beads, grounded beads (mechanically crushing the native chitosan beads to mix the surface and bulk chitosan to get rid of contaminants) and cross-linked beads. They did not see any chromium peak for native chitosan beads after Cr(VI) binding experiments and a small chromium (1~ 2 atom%) $Cr2p_{3/2}$ was observed for the other two samples at 577.3 eV binding energy. However, they did observe that the nitrogen peak was shifting more to the protonated side as seen with our samples (Table 4.4).

Table 4.3 Surface atomic composition of HMWchitosan: PEO (90:10) blends with different fiber diameter before and after metal binding.

	Fiber Diameter (nm)	Atom%			C/N ratio	C/O ratio
		C1s	N1s	O1s		
Before Cr(VI) binding	80	66.19	3.46	30.1	19.13	2.19
	113	65.58	4.44	29.97	14.77	2.18
	130	72.49	1.67	25.84	43.41	2.81
After Cr(VI) binding	80	71.33	2.76	25.42	25.84	2.76
	113	73.72	3.89	21.86	18.95	3.37
	130	86.63	1.51	11.17	57.37	7.75

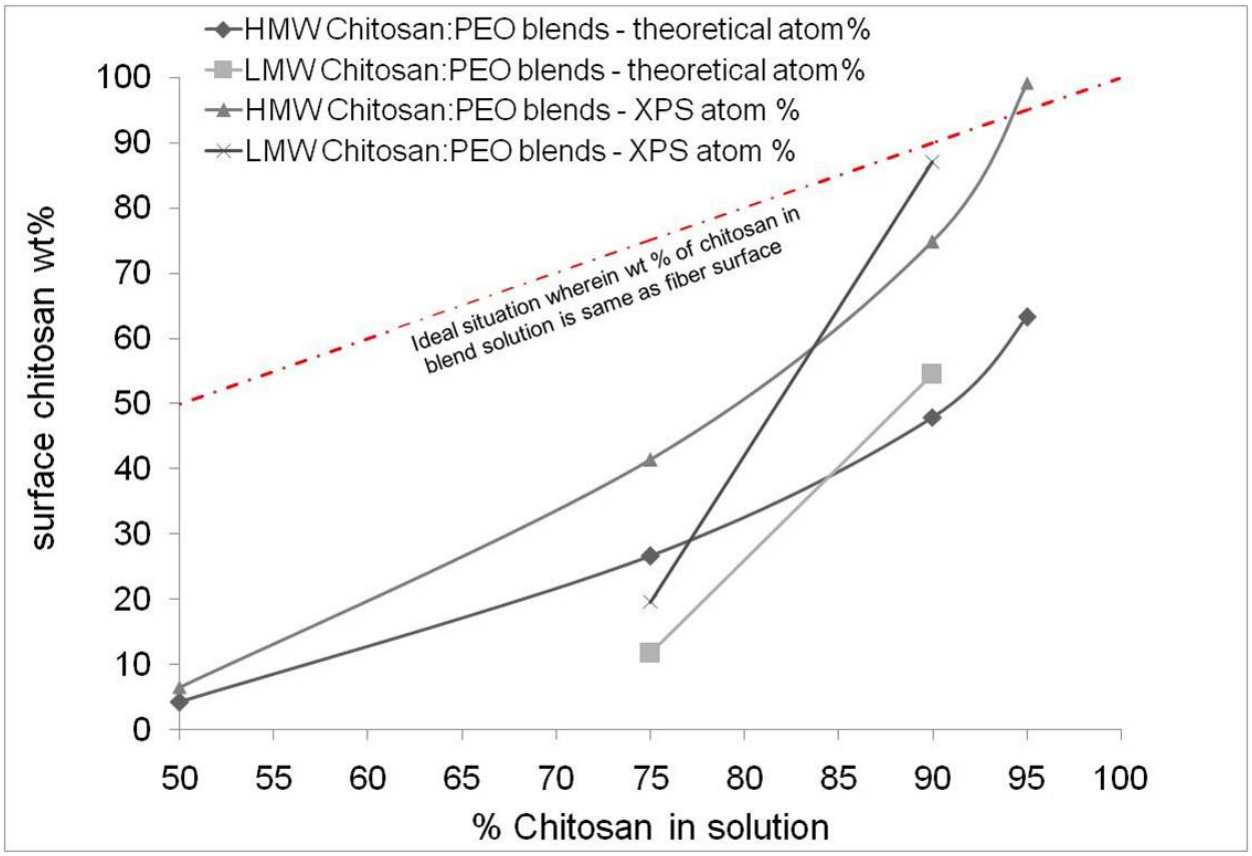

Figure 4.14 Calculated surface chitosan wt% vs. chitosan wt% in solution.

Table 4.4 Surface protonated N1s (atom %) before and after metal binding.

	Fiber diameter (nm)/ %DDA	Protonated N1s (atom%)	
		before metal binding	after metal binding
Different diameter 90% chitosan/PEO blends	80	10.48	86.12
	113	76.99	31.12
	130	13.39	56.76
Different DDA 90% chitosan/PEO blends	80	76.99	31.12
	70	2.92	8.62
	67	10.12	12.59

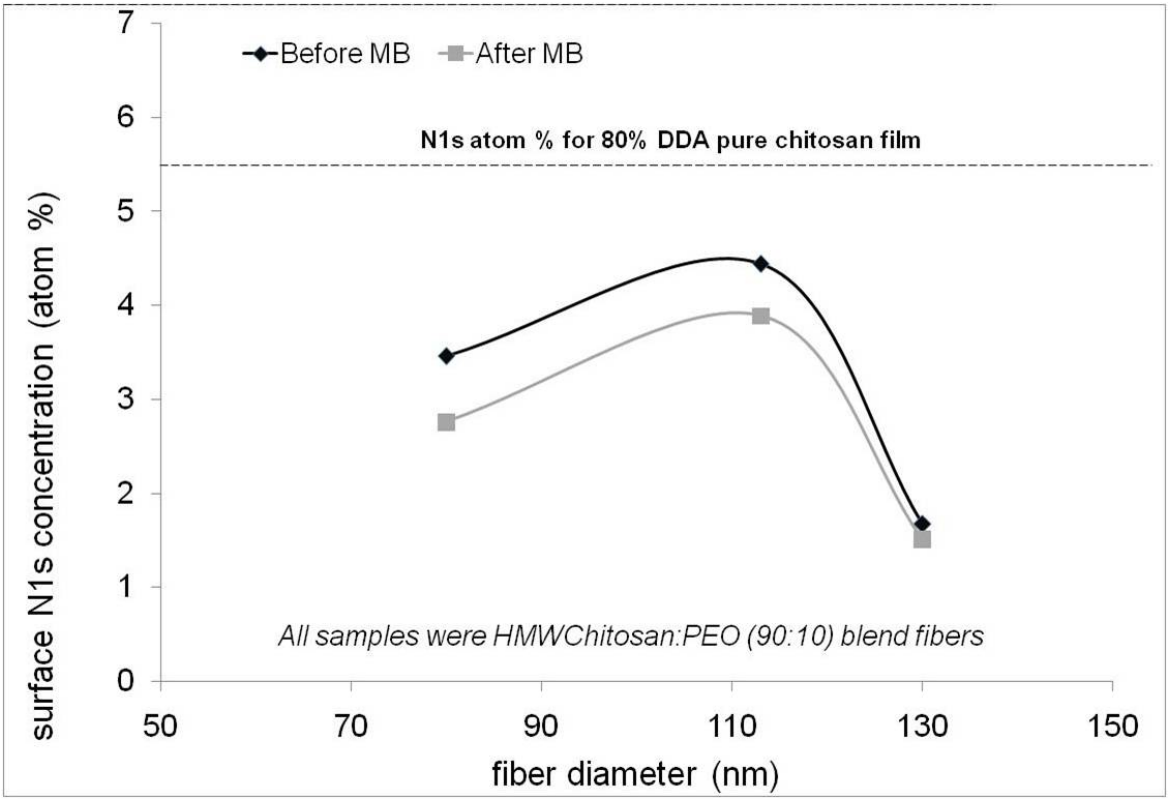

Figure 4.15 Surface nitrogen composition (atom%) vs. fiber diameter for HMWChitosan:PEO (90:10) blend fibers.

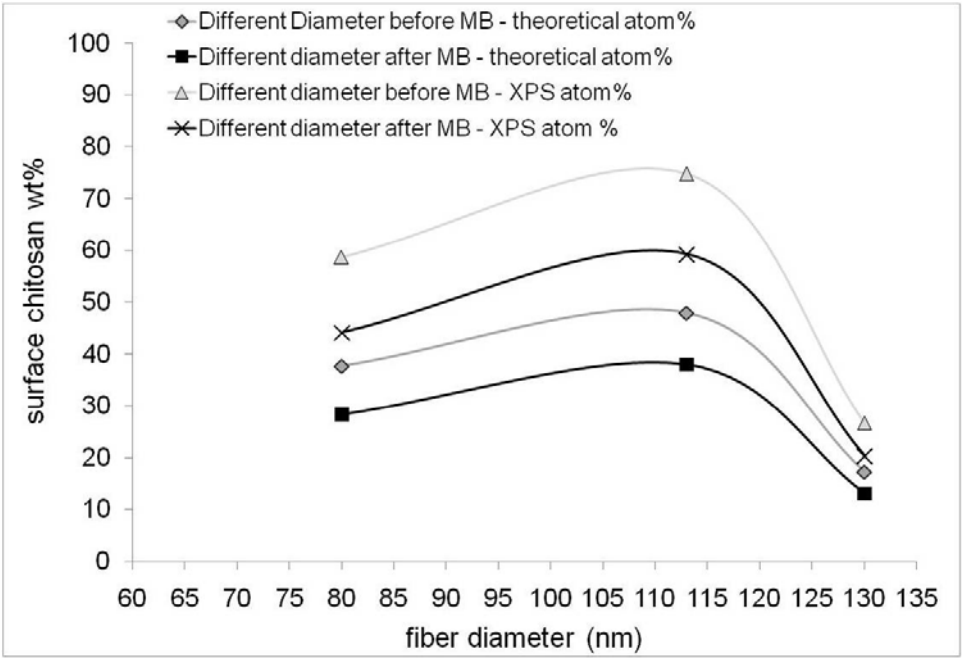

Figure 4.16 Surface chitosan wt% with increasing fiber diameter in HMWchitosan:PEO (90:10) blend solutions before and after metal binding.

Table 4.5 Surface atomic composition of HMWchitosan:PEO (90:10) blends with different %DDA chitosan before and after metal binding.

	%DDA	Atom%			C/N ratio	C/O ratio
		C1s	N1s	O1s		
Before Cr(VI) binding	80	65.58	4.44	29.97	14.77	2.19
	70	64.21	4.03	31.75	15.93	2.02
	67	65.73	3.69	30.33	17.81	2.17
After Cr(VI) binding	80	73.72	3.89	21.86	18.95	3.37
	70	66.62	4.86	27.86	13.71	2.39
	67	66.31	4.78	28.12	13.87	2.36

Table 4.5 shows the atom% data of HMWchitosan: PEO (90:10) blend fibers fabricated using chitosan of varying % DDA before and after metal binding. Before binding it can be seen that with decreasing % DDA the surface nitrogen content decreases as expected theoretically (as %DDA decreases from 80 to 70 to 67, atom% N decreases theoretically from 8.26 to 8.06 to 8 respectively). The surface chitosan % is however not affected by the chitosan DDA, all blends have 90% chitosan in solution and the XPS data also shows that surface chitosan content is also

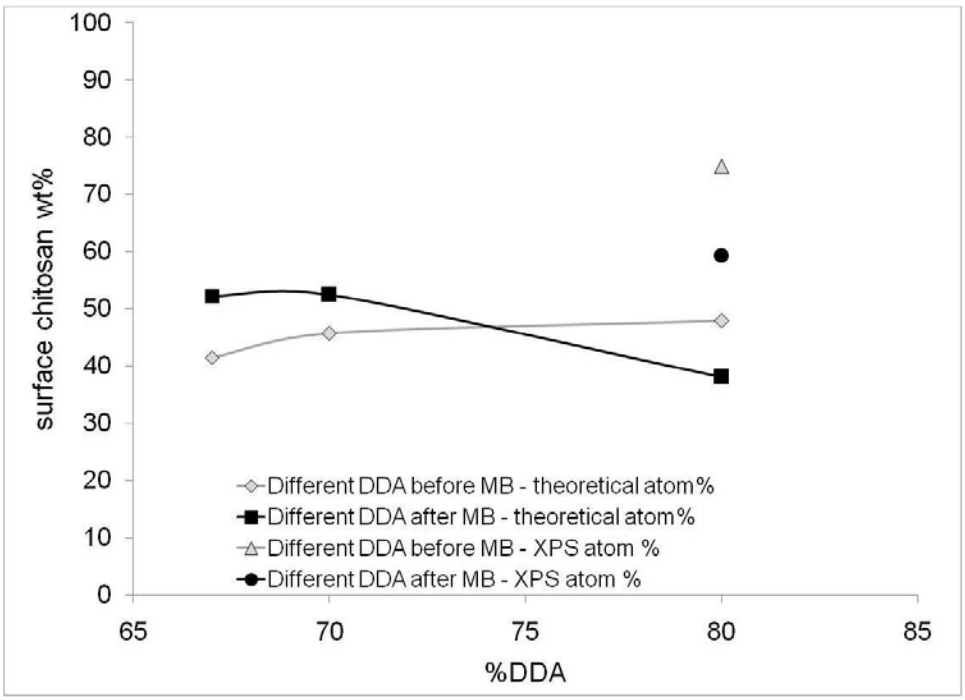

Figure 4.17 Surface chitosan (wt%) with decreasing % DDA chitosan in HMWchitosan:PEO (90:10) blend solutions before and after metal binding.

similar (Figure 4.17)). As seen in case of samples of varying fiber diameter after metal binding the surface nitrogen concentration decreases and the C/O ratio increases (Table 4.4).

4.2.2 XPS – Chitosan/PAAm blends.

The elemental C1s and N1s XPS scans are as shown in Figure 4.18. It can be seen that similar to chitosan/PEO blends in Figure 4.13 with decreasing % chitosan in blend solution the C1s and N1s peak lose their definite shoulder peaks and just broaden like the pure PAAm film peaks. Pure PAAm N1s peak does not show the presence of a prominent protonated peak like the pure chitosan film. Curve fitting of the pure PAAm N1s peak (Figure 4.11) shows presence of 2 atom % protonated nitrogen. It can be seen that as expected with increasing % PAAm in blend solution the surface nitrogen content increases and the C/N ratio decreases (Table 4.6) however an increase in nitrogen atom % will not translate into enhanced surface activity as the amide linkage from PAAm is not easily protonated.[185]

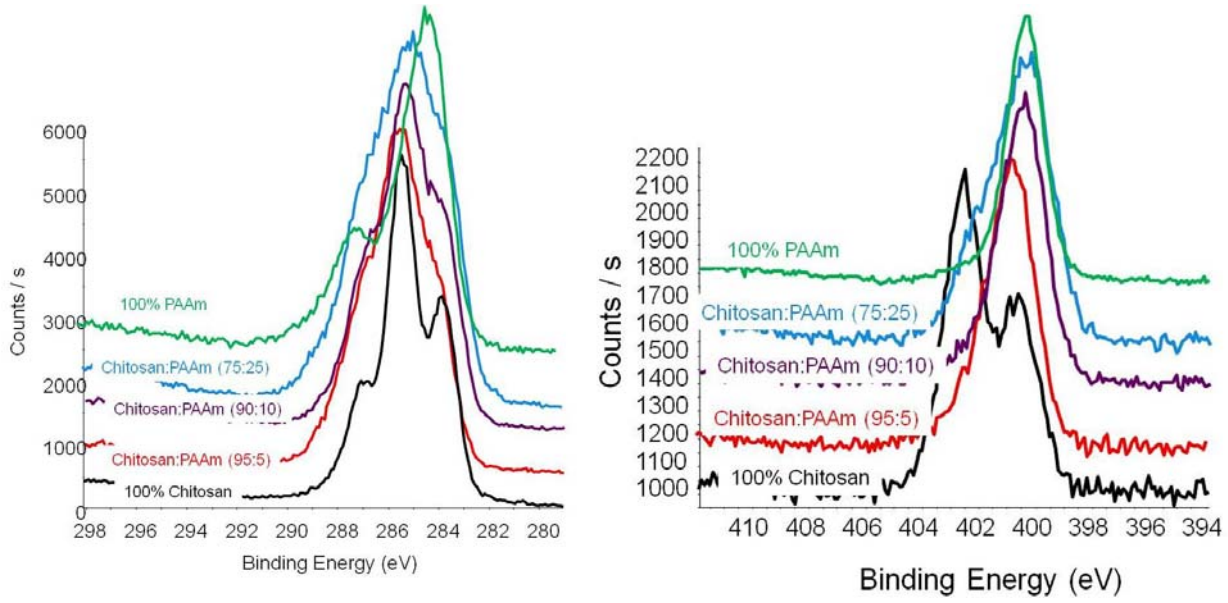

Figure 4.18 C1s (left) and N1s (right) elemental scans of chitosan/PAAm blend fibers with decreasing % chitosan in blend fiber.

Calculation of surface chitosan wt%

As in case of chitosan/PEO blends similar analysis to calculate chitosan weight fraction in chitosan/PAAm blends is done. Let Nn be number of nitrogen atoms and Nc be number of carbon atoms in chitosan/PAAm blend fibers and the C/N ratio which Nc/Nn or "r". From XPS we know "r" and knowing that theoretically for each chitosan repeat unit there 6.4 atoms of carbon and 1 atom of nitrogen, and for each PAAm repeat unit there are 3 atoms of carbon and 1 atom of nitrogen we can obtain surface chitosan concentration in weight basis. Surface chitosan wt% calculated using this hypothesis will be referred to as "calculations based on theoretical # of C".

$$Nc = \frac{Wt\ of\ chitosan}{mol.wt\ of\ chitosan\ rpt\ unit}(\#of\ C\ atoms\ perchitosan\ rpt\ unit) + \frac{Wt\ of\ PAAm}{mol.wt\ of\ PAAm\ rpt\ unit}(\#of\ C\ atoms\ perPAAm\ rpt\ unit)$$

$$Nn = \frac{Wt\ of\ chitosan}{mol.wt\ of\ chitosan\ rpt\ unit}(\#of\ N\ atoms\ perchitosan\ rpt\ unit) + \frac{Wt\ of\ PAAm}{mol.wt\ of\ PAAm\ rpt\ unit}(\#of\ N\ atoms\ perPAAm\ rpt\ unit)$$

$$Nc = \frac{Wt\ of\ chitosan}{169.4}(6.4) + \frac{Wt\ of\ PAAm}{72}(3\ )$$

$$Nn = \frac{Wt\ of\ chitosan}{169.4}(1) + \frac{Wt\ of\ PAAm}{72}(1\ )$$

$$\frac{Nc}{Nn} = \frac{\frac{Wt\ of\ chitosan}{169.4}(6.4) + \frac{(1 - Wt\ of\ chitosan)}{72}(3\ )}{\frac{Wt\ of\ chitosan}{169.4}(1) + \frac{(1 - Wt\ of\ chitosan)}{72}(1\ )}$$

$$Wt\ of\ chitosan = \frac{0.042 - 0.0138\frac{Nc}{Nn}}{0.00388 - 0.0079\frac{Nc}{Nn}}$$

However as seen from XPS results of pure chitosan films the "C/N" ratio for 80% DDA pure chitosan film is 10.91 compared to theoretical 6.4 and therefore the above equations will not be able to accurately predict surface chitosan wt%. To get a better estimate of surface chitosan wt% instead of using theoretical values of # of C and N atoms we use the values obtained from XPS for pure chitosan and PAAm. Hence, # of C atoms per chitosan repeat unit is 6.96 and # of C atoms per PAAm repeat unit is 3.36. Therefore using the data from XPS surface analysis the weight of chitosan is given by the following equations. Surface chitosan wt% calculated using this hypothesis will be referred to as "calculations based on experimental # of C".

$$Nc = \frac{Wt\ of\ chitosan}{169.4}(6.96) + \frac{Wt\ of\ PAAm}{72}(3.36)$$

$$Nn = \frac{Wt\ of\ chitosan}{169.4}(0.64) + \frac{Wt\ of\ PAAm}{72}(0.69)$$

$$\frac{Nc}{Nn} = \frac{\frac{Wt\ of\ chitosan}{169.4}(6.96) + \frac{(1 - Wt\ of\ chitosan)}{72}(3.36\ )}{\frac{Wt\ of\ chitosan}{169.4}(0.64) + \frac{(1 - Wt\ of\ chitosan)}{72}(0.69\ )}$$

$$Wt\ of\ chitosan = \frac{0.0468 - 0.0096\frac{Nc}{Nn}}{0.0056 - 0.0058\frac{Nc}{Nn}}$$

Actually while calculating the surface chitosan wt% using the theoretical "C" and "N" atomic values we see that results show surface chitosan content is always greater than 100% which is practically impossible, hence we need to use the method using values from XPS scans of pure chitosan and PAAm films (Figure 4.19). The surface chitosan concentration is closer to the ideal surface chitosan concentration (*i.e.* if solution chitosan content = surface chitosan content) compared to chitosan/PEO blends. The solubility parameter for chitosan, PAAm, acetic acid and water are 45.6, 30.6, 21.4 and 47.8 $J^{1/2}/cm^{3/2}$ respectively as calculated by the Hoftyzer and Van Krevelen method described earlier. Solubility parameter of PAAm and chitosan are closer in magnitude compared to chitosan/PEO blends suggesting greater chances of mixing in chitosan/PAAm blends.

The surface atomic composition of electrospun fibers of chitosan/PAAm blends is as shown in Table 4.6. The surface chitosan content (Figure 4.19) also decreases with increasing fiber diameter for all blend ratios; similar to what has been observed for chitosan/PEO blends. However the surface chitosan content is in closer agreement with original chitosan concentration in solution then what was observed for chitosan/PEO blends. Figure 4.20 and Figure 4.21 shows a plot of surface nitrogen concentration (atom %) with decreasing % chitosan in blend solutions and increasing fiber diameter respectively. The surface nitrogen content increases with decreasing PAAm content and increasing fiber diameter. However this increase in surface nitrogen content does not necessarily mean increased surface properties because the protonated component N peak decreases with decreasing % chitosan in blend solution (Table 4.7).

Table 4.6 Surface atomic composition of chitosan:PAAm blends with decreasing chitosan content spun at different spinning temperatures to obtain different diameter fibers.

%Chitosan in solution	Spinning solution temperature (°C)	Fiber diameter (nm)	Atom %			C/N ratio
			C1s	N1s	O1s	
100 %	Pure Chitosan film		61.11	5.6	28.18	10.91
95	RT	155.58	74.74	6.27	20.61	11.92
95	40	162.41	62.75	6.04	30.83	10.39
95	70	286.49	61.4	6.43	29.94	9.55
90	RT	50.85	62.44	6.79	30.2	9.20
90	40	63.58	61.18	6.93	30.59	8.83
90	70	306.67	61.48	6.94	31.01	8.86
75	RT	131.61	63.72	7.62	28.1	8.36
75	40	304.69	62.7	7.82	28.69	8.02
75	70	315.00	61.23	8.94	29.31	6.85
0%	Pure PAAm film		67.17	13.73	18.56	4.89

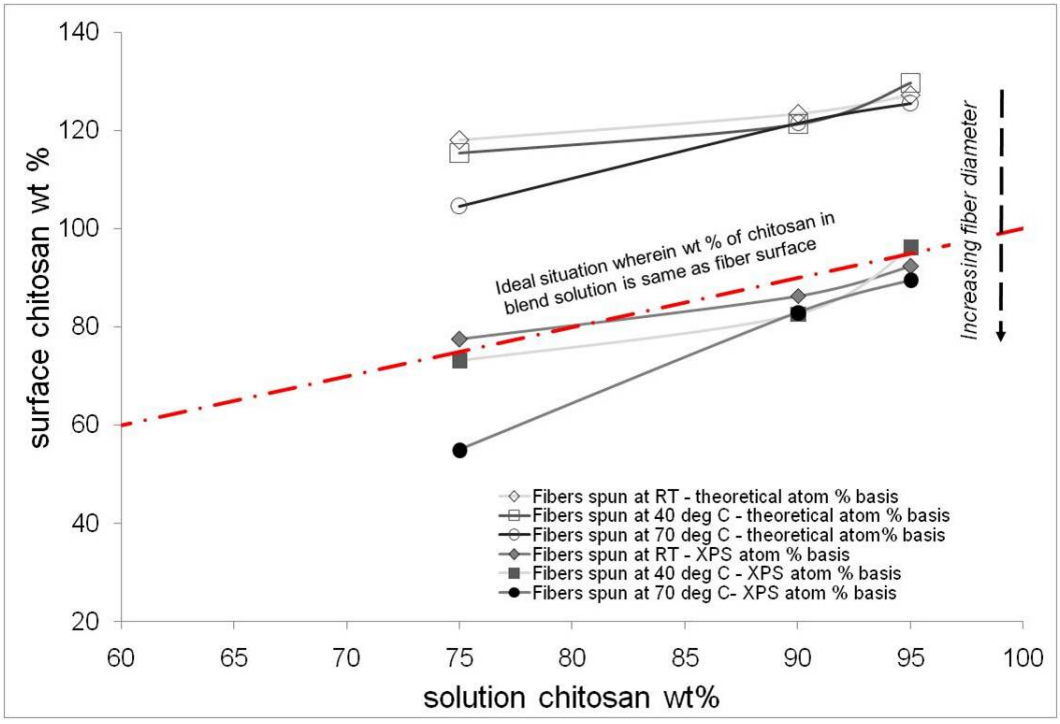

Figure 4.19 Surface chitosan wt % for chitosan:PAAm blend solutions with increasing % chitosan in solution.

Table 4.7 Surface protonated N1s (atom %) content with varying blend ratios and fiber diameter for Chitosan:PAAm blends

%Chitosan in solution	Spinning solution temperature (°C)	Fiber diameter (nm)	Protonated N1s (atom %)
100 %	Pure Chitosan film		58.48
95	RT	155.58	10.76
95	40	162.41	9.18
95	70	286.49	12.77
90	RT	50.85	10.5
90	40	63.58	8.88
90	70	306.67	9
75	RT	131.61	25.89
75	40	304.69	35.85
75	70	315.00	35.34
0%	Pure PAAm film		8.19

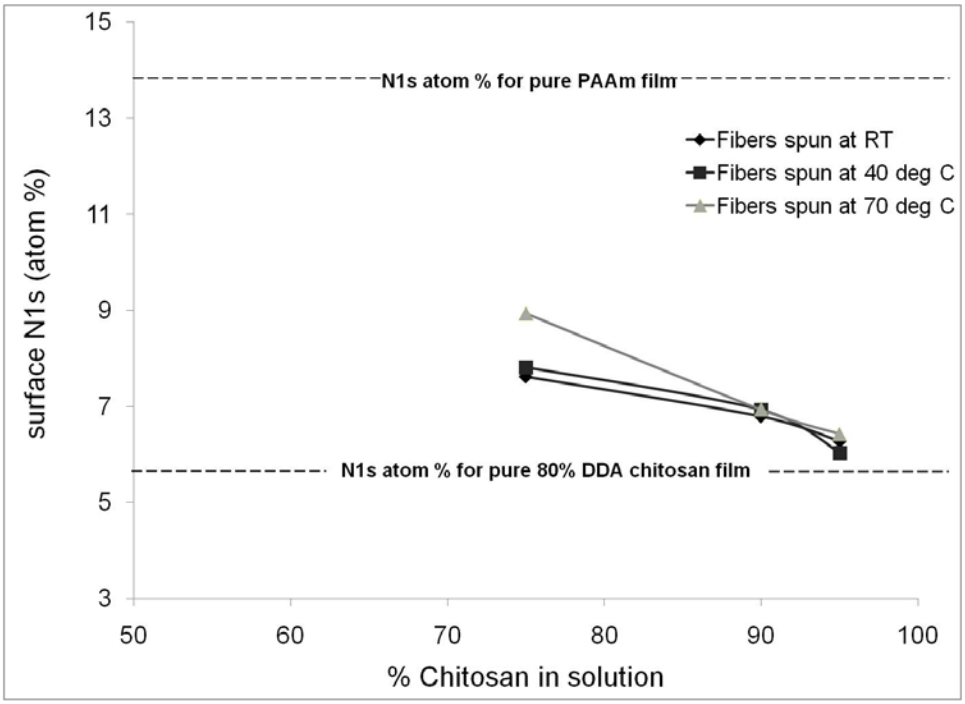

Figure 4.20 Surface nitrogen atom% for chitosan:PAAm blend solutions with increasing % chitosan in solution.

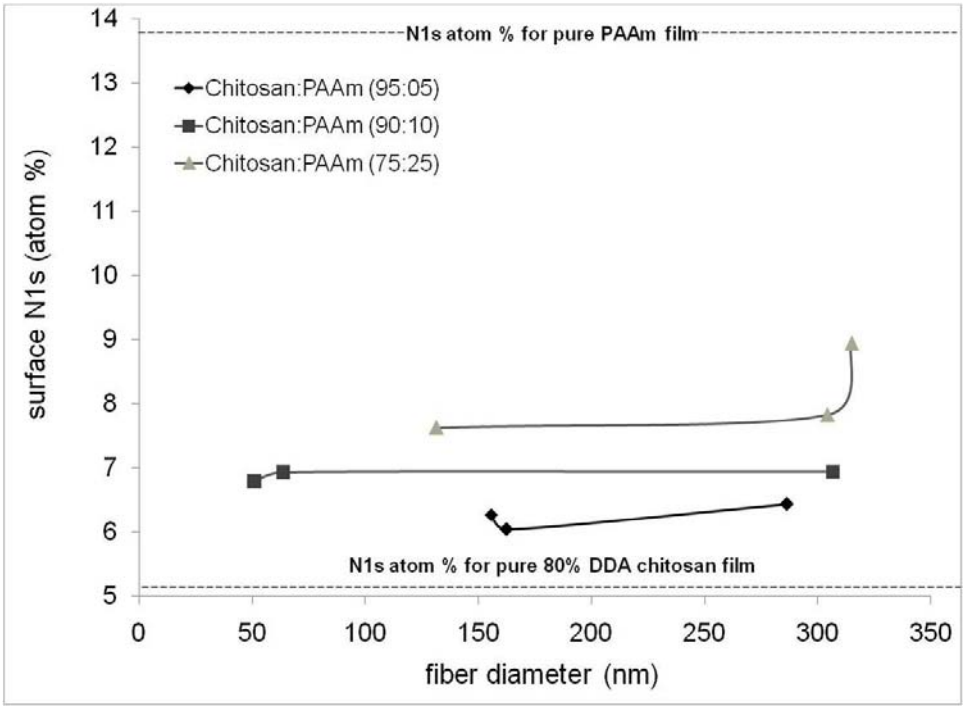

Figure 4.21 Surface nitrogen atom% for chitosan:PAAm blend solutions with increasing fiber diameter.

4.2.3 Summary – XPS chitosan blend fibers.

The surface XPS analysis of chitosan blend fibers with both PEO and PAAm show similar results. From the XPS analysis of blend fiber samples it can be concluded that:

- With increasing % PEO in blend solution surface nitrogen content decreases.
- With increasing % PAAm in blend solution overall surface nitrogen increases, however protonated nitrogen peak decreases.
- With increasing fiber diameter the surface chitosan content decreases.
- Chitosan % DDA does not have any effect on surface chitosan content, but as expected the nitrogen content decreases slightly with decreasing % DDA.
- Surface nitrogen concentration is always lower for LMW chitosan blends compared to HMW chitosan blends.
- After metal binding experiments the surface un-protonated nitrogen content decreases but no chromium peaks are seen.

5. Surface Properties – Results & Discussion

5.1 Metal binding - Chitosan/PEO blends.

The Cr (VI) binding properties of chitosan/PEO blend fibers were studied using the procedure outlined in section 2.3.2. Effect of chitosan content in electrospun chitosan/PEO blend nanofibers, molecular weight of chitosan, and degree of deacetylation of chitosan were studied on the metal binding efficiency of chitosan/PEO blend nanofibers.

5.1.1 Effect of chitosan/PEO blend ratios and molecular weight of chitosan.

Metal binding occurs due to the electrostatic attraction between the dissociated CrO_4^{2-} ion in solution and NH_3^+ ion on the chitosan fiber surface[186]. No significant change in pH of 5 mg/L K_2CrO_4 solutions upon immersion of chitosan/PEO blend fibers was observed. The pH of the prepared K_2CrO_4 solution was 7.3. After immersion of HMW chitosan/PEO (90:10) fibers for 3 hours, the pH decreased to 7.0 (80% DDA), 6.8 (70% DDA), and 6.7 (67% DDA). Hence, it is safe to assume that all metal binding took place at pH ~ 6.5 – 7.0 and as known from literature chitosan is 50% protonated at pH ~ 6.5.[22]

Figure 5.1 shows the amount of chromium bound (mg Cr per g chitosan) for blend fibers with different chitosan: PEO blend ratios. HMW chitosan: PEO (90:10) blends show the highest amount of Cr bound per g chitosan. It can be observed that metal binding is strongly related to the % chitosan in the blend solution, and molecular weight of chitosan. With decreasing % chitosan in blend fiber, the binding capacity of the fibers decreased. As discussed in section 4.2.1 with decreasing chitosan % in blend solution fiber surface nitrogen atom % decreased which would offer fewer binding sites for Cr (VI) binding resulting in lower binding capacities. Figure 5.2 shows the binding capacity of HMWchitosan:PEO blends with varying % chitosan in blend solution plotted as function of surface nitrogen atom %. The binding capacity of blends made using high molecular weight chitosan was seen to be higher. High molecular weight chitosan would offer higher number of available $–NH_3^+$ sites for metal binding for similar surface area fibers (XPS results in Figure 4.12 also show surface nitrogen concentration is higher for HMW blends compared to LMW blends at same blend ratio) due to longer chain lengths and higher degree of protonation[187]. The high binding capacity observed for HMW chitosan fibers could

also be result of thinner fibers providing higher surface (Figure 3.5) compared to LMW chitosan blends. To rule out the possibility of association of PEO with the metal ions a 3 wt% electrospun HMW PEO fiber mat was also tested for metal binding and the results showed no binding.

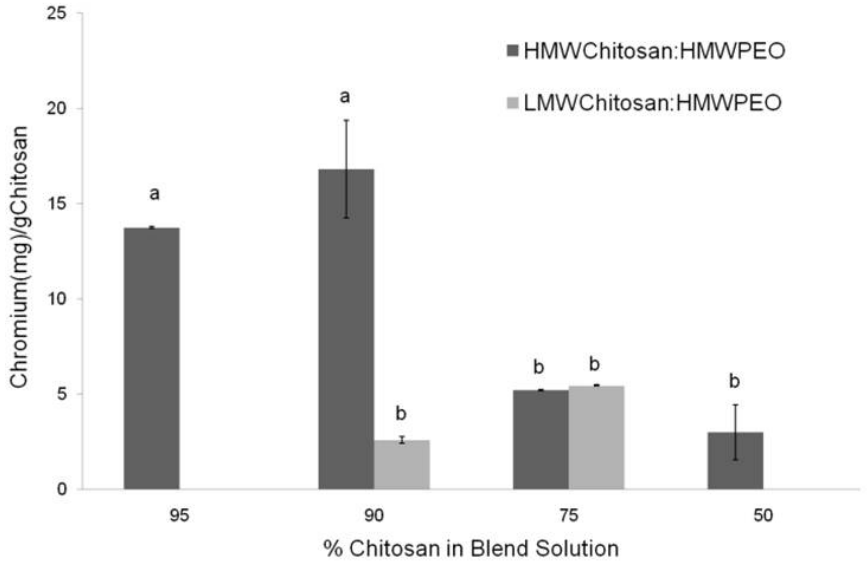

Figure 5.1 Metal binding of chitosan/PEO blend fibers at different % of chitosan in solution (Error bars represent standard deviation (n=3), letters indicate significant difference at $p<0.05$)

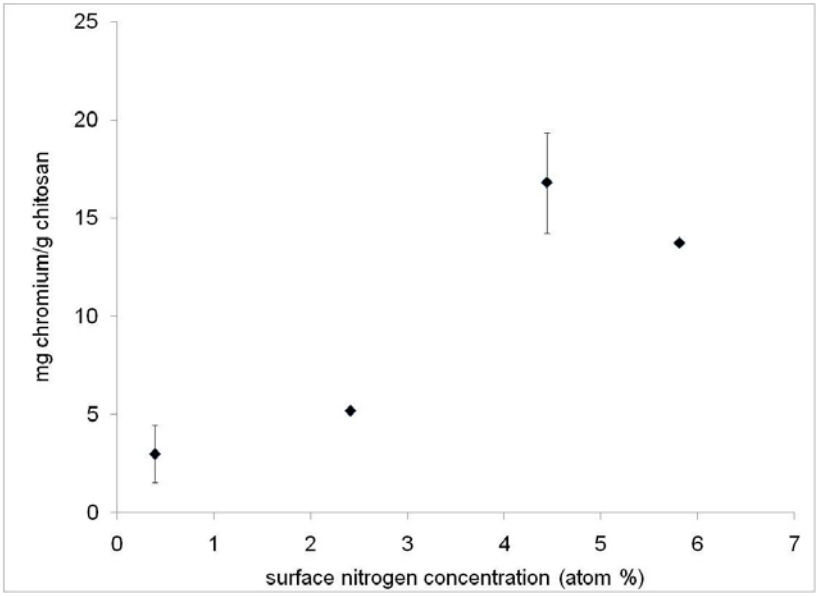

Figure 5.2 Metal binding of HMWchitosan:PEO blend fibers at different % of chitosan in solution as function surface nitrogen atom % (Error bars represent standard deviation (n=3), letters indicate significant difference at $p<0.05$)

5.1.2 Effect of degree of deacetylation of chitosan.

The effect of degree of deacetylation on the metal binding capacity of chitosan/PEO (90:10) blend fibers was also studied. Solutions of 1.33 wt% HMW chitosan of varying degrees of deacetylation (80% DDA, 70% DDA and 67%DDA) with PEO in 75% acetic acid were electrospun to form non-woven mats. From the SEM images in Figure 5.3 it can be seen that at 67% DDA we did not get a uniform fiber mat as obtained at 70 and 80% DDA suggesting the influence of degree of deacetylation on fiber formation; increased DDA from 67% to 70% led to improved fiber formation with increased fiber diameter. Similar results have been obtained with chitosan/poly (vinyl alcohol) blends in which using chitosan of increasing degree of deacetylation lead to more uniform beadless fiber mat formation[112]. The metal binding capacity as shown in Figure 5.2 was highest at 80% DDA as expected because of the increase in number of available $–NH_3^+$ sites for metal binding (as shown in Table 4.5) and there was no significant statistical difference between the 67% (7.35 mg chromium/g chitosan) and 70% DDA (4.44 mg chromium/ g chitosan) chitosan/PEO blend fibers. The slight increase at 67% DDA (45.5 nm) could be due to thinner fibers formed compared to 70% DDA (62.4 nm) resulting in increased surface area. The metal binding capacity in chitosan blend fibers is significantly higher than that observed for similar blend ratio chitosan/PEO blend films[188]. A 93 μm thick LMW Chitosan/PEO (90:10) blend film showed binding capacity of 0.44 mg chromium/g chitosan. Electrospun fibers exhibit greater binding capacity due to the high surface area to mass offered by the fibers compared to films.

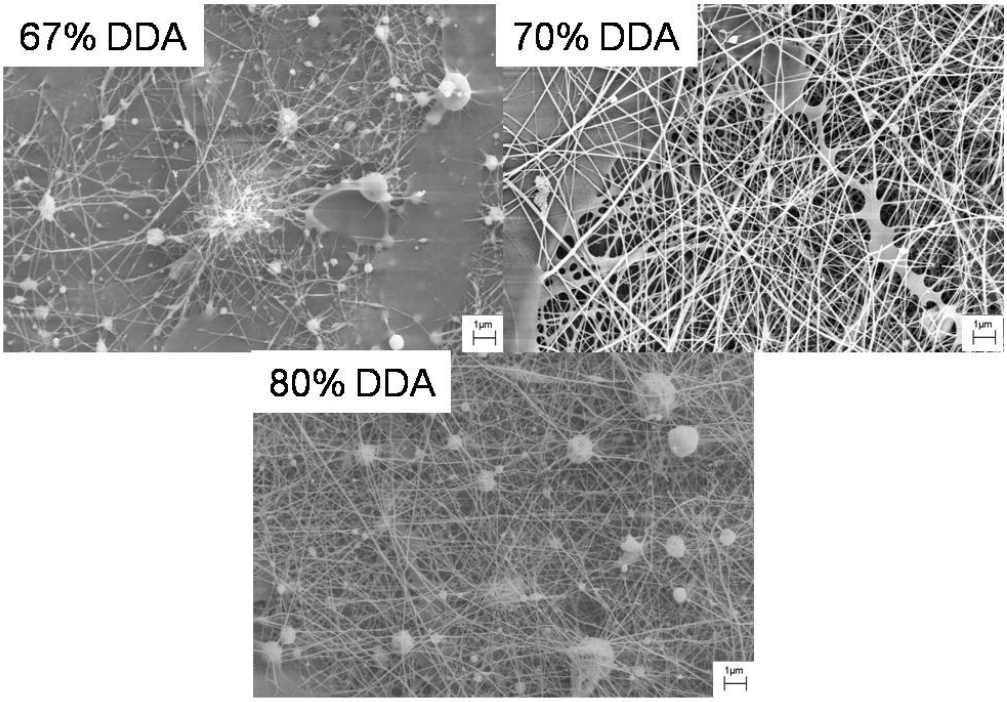

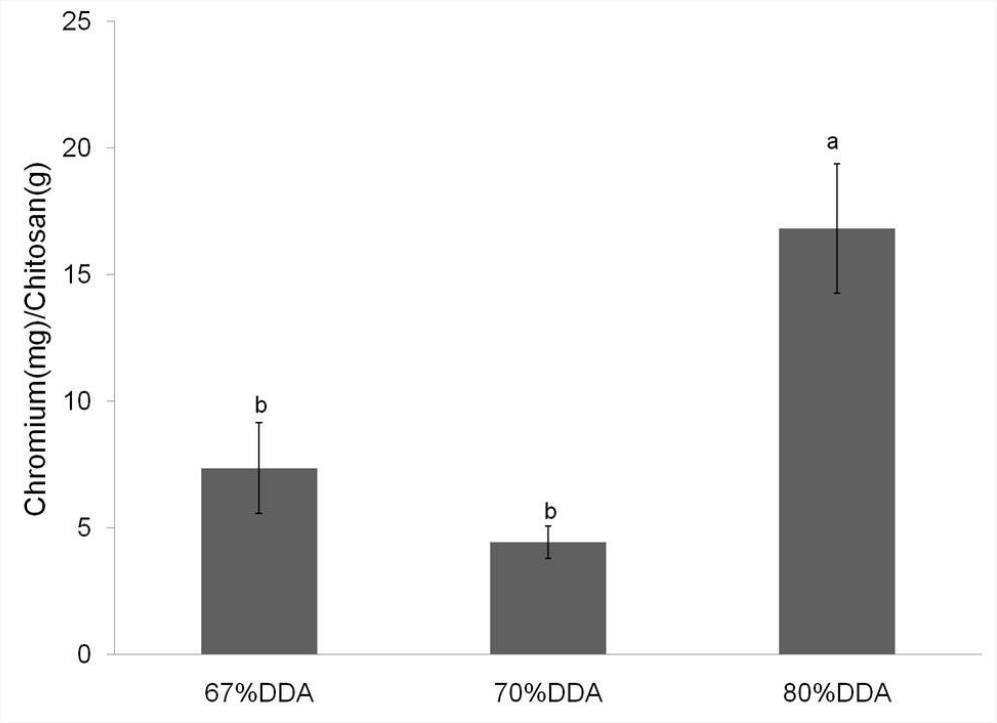

Figure 5.3 SEM images and metal binding of HMW chitosan: HMW PEO (90:10) blend fibers at different DDA (Error bars represent standard deviation (n=3), letters indicate significant difference at $p<0.05$).

5.1.3 Comparison of experimental results with model developed in Chapter 4.

Figure 5.4 shows the comparison of mg chromium/g chitosan values of the experimentally observed data, and that calculated using the model developed in section 4.1. All the data are being compared at similar fiber diameters. It can be seen that the experimental data is mostly higher than the calculated values from the model. This is understandable because in reality the degree of protonation of chitosan in solution can be higher than the assumed 50%. In the model data it seems that 80% DDA chitosan has lower binding capacity than 67 or 70% DDA chitosan, this is because 80% DDA chitosan fibers have diameter of 117 nm compared to 45.5 and 62.4 nm for 67 and 70% DDA respectively. For this range of fiber diameters the effect of fiber size is more pronounced then the effect of % DDA. Similar observations can be made for the effect of % chitosan in blend fiber. Fiber diameter of fibers made using 90% and 75% chitosan in blend solution is statistically same (Figure 3.5). The theoretical binding capacity also looks to be similar (3.76 and 3.13 mg chromium/ g chitosan for 90% and 75% chitosan in blend fiber respectively) compared to very low theoretical binding capacity shown by 315 nm thick 50 % chitosan blend fibers. Chromium ions can be bound by forming either ionic or coordination bonds with hydroxyl or un-protonated amine sites (as has been suggested by Guibal[16]) in solution contributing to the increased binding capacity observed experimentally compared to the model results. As these experiments are conducted in aqueous media another possibility for high binding results observed experimentally is that since chitosan is partially soluble in water and PEO is completely soluble during the testing the fiber surface could be disintegrating. Upon interaction with water, the surface chitosan chains may be swelling leading to diffusion of chromium to the bulk of the fiber causing increase in binding capacity due to the additional availability of binding sites. This effect will be further discussed in Chapter 6 wherein we have studied the dynamic filtration of these espun chitosan coated filtration membranes.

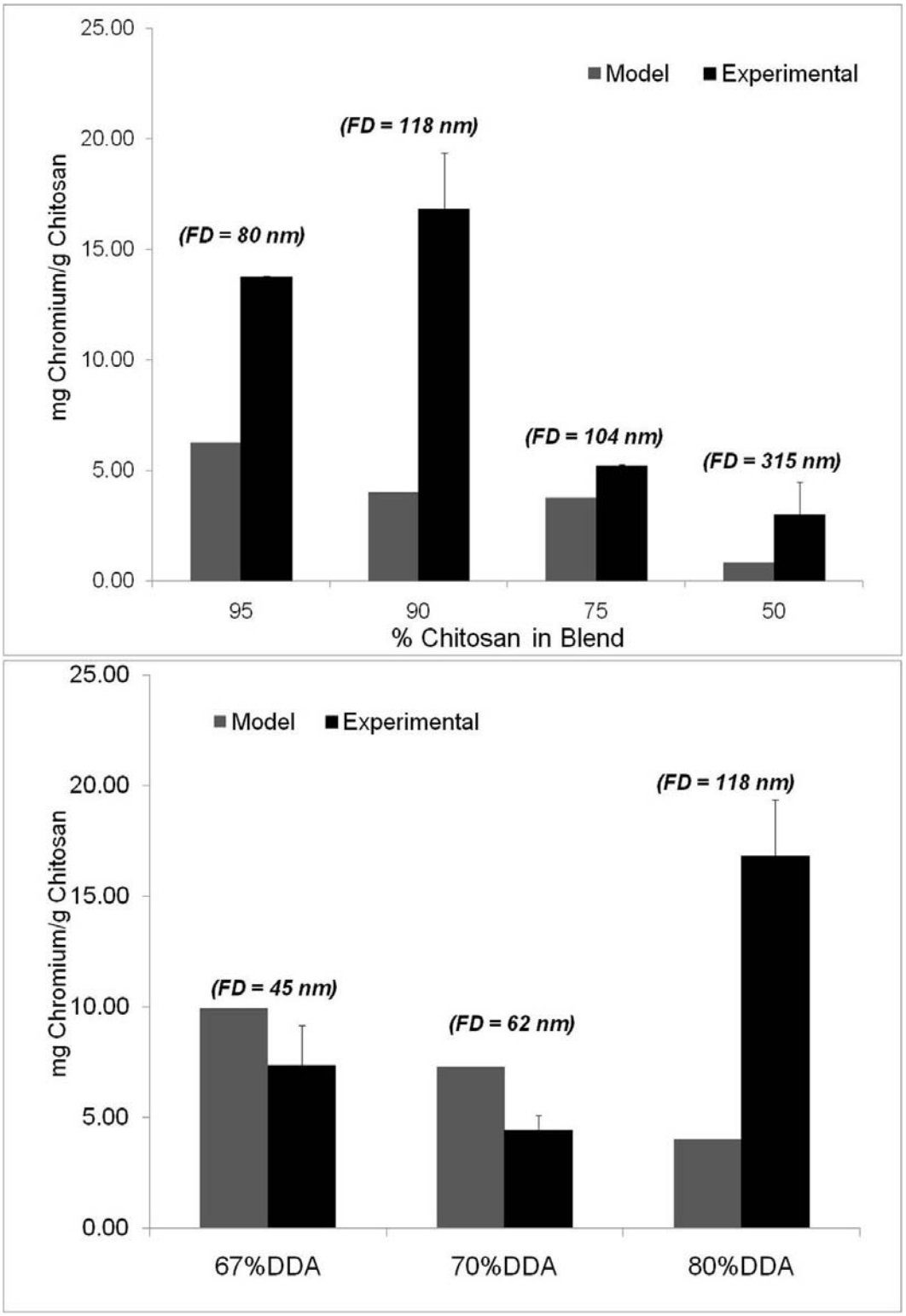

Figure 5.4 Comparison of experimental and calculated values for Cr (VI) binding capacity as function of % chitosan in blend (top), and % DDA (bottom). (Error bars represent standard deviation (n=3), letters indicate significant difference at $p<0.05$).

5.2 Metal binding - Chitosan/PAAm blends.

As the effect of % DDA in chitosan had been studied in Cr (VI) binding studies of chitosan/PEO blends. For chitosan/PAAm blends only the effect of % chitosan in blend fiber, molecular weight of chitosan and fiber diameter of chitosan/PAAm blend fibers (formed by spinning solutions at varying temperatures, section 3.3.2) was studied.

Figure 5.5 shows the Cr (VI) binding capacity vs. % chitosan in blend of chitosan/PAAm blend nanofibers. The results once again show that the blends containing higher molecular weight chitosan and higher % chitosan in blend fiber show greater binding capacity. Figure 5.6 shows the Cr (VI) binding capacity vs. fiber diameter for 1.4 wt% HMW Chitosan:PAAm (90:10) blend fibers formed by spinning the solution at varying temperatures. Also plotted on the secondary axis is the surface nitrogen atom % vs the fiber diameter. It can be seen that with increasing fiber diameter the surface nitrogen content does not change, hence the binding capacity remain unaffected by change in diameter. These results contradict the predicted values from the model and belief that with increasing fiber diameter or decreased surface area to mass ratio binding capacity should be decreased, but in the model also major change in binding capacity with fiber diameter occurs at diameters above 300 nm.

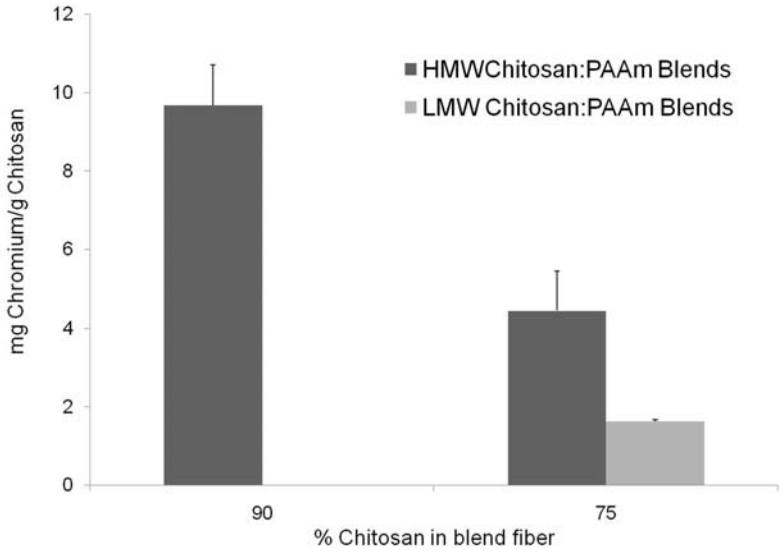

Figure 5.5 Metal binding of chitosan/PAAm blend fibers at varying % chitosan in blend fiber (Error bars represent standard deviation (Error bars represent standard deviation (n=3), letters indicate significant difference at $p<0.05$, n=3)

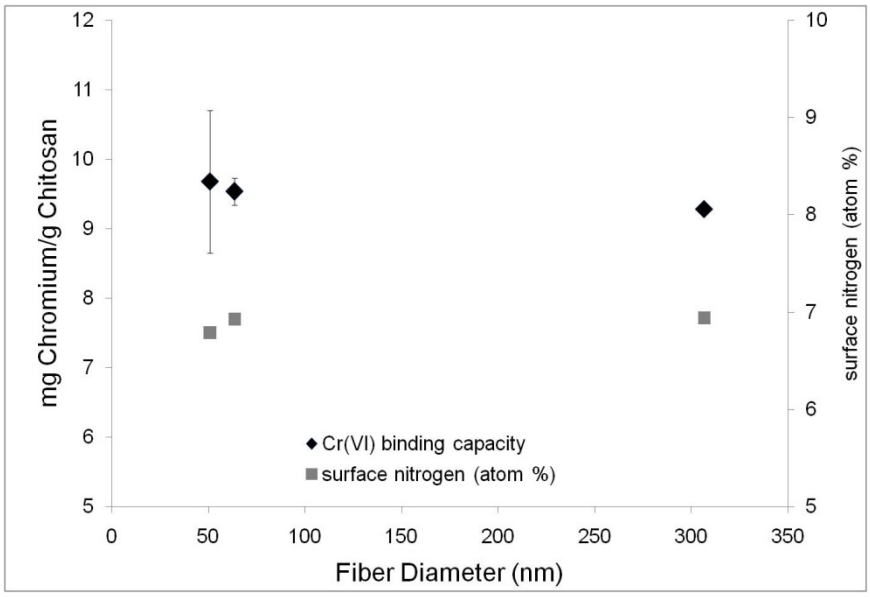

Figure 5.6 Cr (VI) binding capacity (primary axis), surface nitrogen atom % (secondary axis) vs. fiber diameter for 1.4 wt% HMW Chitosan:PAAm (90:10) blend fibers formed by spinning the solution at varying temperatures. (Error bars represent standard deviation (n=3), letters indicate significant difference at $p<0.05$, n=3)

5.3 Anti-microbial properties of Chitosan/PEO blends.

The anti-microbial properties of chitosan/PEO blend fibers were measured using the procedure outlined in section 2.3.3. Chitosan fibers exhibit anti-microbial properties due to the positively charged NH_3^+ on the surface which can bind to the negatively charged components of the bacterial cell wall and inhibit the growth of the cell and eventually kill the micro organism. Effect of chitosan content in electrospun chitosan/PEO blend nanofibers, molecular weight of chitosan, and degree of deacetylation of chitosan were studied on anti-microbial performance of chitosan/PEO blend nanofibers.

In anti-microbial studies usually the reduction in microbial activity is reported on log basis however since all our analysis so far has been based on weight of chitosan we have also plotted data based on reduction in bacteria divided by weight of film. Figure 5.7 shows a plot of effect of % chitosan in blend fiber and molecular weight of chitosan in blend fiber on the anti-microbial effectiveness of chitosan/PEO blend fibers. As the weight of all the fiber mats studied was not same, the weight of the fiber mats is being plotted on the secondary y-axis to better correlate the anti-microbial properties with fiber structure and composition. We see a 2.5-3.0 log

reduction in cfu (colony forming unit) indicating a bacteriostatic effect, this value is similar to ones obtained for 35 μm thick films of chitosan:PEO blends with similar blend ratios, but the mass of chitosan in films was up to 10 times higher than that in the fibers.[188] There is no statistical difference in log reduction with increasing PEO content. To better understand the anti-microbial data # of cfu (colony forming units) reduced per g of chitosan was calculated and plotted as shown in Figure 5.7. When the anti-microbial test data is normalized to weight (Figure 5.8) then we can observe a trend that with increasing % PEO in blend fiber and decreasing molecular weight of chitosan leads to reduction in anti-microbial properties. The effect of molecular weight on anti-bacterial activity of chitosan is not fully understood, some groups have suggested there is a threshold molecular weight ~ 220 kDa until which the anti-microbial activity increases with increasing chitosan molecular weight. However upon exceeding this threshold molecular weight the anti-microbial activity decreases because they believe the molecules pack more densely leading to increased inter and intra-molecular hydrogen bonding utilizing some of the available protonated amine sites.[30] Figure 5.8 shows a plot of effect of increasing chitosan % DDA for 1.33 wt% HMW chitosan: PEO (90:10) blend fibers. Figure 5.9 shows the same data normalized to the weight of the fibers *i.e.* # cfu reduced per gram of chitosan is plotted against DDA. Although one would expect an increase in anti-microbial activity with increasing % DDA because of the increase of # of available protonated amine sites, results from Figures 5.9 and 5.10 show the contrary. The slight decrease in anti-microbial activity with increasing % DDA could be because fibers formed at 80% DDA have larger fiber diameter (118 nm) compared to the fibers formed using 70 and 67% DDA (62 and 45 nm respectively). This increase in fiber diameter would lead to greater reduction in # available of protonated $–NH_3^+$ amine sites then would be increased by increasing % DDA. The # of available protonated $–NH_3^+$ sites at respective fiber diameters and % DDA for the 80% DDA and 70% DDA chitosan as calculated by our model (Appendix 3) are 2.15E+19 and 3.52E+19 which means the thinner 70% DDA chitosan fibers have higher number of protonated amine sites which could result in better anti-microbial activity.

During all the anti-microbial tests a positive control of bacteria with no fiber sample, and negative control of fibers with no bacteria was also tested for 6 hrs to make sure that bacteria did not grow on its own. Pure PEO fibers were also tested for their anti-microbial efficiency and were found to have ~ 0 log reduction.

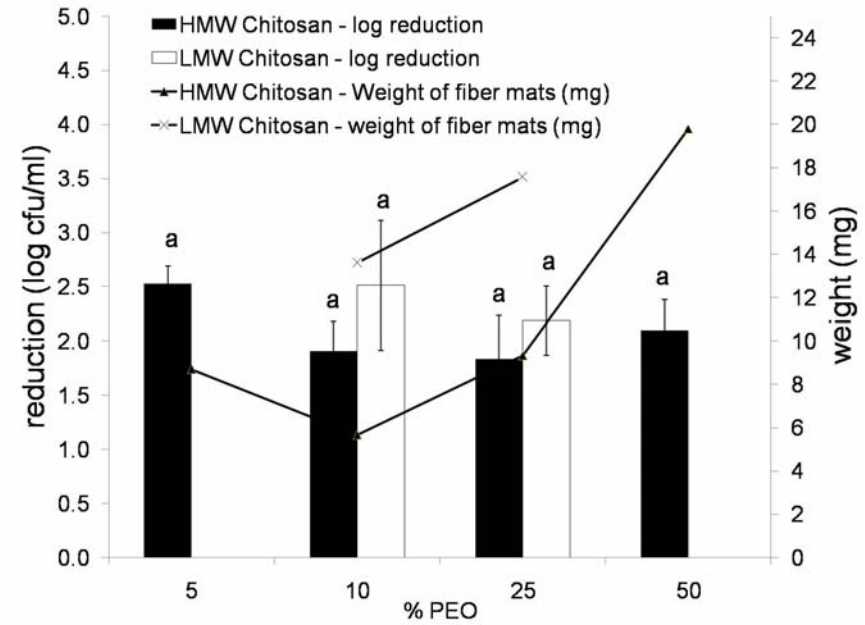

Figure 5.7 Effect of % chitosan in blend fiber and molecular weight of chitosan in blend fiber on the anti-microbial effectiveness of chitosan/PEO blend fibers. (Error bars represent standard deviation (n=3), letters indicate significant difference at $p<0.05$, n=3)

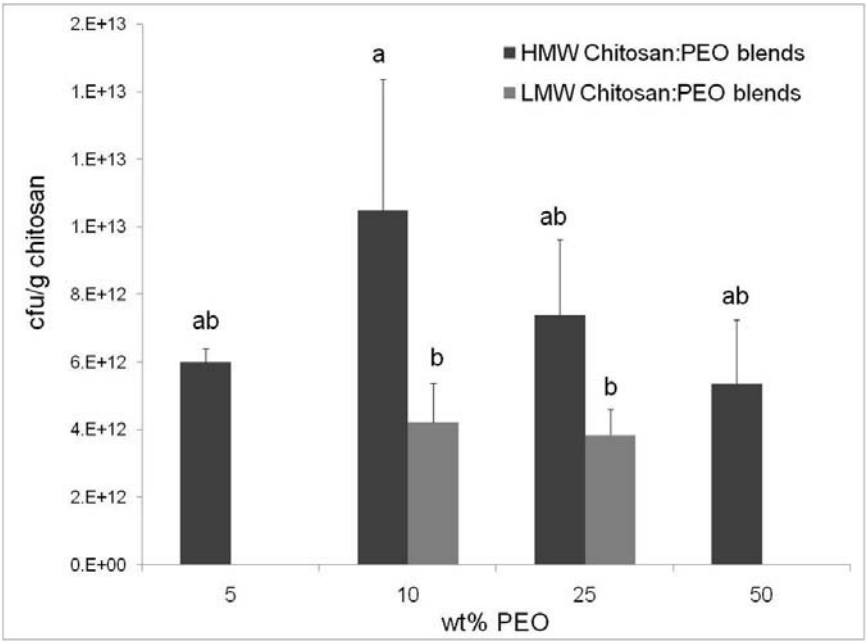

Figure 5.8 Effect of % chitosan in blend fiber and molecular weight of chitosan in blend fiber on the anti-microbial effectiveness of chitosan/PEO blend fibers. (Error bars represent standard deviation (n=3), letters indicate significant difference at $p<0.05$, n=3)

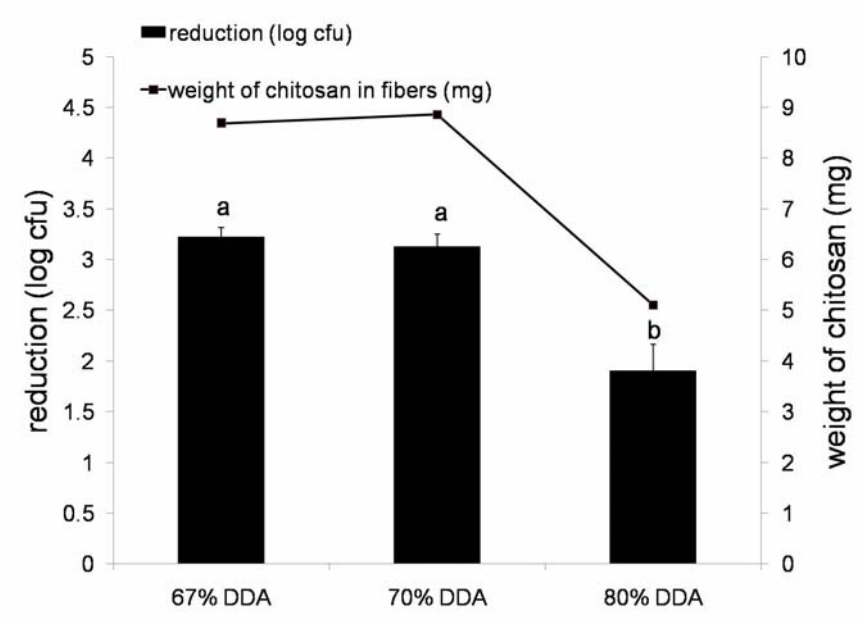

Figure 5.9 Anti-microbial activity of HMW Chitosan:PEO (90:10) blend fibers as function of chitosan % DDA. (Error bars represent standard deviation (n=3), letters indicate significant difference at $p<0.05$, n=3)

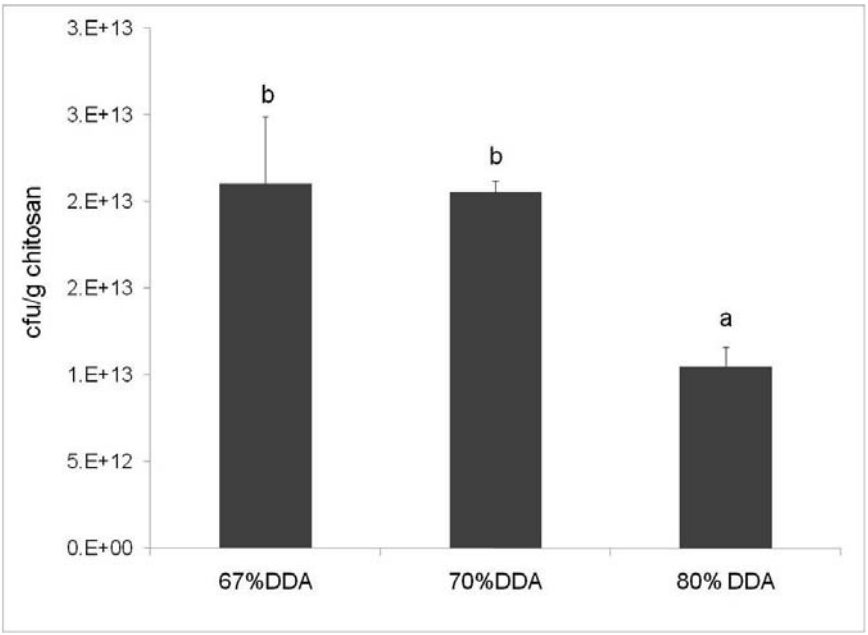

Figure 5.10 Reduction in # of cfu/g of chitosan for HMW Chitosan:PEO (90:10) blend fibers made with increasing chitosan % DDA. (Error bars represent standard deviation (n=3), letters indicate significant difference at $p<0.05$, n=3)

5.4 Anti-microbial properties of Chitosan/PAAm blends.

The effect of % chitosan in blend and molecular weight of chitosan used for fabricating the fibers on the anti-microbial effectiveness of chitosan/PAAm blend fibers was studied. All samples used were of nearly same weight to make a more direct comparison of results. Table 5.1 summarizes the anti-microbial efficiencies of chitosan/PAAm fibers. From the data it can be observed that for all samples there was ~ 3 log reduction in bacteria after 6 hrs. The # of cfu reduced per g of chitosan has also been tabulated in Table 5.1. It can be seen that at same blend ratio with increasing fiber diameter and decreasing chitosan molecular weight there was decrease in anti-microbial efficiency. The physical structure of the fiber mats also after 6 hrs of testing had disintegrated compared to the chitosan/PEO fibers as PAAm is highly hydrophilic which could have affected the test and the results.

Table 5.1 Anti-microbial properties of Chitosan/PAAm blend nanofibers

Sample	log reduction (cfu/ml)		Fiber Diameter (nm)	cfu / (g chitosan)
	Average	Std.Dev		
1.4 wt% HMW Chitosan:PAAm (90:10) espun @ 70°C	3.34	0.12	305	2.14E+13
1.4 wt% HMW Chitosan:PAAm (75:25) espun @ 25°C	3.11	0.35	132	2.61E+13
1.4 wt% HMW Chitosan:PAAm (75:25) espun @ 70°C	3.17	0.19	328	2.47E+13
2.85wt%LMW Chitosan:PAAm (75:25) espun @ 70°C	3.15	0.04	421	1.96E+13

5.5 Summary – Surface properties of chitosan blend fibers.

These results validate the theory that protonated amine sites are the main reason for the anti-microbial and metal binding properties of chitosan blend fibers. Increased metal binding and anti-microbial properties are seen for both chitosan/PEO and chitosan/PAAm blend fibers with:

- Increased % chitosan in blend fiber.
- Fibers fabricated using higher molecular weight chitosan.
- Reduced fiber diameter or increased surface area to mass ratio.
- Chitosan with increased % DDA.

Therefore, in the second part of this research wherein these electrospun mats would be tested for their filtration properties by spinning onto a spunbonded PP substrate, mats of chitosan/PEO and chitosan/PAAm blends were fabricated with 90% chitosan in blend solution and using only high molecular weight chitosan.

6. Filter Performance – Results & Discussion

The goal of this research is to develop chitosan based nanofibrous filtration media which possess enhanced filtration efficiencies owing to the positive charge on filter fiber surface and size effect of nanofibers. As seen in Chapter 5, nanofibers with higher chitosan % in blend solution (90%), higher molecular weight (HMW Chitosan) and higher degree of deacetylation (80% DDA) exhibited the highest metal binding and anti-microbial efficiencies for both chitosan/PEO and chitosan/PAAm blends.

6.1 Fabrication of chitosan blends nanofibrous filter media.

A nanofibrous filter media comprising of a top layer of chitosan blend nanofibers electrospun on a spunbonded non-woven polypropylene (PP) fiber substrate was fabricated by method as described in section 2.1.3. Spunbonded PP was used a substrate to provide mechanical and structural support to the thin layered electrospun nanofibers. Initially melt-blown nonwoven PP mats were chosen as substrate material as melt-blown mats have thinner fibers and lower pore size compared to spunbonded nonwovens (Fiber diameter and pore size of melt blown PP = 3.2 μm (±1.17 μm), 13.83 μm respectively, fiber diameter and pore size of spun bonded PP = 19.6 μm (±1.33 μm), 47.46 μm respectively). However, as seen in Figure 6.1 it was not possible to electrospin a continuous layer of chitosan fibers on melt-blown PP webs, possibly due to the dense nature of the PP mat acting as an insulator and repelling the charged electrospun fibers away to the surrounding metallic aluminum plate on which it was laid. The melt-blown PP fibers were unsuccessfully coated with gold, coated with chitosan and/or acetic acid to change the surface charge and get a uniform layer of electrospun fibers (Figure 6.1).

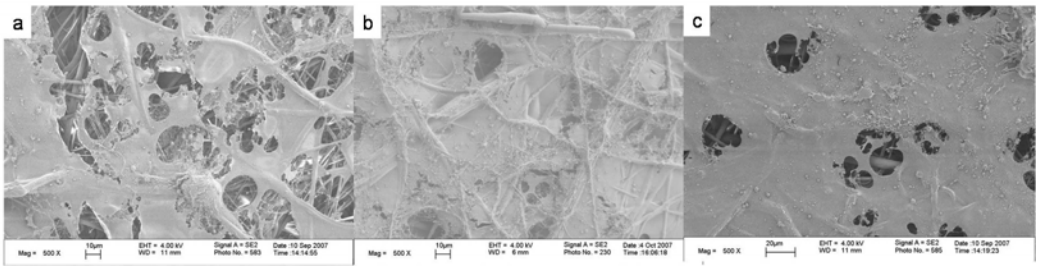

Figure 6.1 SEM images of 1.33 wt% HMW chitosan:PEO (90:10) fibers spun on (a) MB PP substrate, (b) 1% acetic acid coated MB PP substrate, (c) gold sputter coated MB PP substrate.

Electrospinning of chitosan blend solutions on spunbonded PP substrates led to successful fabrication of chitosan based nanofibrous filter media. Filter media of both HMW chitosan/PEO and HMW chitosan/PAAm blends were fabricated with 90% chitosan in blend solution, varying espun layer web density or gsm (which can be achieved by spinning for different time intervals), varying fiber diameter and different DDA chitosan (only for chitosan:PEO blends).

To obtain varying fiber diameter HMW chitosan:PEO blends the strength of the acid solution was varied and a non-ionic surfactant Brij-35 (polyoxyethyleneglycol dodecyl ether) was used. Our collaborators at University of Massachusetts, Amherst, Kriegel et.al[184] have shown that increasing strength of acid reduces solution surface tension with an increase in solution viscosity and addition of 2mM brij-35 leads to increase in solution viscosity with slight increase in solution conductivity and surface tension. Thicker fibers are formed by spinning 1.33 wt% HMW chitosan:PEO (90:10) blends with increasing strength of acetic acid from 75% to 90% and addition of 2mM brij-35 as shown in Figure 6.2 and 6.3. To obtain HMW chitosan:PAAm (90:10) fibers (Figure 6.4) of varying fiber diameter solutions were made and electrospun as described in section 3.3.2 (*i.e.* by spinning at different solution temperatures).

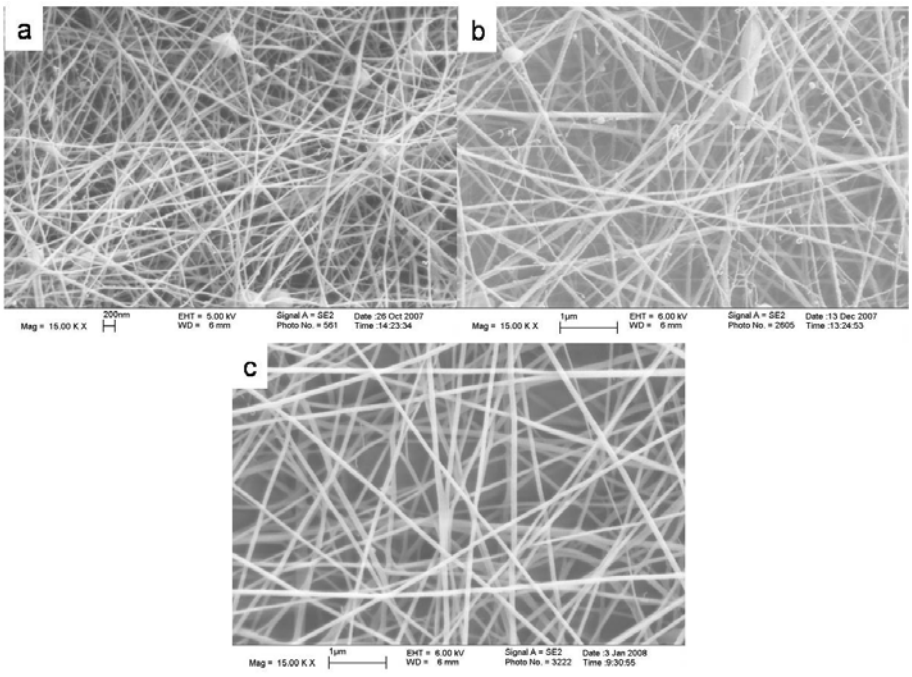

Figure 6.2 SEM images of 1.33 wt% HMW chitosan:PEO (90:10) fibers spun on spunbonded PP (a) using 75% acetic acid, (b) using 90% acetic acid, (c) using 75% acetic acid + 2mM brij-35.

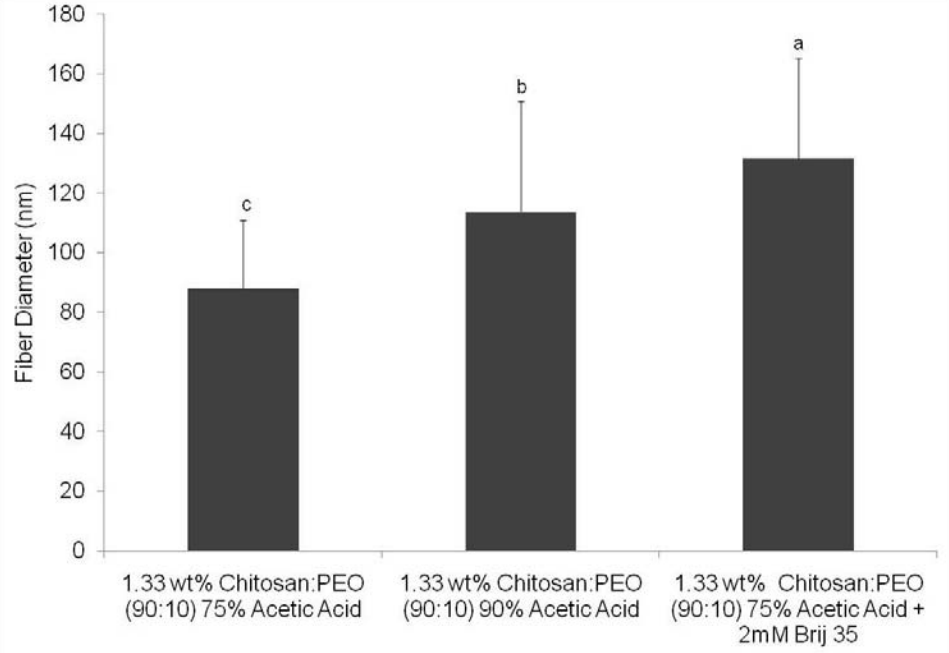

Figure 6.3 Increase in fiber diameter with strength of acid in solvent and addition of surfactant (Error bars represent standard deviation (n=60), letters indicate significant difference at $p<0.05$)

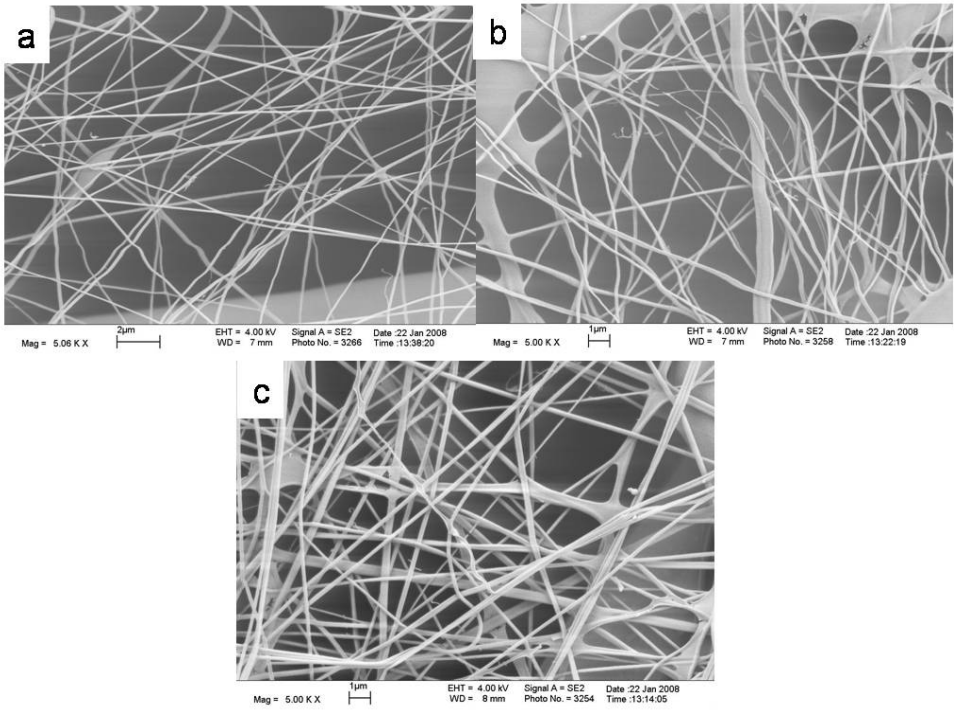

Figure 6.4 SEM images of 1.4 wt% HMW chitosan:PAAm (90:10) fibers spun on spunbonded PP (a) @ RT, (b) @ 40°C, (c) @ 70°C.

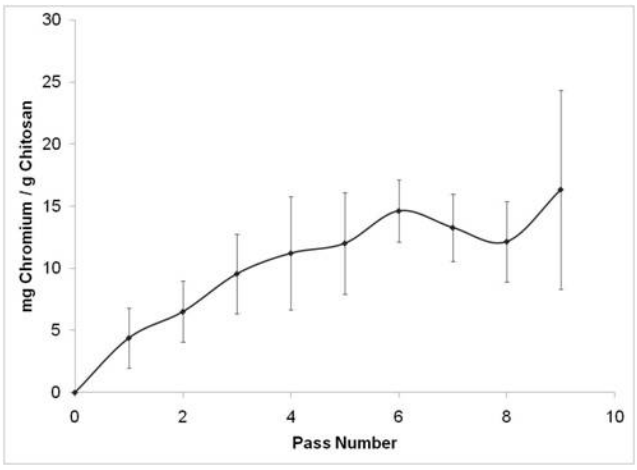

Figure 6.5 mg chromium bound/g chitosan for HMW chitosan:PEO blends after each pass for 10 passes. (Error bars represent standard deviation (n=3))

6.2 Metal binding efficiency of chitosan blends nanofibrous filter media.

6.2.1 Effect of fiber diameter and fiber media gsm.

The dynamic metal binding properties of chitosan blend fiber mats were measured using the procedure described in section 2.4.2. 100 ml of 5 mg/l K_2CrO_4 solution was passed through chitosan nanofibrous filter media ten consecutive times and samples were taken after each pass to see reduction in solution chromium concentration. Figure 6.5 shows the binding capacity achieved after each pass using 1.5 gsm 1.33 wt% HMW chitosan: PEO (90:10) blend fiber mats. It can be seen that with increasing pass number binding efficiency increased. Therefore, for all tests further on mg chromium bound per gram chitosan fiber was calculated after 5^{th} and 10^{th} pass.

Figure 6.6 shows the Cr (VI) binding capacity of HMW chitosan: PEO blend fibers as function of fiber diameter using 0.5 gsm and 1 gsm chitosan nanofibers. It can be seen with increasing fiber diameter binding capacity decreases or remains statistically unchanged. Figure 6.7 shows a plot of binding capacity of 1 gsm HMWchitosan:PEO (90:10) blend fibers with varying fiber diameter plotted along with surface nitrogen concentration (atom %). It can be seen that surface nitrogen content remains unchanged with increasing fiber diameter as explained in section 4.2.1.The binding capacity is statistically similar but shows a decreasing trend with increasing fiber diameter. Our predicted model (Figure 4.6) shows that there is a 30 % drop in

binding capacity between the fiber diameters studied which is well within the standard deviation of the obtained results.

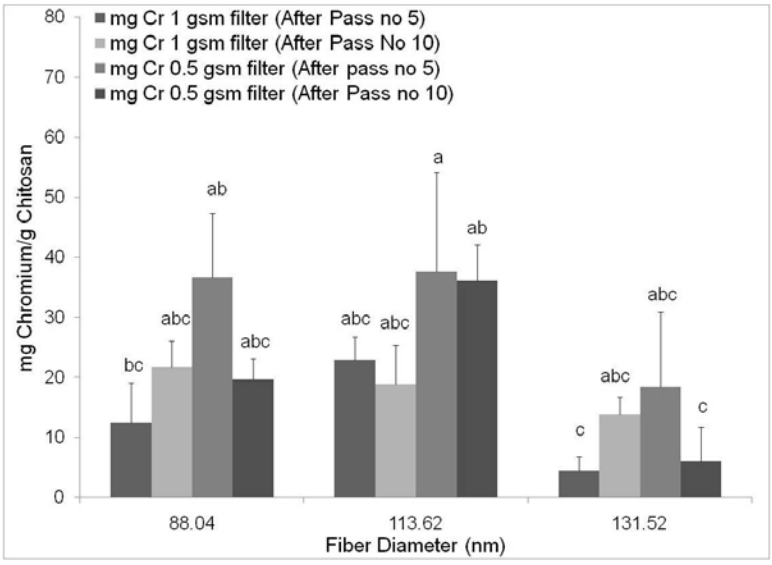

Figure 6.6 Effect of fiber diameter on binding capacity of different gsm HMW chitosan:PEO (90:10) nanofibrous filter media. (Error bars represent standard deviation (n=3), letters indicate significant difference at $p<0.05$)

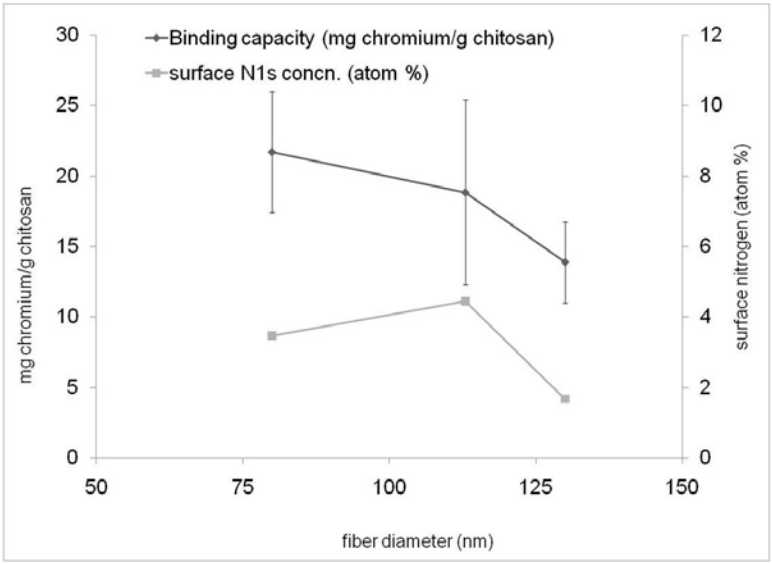

Figure 6.7 Cr(VI) binding capacity and surface nitrogen content vs. fiber diameter for 1 gsm HMWchitosan:PEO (90:10) blend nanofibrous filter media. (Error bars represent standard deviation (n=3))

Figure 6.8 shows the binding capacity as function of fiber diameter for 1gsm HMW chitosan: PAAm (90:10) blend fibers and there is no statistical difference in binding capacity with increasing fiber diameter. Figure 6.9 shows the plot of binding capacity of 1 gsm HMWchitosan:PAAm (90:10) blend fibers along with their surface nitrogen concentration. It can be seen that with increasing fiber diameter surface nitrogen content does not change, which can explain indifference in binding capacity values with increasing fiber diameter. Our predicted model (Figure 4.6) shows that there is a 20 % drop in binding capacity between the fiber diameters studied which is well within the standard deviation of the obtained results. According to the model the effect of fiber diameter is higher when diameter is between 50 – 150 nm above which the effects of % chitosan in blend solution and chitosan % DDA seem to have a greater affect on the binding properties.

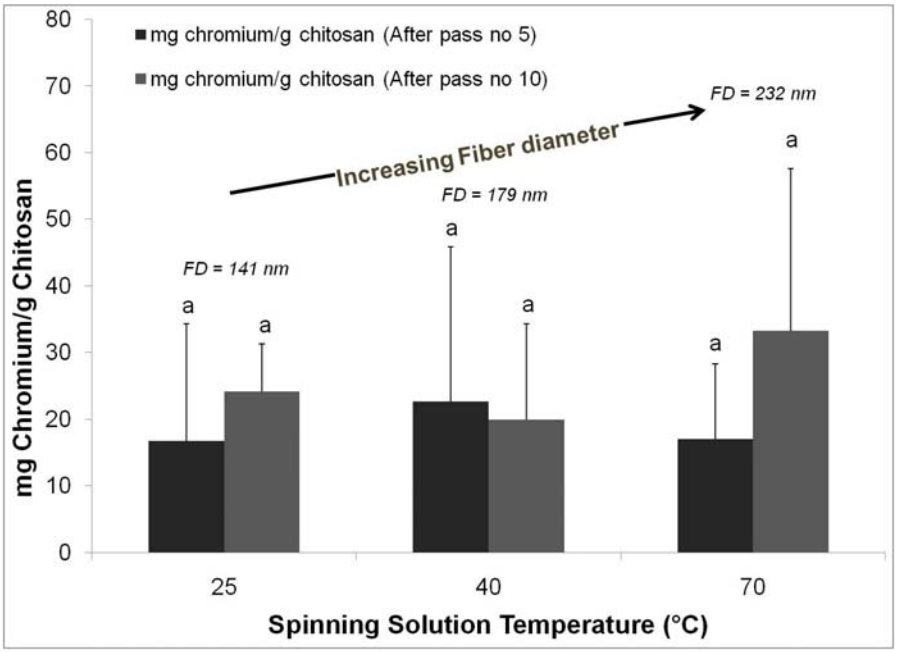

Figure 6.8 Effect of fiber diameter on binding capacity of different gsm HMW chitosan:PAAm (90:10) nanofibrous filter media. (Error bars represent standard deviation (n=3), letters indicate significant difference at $p<0.05$)

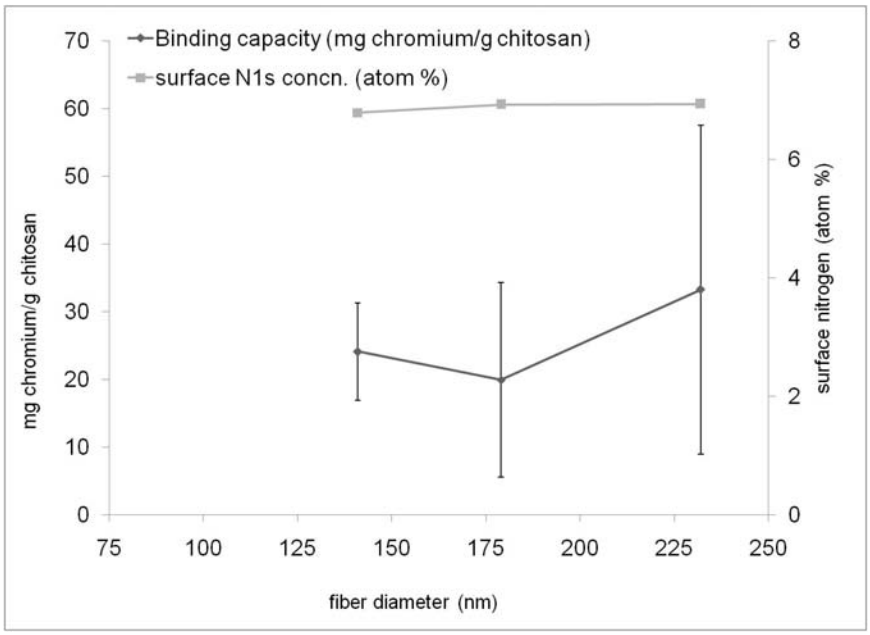

Figure 6.9 Cr(VI) binding capacity and surface nitrogen content vs. fiber diameter for 1 gsm HMWchitosan:PAAm (90:10) blend nanofibrous filter media. (Error bars represent standard deviation (n=3))

Figure 6.10 and 6.11 shows the binding capacity of HMW chitosan:PEO (90:10) and HMW chitosan: PAAm nanofibrous filter media of increasing basis weight (gsm) respectively (constant fiber diameter). It is observed that with increasing gsm for both blend fibers a slight decrease in binding capacity is observed which is statistically mostly insignificant. However it is difficult to comprehend the reason for this slight decrease in binding capacity with increasing web gsm. The % chromium bound does not change with increasing fiber mat gsm (% chromium bound after 10 passes for 0.5 gsm web = 5.67%, 1 gsm web = 6.77% and 1.5 gsm web = 5.4%) which means that the binding efficiency of the fibers is constant irrespective of the basis weight of the mat. The binding activity could be restricted only to the top layers of the espun fiber mat and as will be explained later and shown in Figure 6.12 upon drying of these samples a film is formed on the surface of the fibers. The formation of this film could restrict the binding of chromium to the top few layers forming channels on the fiber surface which would prevent solution effectively wetting the entire depth of the fiber mat.

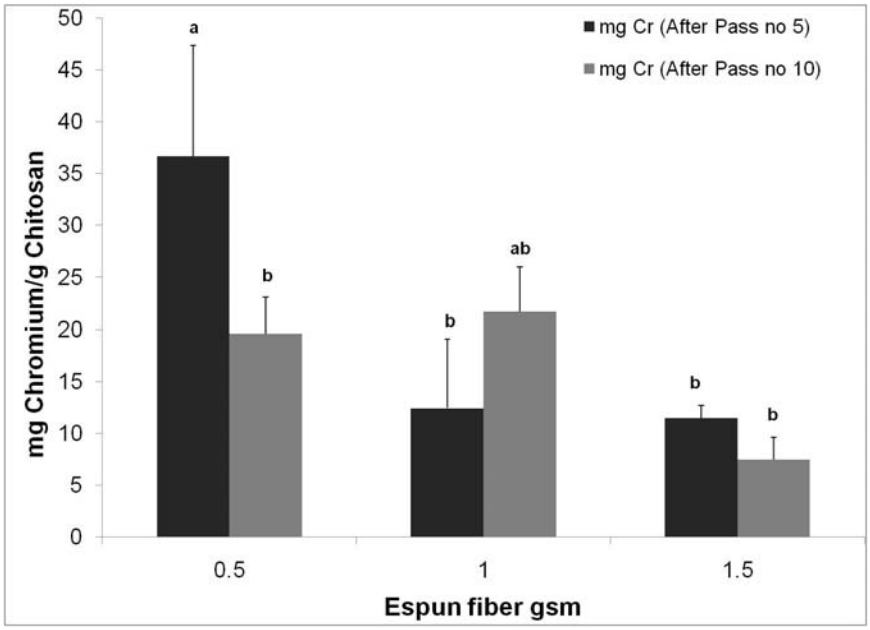

Figure 6.10 Effect of gsm on binding capacity of HMW chitosan:PEO (90:10) nanofibrous filter media. (Error bars represent standard deviation (n=3), letters indicate significant difference at $p<0.05$)

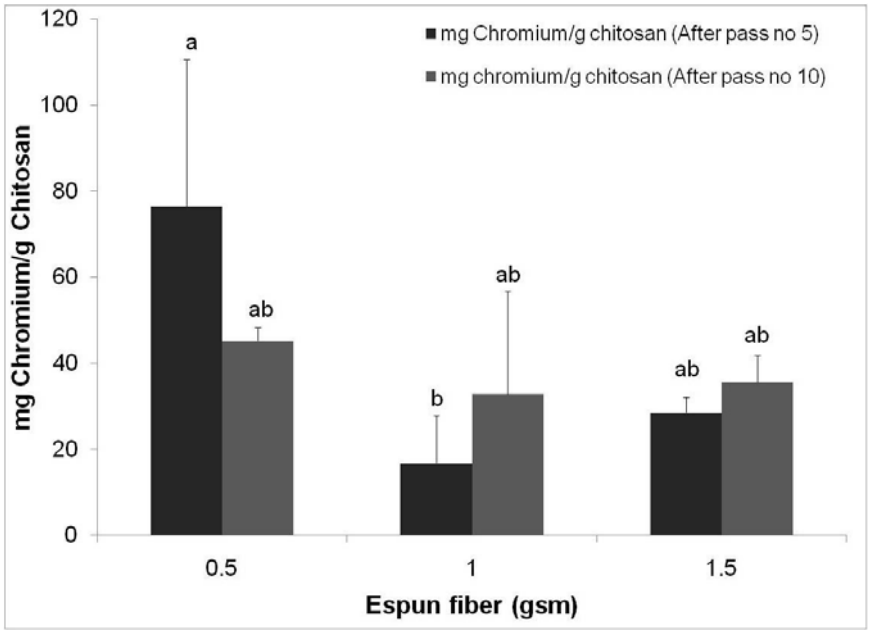

Figure 6.11 Effect of gsm on binding capacity of HMW chitosan:PAAm (90:10) nanofibrous filter media. (Error bars represent standard deviation (n=3), letters indicate significant difference at $p<0.05$)

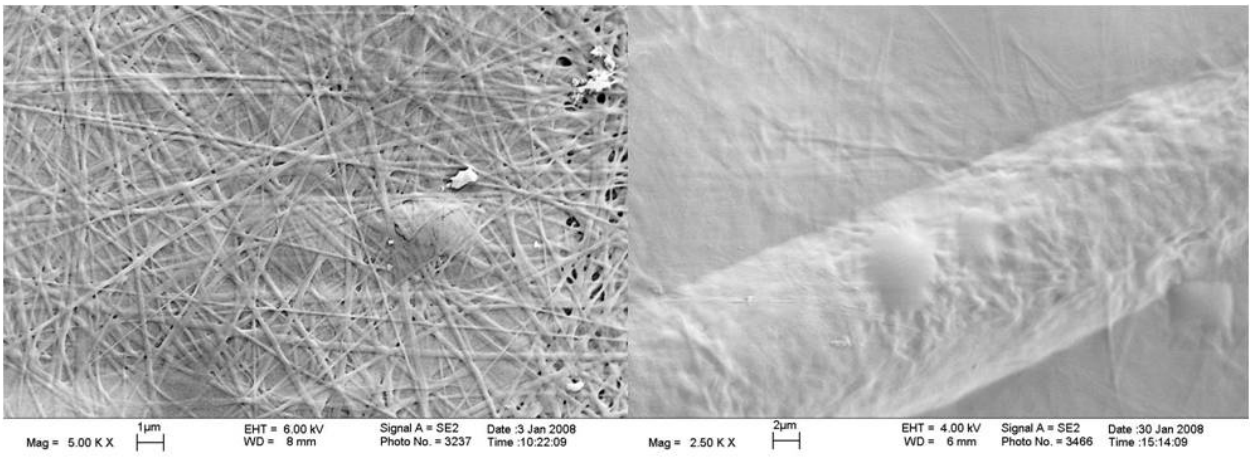

Figure 6.12 SEM images of 1.33 wt% HMW chitosan:PEO (90:10) (left) and 1.4 wt% HMW chitosan: PAAm (90:10) (right) nanofibrous filter media after washing with water.

Looking at the nanofibrous filter media after repeated washing with water using SEM and testing surface composition with XPS it is seen that although a fibrous structure is distinctly visible it is covered by a layer of polymer film. This film could be the incomplete dissolution of the PEO/PAAm from the fibers in solution which upon drying form a film like structure on top of the chitosan nanofibers (Figure 6.12). The surface composition of this layer is as shown in Table 6.1. Looking at the surface nitrogen composition of the films for both the HMWchitosan:PEO (90:10) and HMWchitosan:PAAm (90:10) blend fibers it looks like that the film like layer seen is rich in chitosan. The calculated surface chitosan wt% (calculated as shown in Chapter 4) was found to be 83% for chitosan/PEO blend and 132 % for chitosan/PAAm blends. As has been suggested earlier in section 5.1.3 that during the binding experiments in aqueous medium, chitosan is being partially dissolved in water along with PEO and PAAm. This dissolution of material leads to swelling or partial dissolution of fibrous structure allowing the diffusion of chromium ions to the bulk of the fiber and opening up additional NH_3^+ sites for binding. Upon drying of this wet nanofibrous filter media, formation of polymer film like layer appears on top of the electrospun fiber. This may be a potential reason why we cannot trace Cr content after metal binding experiments using XPS as the Cr bound fibers may be shielded by this polymer film like layer. The formation of this film could also negate the effect of fiber diameter on binding properties as has been seen in Figure 6.7 and 6.9. The swelling of the fiber surface could lead to opening of the fiber structure formation of film like layer and diffusion of chromium ions to the bulk of the fiber reducing the impact of surface chitosan on binding.

Table 6.1 Surface composition of electrospun nanofibrous layer shown in Figure 6.12.

Element	Surface composition HMWchitosan :PEO (90:10) fibers/film (atom %)	Surface composition HMWchitosan :PAAm (90:10) fibers/film (atom %)	Surface composition of pure chitosan film (atom %)	Surface composition of pure PEO film (atom %)	Surface composition of pure PAAm film (atom %)
N	4.83	4.03	5.6		13.73
O	28.42	20.61	28.18	32.39	18.56
C	65.86	74.74	61.11	66.77	67.17
C/N	13.63	18.54	10.91	∞	4.89

6.2.2 Effect of chitosan % DDA.

Figure 6.13 shows the binding capacity of these nanofibrous filter media with increasing % DDA. As has been seen earlier in Figure 5.2, binding capacity increased with increased % DDA even in the dynamic filtration studies. For the 67% and 70% DDA chitosan blend fibrous media there is no increase in binding between 5 and 10 passes as can be seen in the 80% DDA sample. Fibrous media fabricated with lower % DDA chitosan could be getting saturated before or after pass # 5 compared to the 80% DDA chitosan fibrous media.

Comparing metal binding results between the dynamic filtration tests obtained after 20 mins of contact between fibers and metal solution and those discussed in section 5.1 after 3 hrs, it can be seen that higher binding capacity per g of chitosan fiber is observed in the dynamic filtration tests. This could be because of lower weight of fiber mats used in the dynamic tests (wt of filter mats used in dynamic studies is ~ 0.7 – 2.5 g, weight of mats used in section 5.1 > 3 g). Figure 6.14 shows a cross-section view of a 1.5 gsm espun chitosan/PEO blend nanofiber mat on top of 36.5 gsm PP spunbonded web. The thickness of the nanofiber layer is ~ 3 microns. In the literature it has been reported that the binding experiment reaches equilibrium after 12 hrs and after 20 mins only 36 % of available chromium has been bound by chitosan (*i.e.* 37.5 % of maximum chromium ions that can be bound have been bound).[22] Our studies show that after 20 mins only ~ 7-10% of chitosan is bound whereas in results discussed in section 5.1 the binding efficiency after 3 hrs testing is ~ 15 – 30%. The binding capacity after 20 mins in dynamic

filtration tests is approximately 40 % of the maximum binding capacity (*i.e.* binding capacity after 3 hrs) which is similar to literature (Figure 4.3). This validates our assumption in Chapter 4 that the binding kinetics are independent of solution pH and mass of absorbent. The binding capacities observed are significantly (up to 5 magnitudes) higher than those predicted by the model for same sized, blend ratio and %DDA chitosan blend fibers. Our model only accounts for the protonated amine sites on the surface of the fiber but the experimental results and swelling of the fibers leading to formation of film like structure suggest that there is diffusion of chromium through the fiber surface which allows it to bind to protonated amines present in the bulk of the fiber.

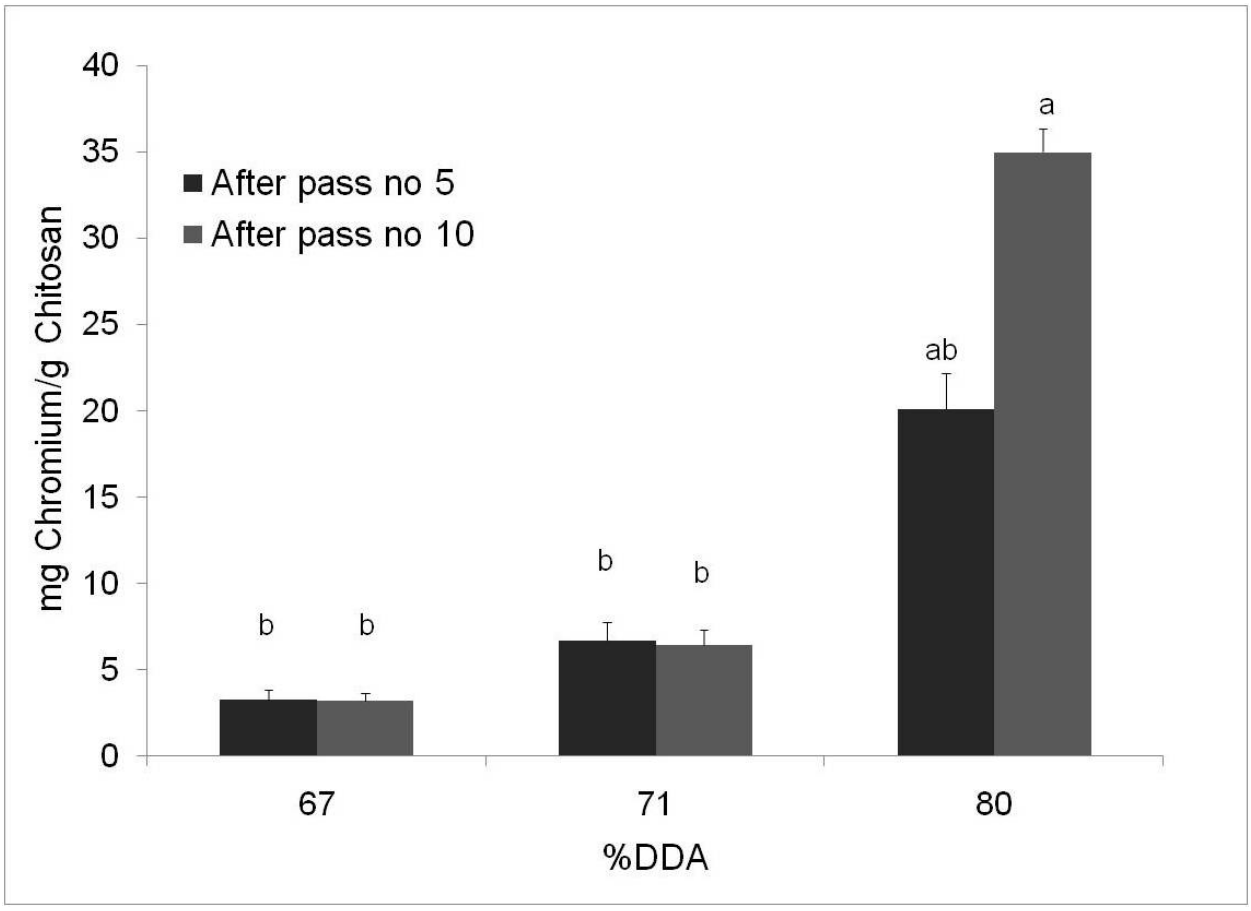

Figure 6.13 Effect of chitosan % DDA on binding capacity of varying DDA HMW chitosan:PEO (90:10) nanofibrous filter media. (Error bars represent standard deviation (n=3), letters indicate significant difference at $p<0.05$)

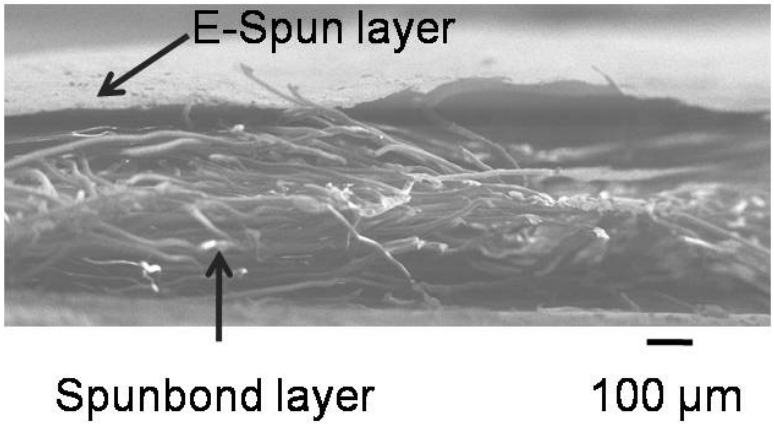

Figure 6.14 SEM cross-section image of 1.5 gsm HMW chitosan: PEO (90:10) espun nanofibrous membrane on spunbonded PP substrate.

6.3 Anti-microbial properties of chitosan blends nanofibrous filter media.

The dynamic anti-microbial properties of chitosan blends nanofibrous filter media were tested using procedure as outlined in section 2.4.3. As had been mentioned earlier, the concentration of Escherichia coli K-12 (10^7 cfu/ml) test microorganism had to be reduced (10^4 cfu/ml) compared to the tests run in section 5.3 as the bacteria overwhelmed the nanofibrous mat (Figure 6.15) and no solution passed through the filter membrane even after 3 hrs. The fiber mat looks like a film after testing because before SEM imaging the sample had to be sterilized which could have melted the polymer fibers partially and formed film on surface.

Figure 6.16 shows the effect of fiber diameter, nanofiber gsm and chitosan DDA on anti-microbial activity of HMW chitosan:PEO (90:10) blend fibers after 1 pass of 10^4 cfu/ml of E-coli K-12. It can be seen that < 0.5 log reduction in bacteria is observed for all samples after ~ 2 mins of contact of fiber with bacterial solution. To understand the kinetics of the anti-microbial activity of chitosan we did a time dependant test wherein bacterial survival after 2mins, 15 mins, 30 mins, 1hr, 2 hr, 4 hr and 6 hr was measured for 1 gsm HMW chitosan:PEO (90:10) blend fibers soaked in 10^7 cfu/ml bacteria solution and results are shown in Figure 6.17. It can be seen that up to 2 hrs there is < 1 log reduction in bacteria and increased activity > 2 log really happens after 4 hrs. Whatever reduction in bacteria was seen in the dynamic filtration test is due to the size effect of the nanofiber which can trap the approximately 0.5 micron sized E-coli bacteria.

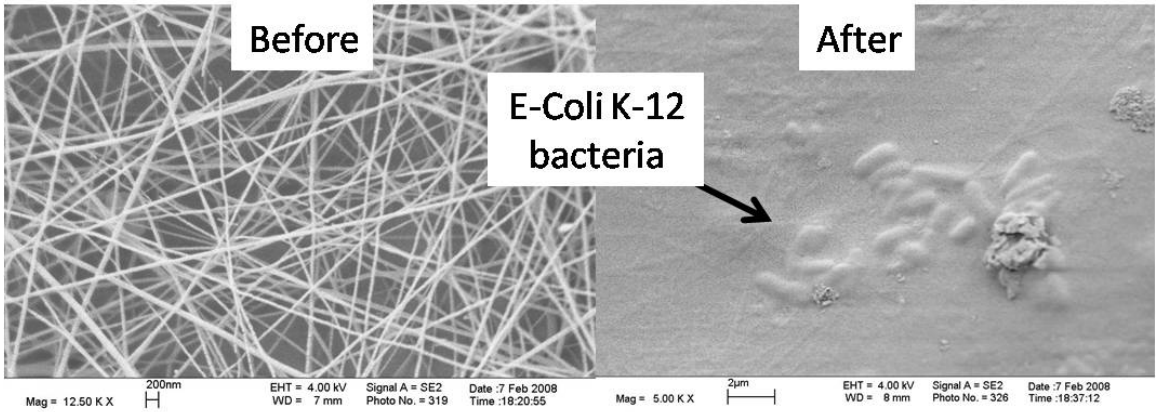

Figure 6.15 SEM image of HMW chitosan:PEO (90:10) nanofibrous filter before and after passing 100 ml of 10^7 cfu/ml E-coli bacteria.

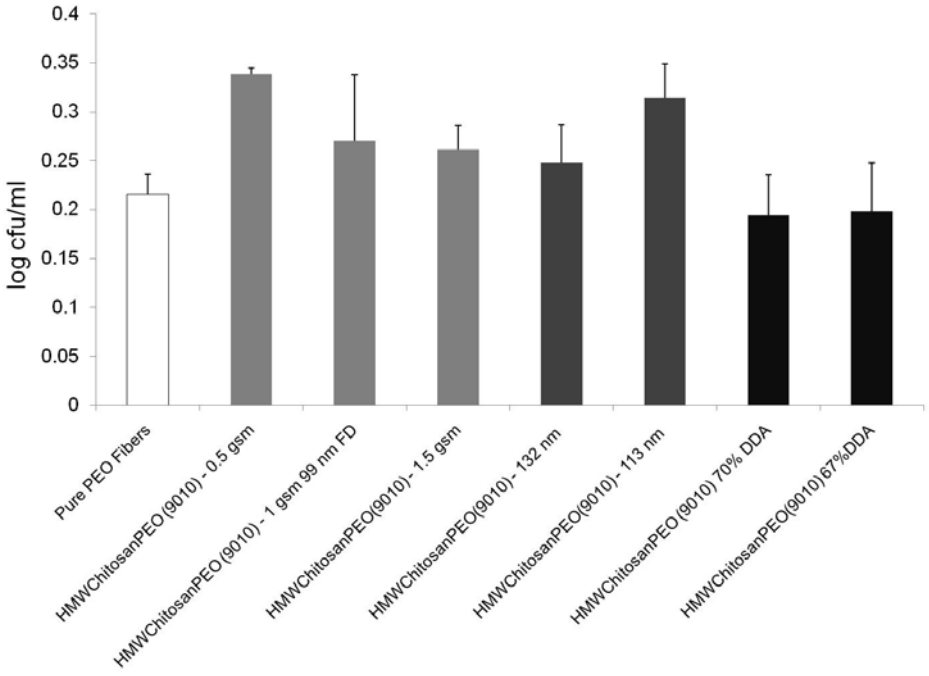

Figure 6.16 Log reduction in E-coli test micro-organism after 1 pass of 100 ml bacteria solution through different gsm, diameter and %DDA chitosan/PEO nanofibrous filter media. (Error bars represent standard deviation (n=3))

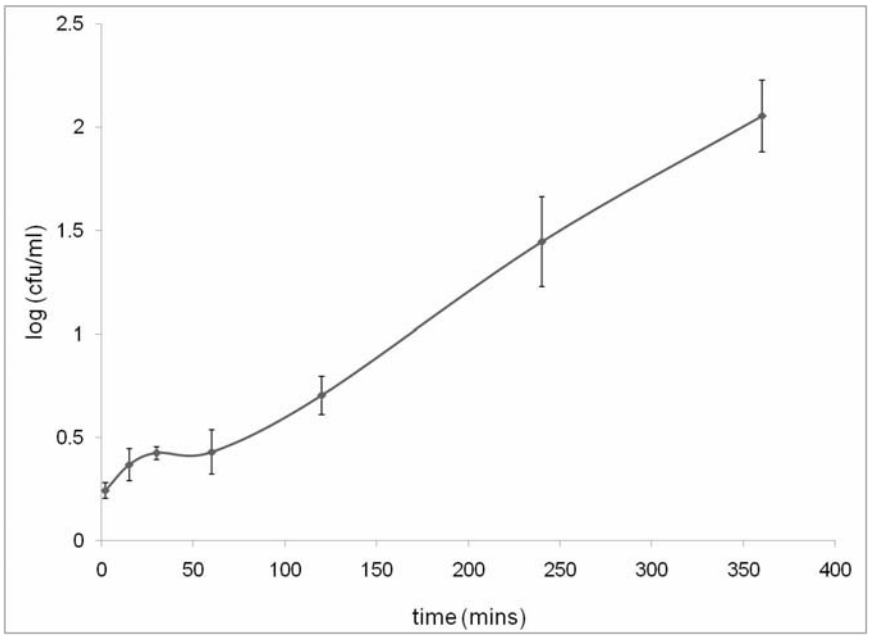

Figure 6.17 Log reduction in E-coli test micro-organism after soaking 1gsm HMW chitosan/PEO (90:10) nanofibrous filter media for different times in bacteria solution. (Error bars represent standard deviation (n=3))

6.4 Latex PS bead filtration efficiency of chitosan blends nanofibrous media.

The applicability of chitosan based nanofibrous filter media to effectively filter out heavy metal ions and micro-organism from pollutant water streams based on the polycationic nature of chitosan has been demonstrated. The particle filtration efficiency of chitosan based nanofibrous filter media was characterized by passing 10 ml of 3 micron sized 200 ppm polystyrene beads through filter media of varying fiber diameter and fiber gsm.

Figure 6.18 shows the SEM images of HMW chitosan/PEO (90:10) blend nanofibrous filter media before and after passing PS beads. It can be seen that the fiber mats appear to be torn after filtration. The mechanical integrity of the mat could have been affected by the pressure exerted by the applied vacuum (~ 2 mm Hg) on the filter membrane during the experiment. Figure 6.19 shows the filtration efficiency of HMW chitosan/PEO (90:10) blend nanofibrous filter media of varying fiber gsm and fiber diameter. With increasing fiber diameter, the PS bead filtration efficiency decreased. This could be due to higher maximum pore size observed with increasing fiber diameter (measured max. pore size of 1 gsm 65 nm diameter fiber = 1.95 μm, measured max. pore size of 1 gsm 110 nm diameter fiber = 2.5 μm). The maximum pore size

was measured as described in section 2.4.1. A filtration experiment was conducted without applying vacuum to the filter media for filtration and varying the fiber media gsm. A 1 gsm nanofibrous filter media of 92 nm fiber diameter and 1.562 microns maximum pore size achieved a 50% filtration efficiency and a similar 3 gsm nanofibrous filter media exhibited 70% filtration efficiency.

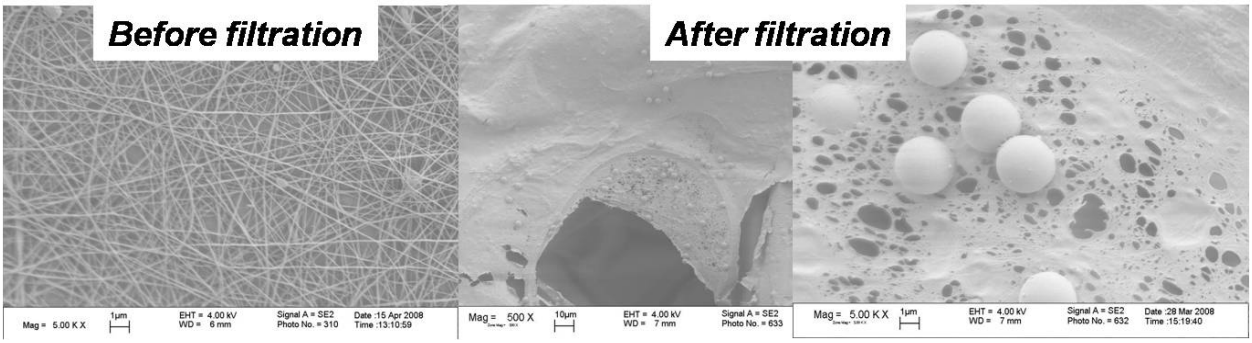

Figure 6.18 SEM images of 1 gsm HMW chitosan:PEO nanofibrous filter media before and after passing 10 ml of 200 ppm 3 μm PS beads.

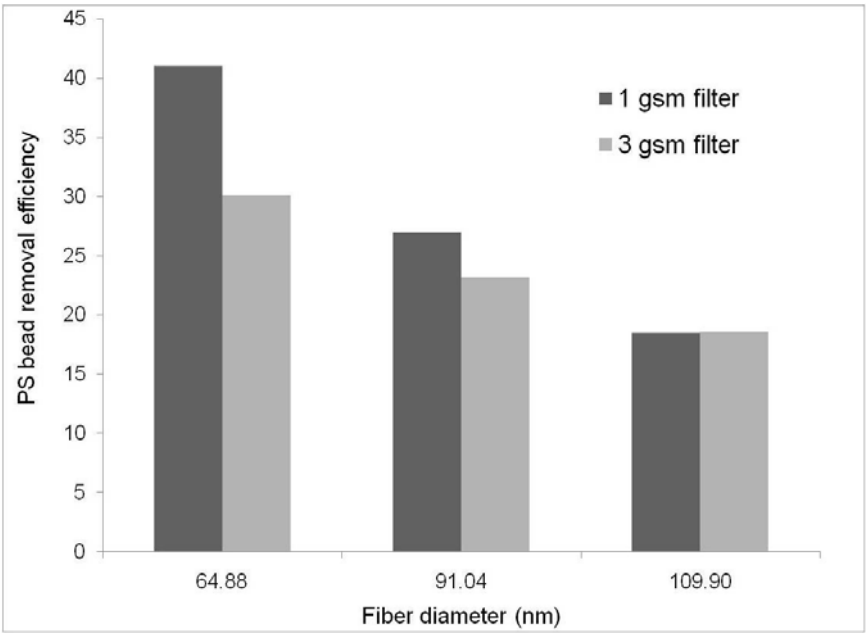

Figure 6.19 PS bead removal efficiency of varying fiber diameter and fiber gsm HMW chitosan:PEO nanofibrous filter media.

Gopal et.al in literature have reported high filtration efficiencies up to 92 % for 1 micron sized PS bead particles[156] using a set-up which had better control over the pressure exerted on the nanofibrous membrane. However, our results obtained do attest to the fact that the chitosan based nanofibrous filter media can effectively filter out particulate media based on size as well as chemical nature of the contaminants.

6.5 Aerosol filtration efficiency of chitosan blends nanofibrous media.

To study the airborne particulate filtration efficiency based on the size of the nanofibers, the aerosol filtration efficiency (Figure 6.20) of 1 gsm HMW chitosan: PEO (90:10) fibers of varying fiber diameters were studied according to the procedure described in section 2.4.4. It can be seen that with increasing fiber diameter the filtration efficiency decreased because the maximum pore size and air permeability increased (Table 6.2). These results show similar trend with those observed for other tested electrospun nanofiber media in literature[147, 153]. The filtration efficiency values are similar to those obtained by Wang et.al[151] (55 % filtration efficiency against 0.6 µm NaCl aerosol particles using a 1 gsm 200 nm diameter and 1.76 µm maximum pore size electrospun poly(vinylalcohol) nanofibers). SEM images of the fiber sample before and after filtration showed no damage to the electrospun layer (Figure 6.21).

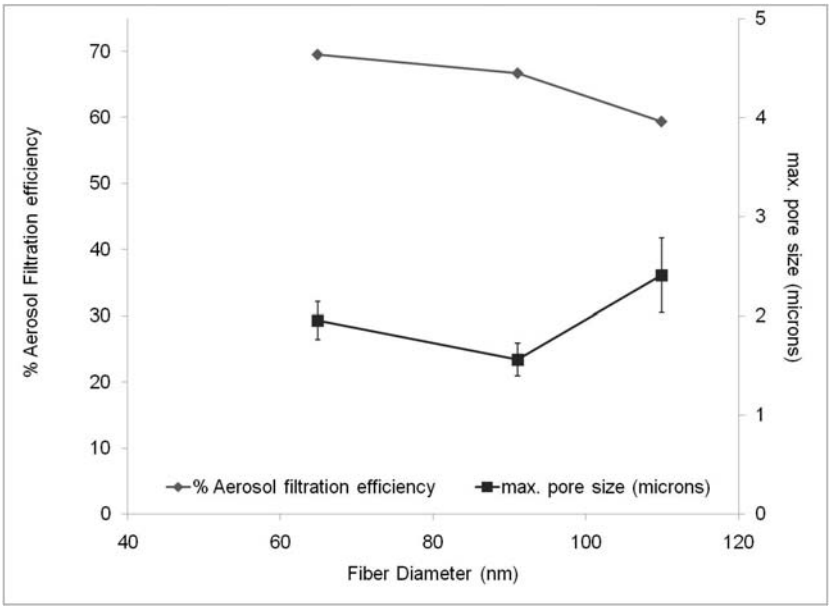

Figure 6.20 Aerosol filtration efficiency and maximum pore size of 1 gsm HMW chitosan:PEO (90:10) nanofibrous filter media. (Error bars represent standard deviation (n=3))

Table 6.2 Air permeability data of 1 gsm HMW chitosan:PEO blend fibers

Fiber Diameter (nm)	Air Permeability (cfm)
64.87	1.29 (± 0.39)
91.04	1.21(± 0.35)
109.84	4.23(± 0.65)

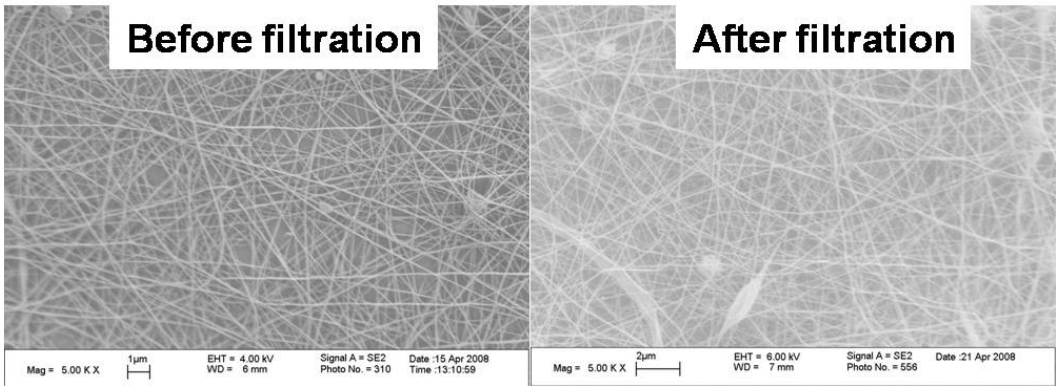

Figure 6.21 SEM images of 1 gsm HMW chitosan:PEO nanofibrous filter media before and after aerosol filtration studies.

7. Conclusions

The work presented herewith demonstrates the applicability of chitosan based nanofibrous filter media to effectively filter out heavy metal ions, pathogenic micro-organisms, and contaminant particulate media from both air and water media. Chitosan based nanofibrous filter media offers the distinct advantage of using both size and surface chemistry of fibers to achieve desired filtration properties compared to nanofibrous filter media fabricated from other synthetic polymers.

Electrospinning of pure chitosan was hindered by its low solubility window in aqueous acid solutions, high degree of inter and intra-chain hydrogen bonding and high solution viscosity. Addition of other synthetic polymers like PEO and PAAm greatly improved the spinnability of chitosan. Fiber formation was strongly dependant on % chitosan in blend solution, viscosity of blend solution (controlled by concentration of polymer in solution, strength of acid and temperature of spinning solution) and synthetic polymer used in blend solution.

We were able to obtain fairly uniform sized electrospun fibers by making blend solutions of both high and low molecular weight chitosan with PEO with very low fractions of PEO (5 %) in the blend solution using acetic acid as the solvent. Fiber formation and size was influenced by blend ratio of the two polymers, polymer concentration, polymer molecular weight and solvent. Heating of the polymer solution with hot air helped improve spinnability by reducing the bead like defects in the formed fibers and enabling the formation of fibers with as low as 5% PEO in the blend solution. TGA analysis of the fibers confirmed the presence of both polymers in the fibers and their blend ratio remained unaltered. Uniform bead-less fibers (fiber diameter ~ 100 nm) were formed with 10% PEO in blend solution by spinning the solution at 70°C.

The advantage of heating the polymer solution during the spinning process was more pronounced for obtaining bead-less fibers of chitosan/PAAm blends. Room temperature spinning solutions were able to form beaded fibers at 75 % chitosan in blend solution, however heating the solution to 70°C enabled us to spin HMWchitosan:PAAm (90:10) blend solutions with ~ 300 nm fiber diameter and < 2% bead density.

A theoretical model was developed to study the change in surface concentration of protonated amine sites and predict maximum Cr (VI) binding efficiency of chitosan nanofibers with respect to fiber diameter, % chitosan in blend solution, and %DDA of chitosan. The model

predicted that size of the fiber (> 400 nm) had a greater effect on binding capacity compared to % chitosan in blend solution or chitosan % DDA. However, for smaller sized fibers % chitosan in blend solution affected the binding efficiency of chitosan blend fibers.

XPS analysis of chitosan blend fibers show that with decreasing % chitosan in blend solution the surface nitrogen concentration decreases for chitosan/PEO blend solutions as expected. From the surface atomic compositions of blend fibers obtained using XPS we were able to calculate the surface chitosan composition (wt %) which decreased with decreasing chitosan in blend solutions. However as % chitosan in solution decreased the % chitosan in fiber surface decreased in a non-linear fashion with only 4-7 wt % chitosan on fiber surface for chitosan:PEO (50:50) blend fibers. For chitosan/PAAm blend fibers although surface nitrogen concentration increased with decreasing chitosan content it did not lead to increase in surface properties. The amide linkage in polyacrylamide is not easily protonated like chitosan as has been shown by the XPS data.

Chitosan blend nanofibers were highly effective in binding Cr(VI) metal ions and binding efficiency was a function of % chitosan in blend solution, molecular of weight, % DDA of chitosan and synthetic polymer used in blend solutions. Results showed similar trend in binding efficiency when compared with theoretically developed model. The metal binding capacity in chitosan blend fibers is significantly higher than that observed for similar blend ratio chitosan/PEO blend films[188]. A 93 μm thick Chitosan/PEO (90:10) blend film showed binding capacity of 0.44 mg chromium/g chitosan whereas the same blend ratio fibers showed 16 mg chromium/g chitosan binding capacity. Electrospun fibers exhibit greater binding capacity due to the high surface area to mass offered by the fibers compared to films.

Chitosan blend nanofibers showed 2-3 log reduction in E-coli K-12 micro-organism and reduction efficiency was a function of % chitosan in blend solution. This value is similar to ones obtained for 35 μm thick films of chitosan:PEO blends with similar blend ratios, but the mass of chitosan in films was up to 10 times higher than that in the fibers.

Nanofibrous filter media using chitosan based electrospun nanofibers were successfully fabricated by electrospinning onto spunbonded PP non-woven substrates. Dynamic metal binding efficiencies using as little 0.5 gsm of nanofibrous filter media showed promising results (binding capacity up to 35 mg chromium/ g chitosan) for commercial applicability of these filters. The nanofibrous filter media however was unable to achieve desired anti-microbial

effectiveness because of the slow reaction between the protonated amine in chitosan and negative components of the bacterial cell wall. Air and water filtration efficiencies of the nanofibrous filter media measured using aerosol and PS beads suspended in water respectively showed high efficiencies which correlated with the fibrous media size and shape. However the nanofibrous layer lacked mechanical strength to with stand pressure applied during the PS bead filtration which affected the results.

Electrospun chitosan based nanofibrous filter media definitely offers great potential as a pre-filter material owing to its excellent metal-binding capacities, anti-microbial properties and physical filtration efficiencies.

7.1 Future Work.

The future work towards the optimization of the development of chitosan based nanofibrous filter media with maximum metal binding and anti-microbial properties can be:

1. The XPS data of the blend nanofibers suggest that surface chitosan concentration is different from the bulk and using transmission electron microscopy phase imaging or atomic force microscopy (force modulation mode) or dynamic mechanical analysis methods further studies should be done to try and understand phase morphology development occurring during the spinning process in the fibers.
2. Consistently higher binding efficiencies then those predicted by the model indicate that binding occurs by diffusion of chromium through the fibers potentially by swelling of the polymers. The binding mechanism needs to be further studied probably by varying initial chromium concentrations in solution.
3. SEM images of nanofibrous filter media washed with water or even after metal binding experiments show the formation of a film like layer. Although XPS analysis of the surface indicates that the film is rich in chitosan, studies need to be done to understand the film formation and its prevention by either cross-linking the chitosan or making fibers of chitosan blends with hydrophobic polymers.
4. As seen in the PS latex beads test, mechanical integrity of the nanofiber layer is weak. A potential way of overcoming this problem in the future would be to develop a sandwich filter with a top layer of melt blown PP, a middle layer of the electrospun chitosan and a bottom substrate layer of spun bonded PP.

5. The economic viability of chitosan nanofibrous filter media lie with its regeneration capacity. The Cr(VI) binding mechanism is a reversible process and studies need to be done to understand this reverse reaction for the electrospun fibers *i.e.* if we can desorb the absorbed heavy metal ions by increasing solution pH and reuse the fibers.
6. Binding and anti-microbial studies can be extended to other metal species and gram negative or gram positive bacteria. The effect of different metal ions or micro-organisms, and effect of solution pH can be studied on nanofibrous filter media performance.

References

References.

1. Kaur, S.; Gopal, R.; Ng, W. J.; Ramakrishna, S.; Matsuura, T., Next-generation fibrous media for water treatment. *Mrs Bulletin* **2008,** 33, (1), 21-26.
2. Wang, J.; Kim, S. C.; Pui, D. Y., Investigation of the figure of merit for filters with a single nanofiber layer on a substrate. *Journal of Aerosol Science* **2008,** 39, (4), 323-334.
3. Cauchie, H. M., Chitin production by arthropods in the hydrosphere. *Hydrobiologia* **2002,** 470, (1-3), 63-96.
4. Roberts, G. A. F., *Chitin Chemistry*. The MacMillan Press Ltd: London, 1992.
5. Wu, T.; Zivanovic, S.; Draughon, F. A.; Sams, C. E., Chitin and chitosan - Value-added products from mushroom waste. *Journal of Agricultural and Food Chemistry* **2004,** 52, (26), 7905-7910.
6. Angelova, N. M., N.; Rashkov, I.; Maximova, V.; Bogdanova, S.; Domard, A., Preparation and properties of modified chitosan films for drug release. *Journal of Bioactive and Compatible Polymers* **1995,** 10, (4), 285-98.
7. Selmer-Olsen, E. R., H. C.; Pehrson, R., A novel treatment process for dairy wastewater with chitosan produced from shrimp-shell waste. *Water Science and Technology* **1996,** 34, 33-40.
8. Doshi, J.; Reneker, D. H., ELECTROSPINNING PROCESS AND APPLICATIONS OF ELECTROSPUN FIBERS. *Journal of Electrostatics* **1995,** 35, (2-3), 151-160.
9. Subbiah, T.; Bhat, G. S.; Tock, R. W.; Pararneswaran, S.; Ramkumar, S. S., Electrospinning of nanofibers. *Journal of Applied Polymer Science* **2005,** 96, (2), 557-569.
10. Formhals, A. Method and Apparatus for Spinning. 2,160,962, 1939.
11. Goosen, M., *Application of Chitin and Chitosan,*. Technomic Publishing Co: Lancaster-Basel, PA, 1997.
12. Gupta, K. C.; Kumar, M., An overview on chitin and chitosan applications with an emphasis on controlled drug release formulations. *Journal of Macromolecular Science-Reviews in Macromolecular Chemistry and Physics* **2000,** C40, (4), 273-308.
13. Neto, C. G. T.; Giacometti, J. A.; Job, A. E.; Ferreira, F. C.; Fonseca, J. L. C.; Pereira, M. R., Thermal Analysis of Chitosan Based Networks. *Carbohydrate Polymers* **2005,** 62, (2), 97-103.
14. Dutta, P. K.; Ravikumar, M. N.; Dutta, J., Chitin and chitosan for versatile applications. *Journal of Macromolecular Science-Polymer Reviews* **2002,** C42, (3), 307-354.
15. Chen, R. H.; Hwa, H. D., Effect of molecular weight of chitosan with the same degree of deacetylation on the thermal, mechanical, and permeability properties of the prepared membrane. *Carbohydrate Polymers* **1996,** 29, (4), 353-358.
16. Guibal, E., Interactions of metal ions with chitosan-based sorbents: a review. *Separation and Purification Technology* **2004,** 38, (1), 43-74.
17. Trung, T. S.; Thein-Han, W. W.; Qui, N. T.; Ng, C. H.; Stevens, W. F., Functional characteristics of shrimp chitosan and its membranes as affected by the degree of deacetylation. *Bioresource Technology* **2006,** 97, (4), 659-663.
18. Sorlier, P.; Denuziere, A.; Viton, C.; Domard, A., Relation between the Degree of Acetylation and the Electrostatic Properties of Chitin and Chitosan. *Biomacromolecules* **2001,** 2, (3), 765-772.
19. Kawamura, Y.; Mitsuhashi, M.; Tanibe, H.; Yoshida, H., Adsorption of metal ions on polyaminated highly porous chitosan chelating resin. *Ind. Eng. Chem. Res.* **1993,** 32, (2), 386-391.

20. Babel, S.; Kurniawan, T. A., Low-cost adsorbents for heavy metals uptake from contaminated water: a review. *Journal of Hazardous Materials* **2003,** 97, (1-3), 219-243.
21. Schmuhl, R.; Krieg, H. M.; Keizer, K., Adsorption of Cu(II) and Cr(VI) ions by chitosan: Kinetics and equilibrium studies. *Water Sa* **2001,** 27, (1), 1-7.
22. Udaybhaskar, P.; Iyengar, L.; Rao, A., HEXAVALENT CHROMIUM INTERACTION WITH CHITOSAN. *Journal of Applied Polymer Science* **1990,** 39, (3), 739-747.
23. Juang, R.-S.; Shiau, R.-C., Metal removal from aqueous solutions using chitosan-enhanced membrane filtration. *Journal of Membrane Science* **2000,** 165, (2), 159-167.
24. Milot, C.; McBrien, J.; Allen, S.; Guibal, E., Influence of physicochemical and structural characteristics of chitosan flakes on molybdate sorption. *Journal of Applied Polymer Science* **1998,** 68, (4), 571-580.
25. Guibal, E.; Jansson-Charrier, M.; Saucedo, I.; Cloirec, P. L., Enhancement of Metal Ion Sorption Performances of Chitosan: Effect of the Structure on the Diffusion Properties. *Langmuir* **1995,** 11, (2), 591-598.
26. Krajewska, B., Membrane-based processes performed with use of chitin/chitosan materials. *Separation and Purification Technology* **2005,** 41, (3), 305-312.
27. Krajewska, B., Diffusion of metal ions through gel chitosan membranes. *Reactive and Functional Polymers* **2001,** 47, (1), 37-47.
28. Helander, I. M.; Nurmiaho-Lassila, E. L.; Ahvenainen, R.; Rhoades, J.; Roller, S., Chitosan disrupts the barrier properties of the outer membrane of Gram-negative bacteria. *International Journal of Food Microbiology* **2001,** 71, (2-3), 235-244.
29. Lim, S. H.; Hudson, S. M., Review of chitosan and its derivatives as antimicrobial agents and their uses as textile chemicals. *Journal of Macromolecular Science-Polymer Reviews* **2003,** C43, (2), 223-269.
30. Shimojoh, M.; Masaki, K.; Kurita, K.; Fukushima, K., Bactericidal effects of chitosan from squid pens on oral streptococci. *Nippon Nogeikagaku Kaishi-Journal of the Japan Society for Bioscience Biotechnology and Agrochemistry* **1996,** 70, (7), 787-792.
31. Liu, X. F.; Guan, Y. L.; Yang, D. Z.; Li, Z.; De Yao, K., Antibacterial action of chitosan and carboxymethylated chitosan. *Journal of Applied Polymer Science* **2001,** 79, (7), 1324-1335.
32. Tsai, G. J.; Su, W. H., Antibacterial activity of shrimp chitosan against Escherichia coli. *Journal of Food Protection* **1999,** 62, (3), 239-243.
33. Singh, D. K.; Ray, A. R., Biomedical applications of chitin, chitosan, and their derivatives. *Journal of Macromolecular Science-Reviews in Macromolecular Chemistry and Physics* **2000,** C40, (1), 69-83.
34. Brian, S.; Paul, H.; David, W. Nonwoven fabric containing microfungal hyphae fibres 1985.
35. Townsley.Pm, Chromatography of Tobacco Mosaic Virus (Tmv) on Chitin Columns. *Nature* **1961,** 191, (478), 626-&.
36. Hsieh, S. H.; Huang, Z. K.; Huang, Z. Z.; Tseng, Z. S., Antimicrobial and physical properties of woolen fabrics cured with citric acid and chitosan. *Journal of Applied Polymer Science* **2004,** 94, (5), 1999-2007.
37. El-Tahlawy, K. F.; El-Bendary, M. A.; Elhendawy, A. G.; Hudson, S. M., The antimicrobial activity of cotton fabrics treated with different crosslinking agents and chitosan. *Carbohydrate Polymers* **2005,** 60, (4), 421-430.
38. Qin, Y. M.; Zhu, C. J.; Chen, J.; Chen, Y. Z.; Zhang, C., The absorption and release of silver and zinc ions by chitosan fibers. *Journal of Applied Polymer Science* **2006,** 101, (1), 766-771.

39. Gibson, P.; Schreuder-Gibson, H.; Rivin, D., Transport properties of porous membranes based on electrospun nanofibers. *Colloids and Surfaces A: Physicochemical and Engineering Aspects* **2001,** 187-188, 469-481.
40. Reneker, D. H.; Yarin, A. L.; Fong, H.; Koombhongse, S., Bending instability of electrically charged liquid jets of polymer solutions in electrospinning. *Journal of Applied Physics* **2000,** 87, (9), 4531-4547.
41. Reneker, D. H.; Kataphinan, W.; Theron, A.; Zussman, E.; Yarin, A. L., Nanofiber garlands of polycaprolactone by electrospinning. *Polymer* **2002,** 43, (25), 6785-6794.
42. Gupta, P.; Elkins, C.; Long, T. E.; Wilkes, G. L., Electrospinning of linear homopolymers of poly(methyl methacrylate): exploring relationships between fiber formation, viscosity, molecular weight and concentration in a good solvent. *Polymer* **2005,** 46, (13), 4799-4810.
43. Shenoy, S. L.; Bates, W. D.; Frisch, H. L.; Wnek, G. E., Role of chain entanglements on fiber formation during electrospinning of polymer solutions: good solvent, non-specific polymer-polymer interaction limit. *Polymer* **2005,** 46, (10), 3372-3384.
44. Raleigh, L., *London,Edinburgh, and Dublin Phil. Mag. J.* **1882,** 44, 184-186.
45. Taylor, G. I., *Proceedings of the Royal Society,London* **1964,** 280, 383-397.
46. Formhals, A. Process and Apparatus for Preparing Artificial Threads. 1,975,504, 1934.
47. Baumgart.Pk, ELECTROSTATIC SPINNING OF ACRYLIC MICROFIBERS. *Journal of Colloid and Interface Science* **1971,** 36, (1), 71-&.
48. Larrondo, L.; Manley, R. S. J., ELECTROSTATIC FIBER SPINNING FROM POLYMER MELTS .2. EXAMINATION OF THE FLOW FIELD IN AN ELECTRICALLY DRIVEN JET. *Journal of Polymer Science Part B-Polymer Physics* **1981,** 19, (6), 921-932.
49. Fong, H.; Chun, I.; Reneker, D. H., Beaded nanofibers formed during electrospinning. *Polymer* **1999,** 40, (16), 4585-4592.
50. Deitzel, J. M.; Kleinmeyer, J.; Harris, D.; Tan, N. C. B., The effect of processing variables on the morphology of electrospun nanofibers and textiles. *Polymer* **2001,** 42, (1), 261-272.
51. Deitzel, J. M.; Kleinmeyer, J. D.; Hirvonen, J. K.; Tan, N. C. B., Controlled deposition of electrospun poly(ethylene oxide) fibers. *Polymer* **2001,** 42, (19), 8163-8170.
52. Cevat, E.; Dilhan, M. K.; Hongjun, W., A hybrid twin screw extrusion/electrospinning method to process nanoparticle-incorporated electrospun nanofibres. *Nanotechnology* **2008**, (16), 165302.
53. Weitz, R. T.; Harnau, L.; Rauschenbach, S.; Burghard, M.; Kern, K., Polymer nanofibers via nozzle-free centrifugal spinning. *Nano Letters* **2008,** 8, (4), 1187-1191.
54. Shin, Y. M.; Hohman, M. M.; Brenner, M. P.; Rutledge, G. C., Experimental characterization of electrospinning: the electrically forced jet and instabilities. *Polymer* **2001,** 42, (25), 9955-9967.
55. Shin, Y. M.; Hohman, M. M.; Brenner, M. P.; Rutledge, G. C., Electrospinning: A whipping fluid jet generates submicron polymer fibers. *Applied Physics Letters* **2001,** 78, (8), 1149-1151.
56. Spivak, A. F.; Dzenis, Y. A.; Reneker, D. H., A model of steady state jet in the electrospinning process. *Mechanics Research Communications* **2000,** 27, (1), 37-42.
57. Hohman, M. M.; Shin, M.; Rutledge, G.; Brenner, M. P., Electrospinning and electrically forced jets. I. Stability theory. *Physics of Fluids* **2001,** 13, (8), 2201-2220.
58. Hohman, M. M.; Shin, M.; Rutledge, G.; Brenner, M. P., Electrospinning and electrically forced jets. II. Applications. *Physics of Fluids* **2001,** 13, (8), 2221-2236.
59. Huang, Z. M.; Zhang, Y. Z.; Kotaki, M.; Ramakrishna, S., A review on polymer nanofibers by electrospinning and their applications in nanocomposites. *Composites Science and Technology* **2003,** 63, (15), 2223-2253.

60. Teo, W. E.; Ramakrishna, S., A review on electrospinning design and nanofibre assemblies. *Nanotechnology* **2006,** 17, (14), R89-R106.
61. Reneker, D. H.; Yarin, A. L.; Zussman, E.; Xu, H., Electrospinning of nanofibers from polymer solutions and melts. In *Advances in Applied Mechanics, Vol 41*, Elsevier Academic Press Inc: San Diego, 2007; pp 43-195.
62. Schiffman, J. D.; Schauer, C. L., Cross-linking chitosan nanofibers. *Biomacromolecules* **2007,** 8, (2), 594-601.
63. Greiner, A.; Wendorff, J. H., Electrospinning: A fascinating method for the preparation of ultrathin fibres. *Angewandte Chemie-International Edition* **2007,** 46, (30), 5670-5703.
64. Li, D.; Xia, Y. N., Electrospinning of nanofibers: Reinventing the wheel? *Advanced Materials* **2004,** 16, (14), 1151-1170.
65. Tan, K.; Obendorf, S. K., Fabrication and evaluation of electrospun nanofibrous antimicrobial nylon 6 membranes. *Journal of Membrane Science* **2007,** 305, (1-2), 287-298.
66. Krishnappa, R. V. N.; Desai, K.; Sung, C. M., Morphological study of electrospun polycarbonates as a function of the solvent and processing voltage. *Journal of Materials Science* **2003,** 38, (11), 2357-2365.
67. Casper, C. L.; Stephens, J. S.; Tassi, N. G.; Chase, D. B.; Rabolt, J. F., Controlling surface morphology of electrospun polystyrene fibers: Effect of humidity and molecular weight in the electrospinning process. *Macromolecules* **2004,** 37, (2), 573-578.
68. Fong, H.; Liu, W. D.; Wang, C. S.; Vaia, R. A., Generation of electrospun fibers of nylon 6 and nylon 6-montmorillonite nanocomposite. *Polymer* **2002,** 43, (3), 775-780.
69. Yao, L.; Haas, T. W.; Guiseppi-Elie, A.; Bowlin, G. L.; Simpson, D. G.; Wnek, G. E., Electrospinning and stabilization of fully hydrolyzed poly(vinyl alcohol) fibers. *Chemistry of Materials* **2003,** 15, (9), 1860-1864.
70. Desai, K.; Sung, C. M., Electrospinning and phase characterization of polyaniline/polymethyl methacrylate blends. *Abstracts of Papers of the American Chemical Society* **2003,** 226, U442-U442.
71. Deitzel, J. M.; Kosik, W.; McKnight, S. H.; Tan, N. C. B.; DeSimone, J. M.; Crette, S., Electrospinning of polymer nanofibers with specific surface chemistry. *Polymer* **2002,** 43, (3), 1025-1029.
72. Y. Y. Zhao, Q. B. Y. X. F. L. C. W. Y. W., Study on correlation of morphology of electrospun products of polyacrylamide with ultrahigh molecular weight. *Journal of Polymer Science Part B: Polymer Physics* **2005,** 43, (16), 2190-2195.
73. Vetcher, A. A.; Gearheart, R.; Morozov, V. N., Correlation of morphology of electrospun fibers with rheology of linear polyacrylamide solution. *Polymer Journal* **2007,** 39, (8), 878-881.
74. Sarkar, S.; Deevi, S.; Tepper, G., Biased AC electrospinning of aligned polymer nanofibers. *Macromolecular Rapid Communications* **2007,** 28, (9), 1034-1039.
75. Zhang, C.; Yuan, X.; Wu, L.; Han, Y.; Sheng, J., **2005,** - 41, (- 3), - 432.
76. Fennessey, S. F.; Farris, R. J., Fabrication of aligned and molecularly oriented electrospun polyacrylonitrile nanofibers and the mechanical behavior of their twisted yams. *Polymer* **2004,** 45, (12), 4217-4225.
77. Katta, P.; Alessandro, M.; Ramsier, R. D.; Chase, G. G., Continuous electrospinning of aligned polymer nanofibers onto a wire drum collector. *Nano Letters* **2004,** 4, (11), 2215-2218.
78. Um, I. C.; Fang, D. F.; Hsiao, B. S.; Okamoto, A.; Chu, B., Electro-spinning and electro-blowing of hyaluronic acid. *Biomacromolecules* **2004,** 5, (4), 1428-1436.

79. Wang, X. F.; Um, I. C.; Fang, D. F.; Okamoto, A.; Hsiao, B. S.; Chu, B., Formation of water-resistant hyaluronic acid nanofibers by blowing-assisted electro-spinning and non-toxic post treatments. *Polymer* **2005,** 46, (13), 4853-4867.
80. Wang, C.; Chien, H. S.; Hsu, C. H.; Wang, Y. C.; Wang, C. T.; Lu, H. A., Electrospinning of polyacrylonitrile solutions at elevated temperatures. *Macromolecules* **2007,** 40, (22), 7973-7983.
81. Gupta, P.; Wilkes, G. L., Some investigations on the fiber formation by utilizing a side-by-side bicomponent electrospinning approach. *Polymer* **2003,** 44, (20), 6353-6359.
82. Feng, K. An investigation on phase behavior and orientation factor of electrospun nanofibers. The University of Tennessee, Knoxville, 2005.
83. Wei, M.; Kang, B. W.; Sung, C. M.; Mead, J., Core-sheath structure in electrospun nanofibers from polymer blends. *Macromolecular Materials and Engineering* **2006,** 291, (11), 1307-1314.
84. Bianco, A.; Bertarelli, C.; Frisk, S.; Rabolt, J. F.; Gallazzi, M. C.; Zerbi, G., Electrospun polyalkylthiophene/polyethyleneoxide fibers: Optical characterization. *Synthetic Metals* **2007,** 157, (6-7), 276-281.
85. Lim, C. T.; Tan, E. P. S.; Ng, S. Y., Effects of crystalline morphology on the tensile properties of electrospun polymer nanofibers. *Applied Physics Letters* **2008,** 92, (14).
86. McKee, M. G.; Hunley, M. T.; Layman, J. M.; Long, T. E., Solution rheological behavior and electrospinning of cationic polyelectrolytes. *Macromolecules* **2006,** 39, (2), 575-583.
87. Jeong, E. H.; Yang, J.; Youk, J. H., Preparation of polyurethane cationomer nanofiber mats for use in antimicrobial nanofilter applications. *Materials Letters* **2007,** 61, (18), 3991-3994.
88. Ignatova, M.; Markova, N.; Manolova, N.; Rashkov, I., Antibacterial and antimycotic activity of a cross-linked electrospun poly(vinyl pyrrolidone)-iodine complex and a poly(ethylene oxide)/poly(vinyl pyrrolidone)-iodine complex. *Journal of Biomaterials Science-Polymer Edition* **2008,** 19, (3), 373-386.
89. Matthews, J. A.; Wnek, G. E.; Simpson, D. G.; Bowlin, G. L., Electrospinning of collagen nanofibers. *Biomacromolecules* **2002,** 3, (2), 232-238.
90. McManus, M. C.; Boland, E. D.; Simpson, D. G.; Barnes, C. P.; Bowlin, G. L., Electrospun fibrinogen: Feasibility as a tissue engineering scaffold in a rat cell culture model. *Journal of Biomedical Materials Research Part A* **2007,** 81A, (2), 299-309.
91. Wang, Y. K.; Yong, T.; Ramakrishna, S., Nanofibres and their influence on cells for tissue regeneration. *Australian Journal of Chemistry* **2005,** 58, (10), 704-712.
92. Zhang, Y. Z.; Huang, Z. M.; Xu, X. J.; Lim, C. T.; Ramakrishna, S., Preparation of core-shell structured PCL-r-gelatin Bi-component nanofibers by coaxial electrospinning. *Chemistry of Materials* **2004,** 16, (18), 3406-3409.
93. Jing, Z.; Xu, X. Y.; Chen, X. S.; Liang, Q. Z.; Bian, X. C.; Yang, L. X.; Jing, X. B., Biodegradable electrospun fibers for drug delivery. *Journal of Controlled Release* **2003,** 92, (3), 227-231.
94. Verreck, G.; Chun, I.; Rosenblatt, J.; Peeters, J.; Van Dijck, A.; Mensch, J.; Noppe, M.; Brewster, M. E., Incorporation of drugs in an amorphous state into electrospun nanofibers composed of a water-insoluble, nonbiodegradable polymer. *Journal of Controlled Release* **2003,** 92, (3), 349-360.
95. Yoshimoto, H.; Shin, Y. M.; Terai, H.; Vacanti, J. P., A biodegradable nanofiber scaffold by electrospinning and its potential for bone tissue engineering. *Biomaterials* **2003,** 24, (12), 2077-2082.
96. Pedicini, A.; Farris, R. J., Mechanical behavior of electrospun polyurethane. *Polymer* **2003,** 44, (22), 6857-6862.

97. Tsai, P. P.; Roth, J. R.; Chen, W. W., Strength, surface energy, and ageing of meltblown and electrospun nylon and polyurethane (PU) fabrics treated by a one atmosphere uniform glow discharge plasma (OAUGDP (TM)). *Textile Research Journal* **2005,** 75, (12), 819-825.
98. Khil, M. S.; Cha, D. I.; Kim, H. Y.; Kim, I. S.; Bhattarai, N., Electrospun nanofibrous polyurethane membrane as wound dressing. *Journal of Biomedical Materials Research Part B-Applied Biomaterials* **2003,** 67B, (2), 675-679.
99. Zhuo, H. T.; Hu, J. L.; Chen, S. J., Electrospun polyurethane nanofibres having shape memory effect. *Materials Letters* **2008,** 62, (14), 2078-2080.
100. Boland, E. D.; Wnek, G. E.; Simpson, D. G.; Pawlowski, K. J.; Bowlin, G. L., Tailoring tissue engineering scaffolds using electrostatic processing techniques: A study of poly(glycolic acid) electrospinning. *Journal of Macromolecular Science-Pure and Applied Chemistry* **2001,** 38, (12), 1231-1243.
101. Liu, H. Q.; Hsieh, Y. L., Surface methacrylation and graft copolymerization of ultrafine cellulose fibers. *Journal of Polymer Science Part B-Polymer Physics* **2003,** 41, (9), 953-964.
102. Son, W. K.; Youk, J. H.; Park, W. H., Antimicrobial cellulose acetate nanofibers containing silver nanoparticles. *Carbohydrate Polymers* **2006,** 65, (4), 430-434.
103. Chen, L.; Bromberg, L.; Hatton, T. A.; Rutledge, G. C., Electrospun cellulose acetate fibers containing chlorhexidine as a bactericide. *Polymer* **2008,** 49, (5), 1266-1275.
104. Ohkawa, K.; Cha, D. I.; Kim, H.; Nishida, A.; Yamamoto, H., Electrospinning of chitosan. *Macromolecular Rapid Communications* **2004,** 25, (18), 1600-1605.
105. Haiqing Liu, Y.-L. H., Ultrafine fibrous cellulose membranes from electrospinning of cellulose acetate. *Journal of Polymer Science Part B: Polymer Physics* **2002,** 40, (18), 2119-2129.
106. Kim, C. W.; Kim, D. S.; Kang, S. Y.; Marquez, M.; Joo, Y. L., Structural studies of electrospun cellulose nanofibers. *Polymer* **2006,** 47, (14), 5097-5107.
107. Geng, X. Y.; Kwon, O. H.; Jang, J. H., Electrospinning of chitosan dissolved in concentrated acetic acid solution. *Biomaterials* **2005,** 26, (27), 5427-5432.
108. Min, B. M.; Lee, S. W.; Lim, J. N.; You, Y.; Lee, T. S.; Kang, P. H.; Park, W. H., Chitin and chitosan nanofibers: electrospinning of chitin and deacetylation of chitin nanofibers. *Polymer* **2004,** 45, (21), 7137-7142.
109. Mincheva, R.; Manolova, N.; Paneva, D.; Rashkov, I., Preparation of polyelectrolyte-containing nanofibers by electrospinning in the presence of a non-ionogenic water-soluble polymer. *Journal of Bioactive and Compatible Polymers* **2005,** 20, (5), 419-435.
110. Ignatova, M.; Manolova, N.; Rashkov, I., Novel antibacterial fibers of quaternized chitosan and poly(vinyl pyrrolidone) prepared by electrospinning. *European Polymer Journal* **2007,** 43, (4), 1112-1122.
111. Bhattarai, N.; Edmondson, D.; Veiseh, O.; Matsen, F. A.; Zhang, M. Q., Electrospun chitosan-based nanofibers and their cellular compatibility. *Biomaterials* **2005,** 26, (31), 6176-6184.
112. Li, L.; Hsieh, Y. L., Chitosan bicomponent nanofibers and nanoporous fibers. *Carbohydrate Research* **2006,** 341, (3), 374-381.
113. Duan, B.; Dong, C. H.; Yuan, X. Y.; Yao, K. D., Electrospinning of chitosan solutions in acetic acid with poly(ethylene oxide). *Journal of Biomaterials Science-Polymer Edition* **2004,** 15, (6), 797-811.
114. Lou, C. W.; Lin, J. H.; Yen, K. C.; Lu, C. T.; Lee, C. Y., Preparation of polyethylene by electrospinning and the oxide/chitosan fiber membranes evaluation of biocompatibility. *Textile Research Journal* **2008,** 78, (3), 254-257.

115. Matsuda, A.; Kagata, G.; Kino, R.; Tanaka, J., Preparation of chitosan nanofiber tube by electrospinning. *Journal of Nanoscience and Nanotechnology* **2007,** 7, (3), 852-855.
116. Sangsanoh, P.; Supaphol, P., Stability improvement of electrospun chitosan nanofibrous membranes in neutral or weak basic aqueous solutions. *Biomacromolecules* **2006,** 7, (10), 2710-2714.
117. Zhou, Y. S.; Yang, D. Z.; Nie, J., Electrospinning of chitosan/poly(vinyl alcohol)/acrylic acid aqueous solutions. *Journal of Applied Polymer Science* **2006,** 102, (6), 5692-5697.
118. Zhang, Y. Z.; Su, B.; Ramakrishna, S.; Lim, C. T., Chitosan Nanofibers from an Easily Electrospinnable UHMWPEO-Doped Chitosan Solution System. *Biomacromolecules* **2008,** 9, (1), 136-141.
119. Chen, Z. G.; Mo, X. M.; Qing, F. L., Electrospinning of collagen-chitosan complex. *Materials Letters* **2007,** 61, (16), 3490-3494.
120. Park, K. E.; Jung, S. Y.; Lee, S. J.; Min, B. M.; Park, W. H., Biomimetic nanofibrous scaffolds: Preparation and characterization of chitin/silk fibroin blend nanofibers. *International Journal of Biological Macromolecules* **2006,** 38, (3-5), 165-173.
121. Neamnark, A.; Rujiravanit, R.; Supaphol, P., Electrospinning of hexanoyl chitosan. *Carbohydrate Polymers* **2006,** 66, (3), 298-305.
122. Jian, D.; You-Lo, H., Nanofibrous membranes from aqueous electrospinning of carboxymethyl chitosan. *Nanotechnology* **2008**, (12), 125707.
123. Bhattarai, N.; Li, Z. S.; Edmondson, D.; Zhang, M. Q., Alginate-based nanofibrous scaffolds: Structural, mechanical, and biological properties. *Advanced Materials* **2006,** 18, (11), 1463-+.
124. Jiang, H. L.; Fang, D. F.; Hsiao, B. S.; Chu, B.; Chen, W. L., Optimization and characterization of dextran membranes prepared by electrospinning. *Biomacromolecules* **2004,** 5, (2), 326-333.
125. Boland, E. D.; Matthews, J. A.; Pawlowski, K. J.; Simpson, D. G.; Wnek, G. E.; Bowlin, G. L., Electrospinning collagen and elastin: Preliminary vascular tissue engineering. *Frontiers in Bioscience* **2004,** 9, 1422-1432.
126. Zhang, Y. Z.; Ouyang, H. W.; Lim, C. T.; Ramakrishna, S.; Huang, Z. M., Electrospinning of gelatin fibers and gelatin/PCL composite fibrous scaffolds. *Journal of Biomedical Materials Research Part B-Applied Biomaterials* **2005,** 72B, (1), 156-165.
127. Chen, Z. G.; Mo, X. M.; He, C. L.; Wang, H. S., Intermolecular interactions in electrospun collagen-chitosan complex nanofibers. *Carbohydrate Polymers* **2008,** 72, (3), 410-418.
128. Yoo, C. R.; Yeo, I. S.; Park, K. E.; Park, J. H.; Lee, S. J.; Park, W. H.; Min, B. M., Effect of chitin/silk fibroin nanofibrous bicomponent structures on interaction with human epidermal keratinocytes. *International Journal of Biological Macromolecules* **2008,** 42, (4), 324-334.
129. Wang, M.; Yu, J. H.; Kaplan, D. L.; Rutledge, G. C., Production of submicron diameter silk fibers under benign processing conditions by two-fluid electrospinning. *Macromolecules* **2006,** 39, (3), 1102-1107.
130. Xie, J. B.; Hsieh, Y. L., Ultra-high surface fibrous membranes from electrospinning of natural proteins: casein and lipase enzyme. *Journal of Materials Science* **2003,** 38, (10), 2125-2133.
131. Wongsasulak, S.; Kit, K. M.; McClements, D. J.; Yoovidhya, T.; Weiss, J., The effect of solution properties on the morphology of ultrafine electrospun egg albumen-PEO composite fibers. *Polymer* **2007,** 48, (2), 448-457.
132. Torres-Giner, S.; Gimenez, E.; Lagarona, J. M., Characterization of the morphology and thermal properties of zein prolamine nanostructures obtained by electrospinning. *Food Hydrocolloids* **2008,** 22, (4), 601-614.

133. Yao, C.; Li, X. S.; Song, T. Y., Fabrication of zein/hyaluronic acid fibrous membranes by electrospinning. *Journal of Biomaterials Science-Polymer Edition* **2007,** 18, (6), 731-742.
134. Woerdeman, D. L.; Shenoy, S.; Breger, D., Role of chain entanglements in the electrospinning of wheat protein-poly(vinyl alcohol) blends. *Journal of Adhesion* **2007,** 83, (8), 785-798.
135. Fang, X.; Reneker, D. H., DNA fibers by electrospinning. *Journal of Macromolecular Science-Physics* **1997,** B36, (2), 169-173.
136. Ohkawa, K.; Ando, M.; Shirakabe, Y.; Takahashi, Y.; Yamada, M.; Shirai, H.; Yamamoto, H., Preparing chitosan-poly(acrylic acid) composite fibers by self-assembly at an aqueous solution interface. *Textile Research Journal* **2002,** 72, (2), 120-124.
137. Dayal, P.; Liu, J.; Kumar, S.; Kyu, T., Experimental and Theoretical Investigations of Porous Structure Formation in Electrospun Fibers. *Macromolecules* **2007,** 40, (21), 7689-7694.
138. Bellan, L. M.; Cross, J. D.; Strychalski, E. A.; Moran-Mirabal, J.; Craighead, H. G., Individually resolved DNA molecules stretched and embedded in electrospun polymer nanofibers. *Nano Letters* **2006,** 6, (11), 2526-2530.
139. Luu, Y. K.; Kim, K.; Hsiao, B. S.; Chu, B.; Hadjiargyrou, M., Development of a nanostructured DNA delivery scaffold via electrospinning of PLGA and PLA-PEG block copolymers. *Journal of Controlled Release* **2003,** 89, (2), 341-353.
140. Muller, K.; Quinn, J. F.; Johnston, A. P. R.; Becker, M.; Greiner, A.; Caruso, F., Polyelectrolyte functionalization of electrospun fibers. *Chemistry of Materials* **2006,** 18, (9), 2397-2403.
141. Barhate, R. S.; Loong, C. K.; Ramakrishna, S., Preparation and characterization of nanofibrous filtering media. *Journal of Membrane Science* **2006,** 283, (1-2), 209-218.
142. http://208.106.133.230/www.dukescientific.com/pages/page38fa.html?s=979&ss=1298&t=988. In.
143. Barhate, R. S.; Ramakrishna, S., Nanofibrous filtering media: Filtration problems and solutions from tiny materials. *Journal of Membrane Science* **2007,** 296, (1-2), 1-8.
144. Kosmider, K.; Scott, J., Polymeric nanofibres exhibit an enhanced air filtration performance. *Filtration & Separation* **2002,** 39, (6), 20-22.
145. Kristine Graham; Ming Ouyang; Tom Raether; Tim Grafe; Bruce McDonald; Knauf, P. In *Polymeric Nanofibers in Air Filtration Applications*, Fifteenth Annual Technical Conference & Expo of the American Filtration & Separations Society, Galveston,TX, April 9-12, 2002; Galveston,TX, 2002.
146. Ahn, Y. C.; Park, S. K.; Kim, G. T.; Hwang, Y. J.; Lee, C. G.; Shin, H. S.; Lee, J. K., Development of high efficiency nanofilters made of nanofibers. *Current Applied Physics* **2006,** 6, (6), 1030-1035.
147. Maze, B.; Vahedi Tafreshi, H.; Wang, Q.; Pourdeyhimi, B., A simulation of unsteady-state filtration via nanofiber media at reduced operating pressures. *Journal of Aerosol Science* **2007,** 38, (5), 550-571.
148. Podgorski, A.; Balazy, A.; Gradon, L., Application of nanofibers to improve the filtration efficiency of the most penetrating aerosol particles in fibrous filters. *Chemical Engineering Science* **2006,** 61, (20), 6804-6815.
149. Schreuder-Gibson, H. L.; Truong, Q.; Walker, J. E.; Owens, J. R.; Wander, J. D.; Jones, W. E., Chemical and biological protection and detection in fabrics for protective clothing. *Mrs Bulletin* **2003,** 28, (8), 574-578.
150. C. Shin, G. G. C., Water-in-oil coalescence in micro-nanofiber composite filters. *AIChE Journal* **2004,** 50, (2), 343-350.

151. Qin, X.-H.; Wang, S.-Y., Filtration properties of electrospinning nanofibers. *Journal of Applied Polymer Science* **2006,** 102, (2), 1285-1290.
152. Heikkila, P.; Sipila, A.; Peltola, M.; Harlin, A.; Taipale, A., Electrospun PA-66 coating on textile surfaces. *Textile Research Journal* **2007,** 77, (11), 864-870.
153. Yun, K. M.; Hogan Jr, C. J.; Matsubayashi, Y.; Kawabe, M.; Iskandar, F.; Okuyama, K., Nanoparticle filtration by electrospun polymer fibers. *Chemical Engineering Science* **2007,** 62, (17), 4751-4759.
154. Sang, Y.; Li, F.; Gu, Q.; Liang, C.; Chen, J., Heavy metal-contaminated groundwater treatment by a novel nanofiber membrane. *Desalination* **2008,** 223, (1-3), 349-360.
155. Gopal, R.; Kaur, S.; Ma, Z. W.; Chan, C.; Ramakrishna, S.; Matsuura, T., Electrospun nanofibrous filtration membrane. *Journal of Membrane Science* **2006,** 281, (1-2), 581-586.
156. Gopal, R.; Kaur, S.; Feng, C. Y.; Chan, C.; Ramakrishna, S.; Tabe, S.; Matsuura, T., Electrospun nanofibrous polysulfone membranes as pre-filters: Particulate removal. *Journal of Membrane Science* **2007,** 289, (1-2), 210-219.
157. Yoon, K.; Kim, K.; Wang, X. F.; Fang, D. F.; Hsiao, B. S.; Chu, B., High flux ultrafiltration membranes based on electrospun nanofibrous PAN scaffolds and chitosan coating. *Polymer* **2006,** 47, (7), 2434-2441.
158. Kyung-Hye Jung; Huh, M.-W.; Jiang, W. M.; Hee, Y. S.; Bae, H. J.-S.; Hudson, S. M.; Kang, I.-K., Preparation and antibacterial activity of PET/chitosan nanofibrous mats using an electrospinning technique. *Journal of Applied Polymer Science* **2007,** 105, (5), 2816-2823.
159. Fong, H.; Reneker, D. H., Elastomeric nanofibers of styrene-butadiene-styrene triblock copolymer. *Journal of Polymer Science Part B-Polymer Physics* **1999,** 37, (24), 3488-3493.
160. Gao, B. J.; Lv, Y. X.; Jiu, H. F., Synthesis and properties of cationic polyacrylamide containing pyridine quaternary salt. *Polymer International* **2003,** 52, (9), 1468-1473.
161. Gao, B. J.; He, S. X.; Guo, J. F.; Wang, R. X., Antibacterial property and mechanism of copolymer of acrylamide and quaternary salt of 4-vinyl pyridine. *Journal of Applied Polymer Science* **2006,** 100, (2), 1531-1537.
162. Zhao, Y. Y.; Yang, Q. B.; Lu, X. F.; Wang, C.; Wei, Y., Study on correlation of morphology of electrospun products of polyacrylamide with ultrahigh molecular weight. *Journal of Polymer Science Part B-Polymer Physics* **2005,** 43, (16), 2190-2195.
163. Liu, N.; Chen, X. G.; Park, H. J.; Liu, C. G.; Liu, C. S.; Meng, X. H.; Yu, L. J., Effect of MW and concentration of chitosan on antibacterial activity of Escherichia coli. *Carbohydrate Polymers* **2006,** 64, (1), 60-65.
164. Carreau, P.; Kee, D.; Chabra, P., *Rheology of polymeric systems: Principles and applications*. Hanser Publishers: Munich,Germany 1997.
165. Arof, A. K.; Morni, N. M.; Yarmo, M. A., Evidence of lithium-nitrogen interaction in chitosan-based films from X-ray photoelectron spectroscopy. *Materials Science and Engineering B* **1998,** 55, (1-2), 130-133.
166. *Method 7600*. 4 ed.; NIOSH Manual of Analytical Methods (NMAM),National Institute of Occupational Safety and Health: 1994; Vol. 4.
167. Swanson, K. M. J.; Petran, R. L.; Hanlin, J. H. *Culture Methods for Enumeration of Microorganisms; American Public Health Association*; Washington, DC, 2001.
168. Cho, J.; Heuzey, M. C.; Begin, A.; Carreau, P. J., Effect of urea on solution behavior and heat-induced gelation of chitosan-beta-glycerophosphate. *Carbohydrate Polymers* **2006,** 63, (4), 507-518.

169. Li, Q. X.; Song, B. Z.; Yang, Z. Q.; Fan, H. L., Electrolytic conductivity behaviors and solution conformations of chitosan in different acid solutions. *Carbohydrate Polymers* **2006,** 63, (2), 272-282.
170. Cho, J. Y.; Heuzey, M. C.; Begin, A.; Carreau, P. J., Viscoelastic properties of chitosan solutions: Effect of concentration and ionic strength. *Journal of Food Engineering* **2006,** 74, (4), 500-515.
171. Sureeporn Koombhongse; Liu, W.; Reneker, D. H., Flat polymer ribbons and other shapes by electrospinning. *Journal of Polymer Science Part B: Polymer Physics* **2001,** 39, (21), 2598-2606.
172. Desai, K.; Kit, K.; Li, J.; Zivanovic, S., Morphological and Surface Properties of Electrospun Chitosan Nanofibers. *Biomacromolecules* **2008,** 9, (3), 1000-1006.
173. Chaobo Xiao; Lu, Y.; Jing, Z.; Zhang, L., Study on physical properties of blend films from gelatin and polyacrylamide solutions. *Journal of Applied Polymer Science* **2002,** 83, (5), 949-955.
174. Rojas, G.; Silva, J.; Flores, J. A.; Rodriguez, A.; Ly, M.; Maldonado, H., Adsorption of chromium onto cross-linked chitosan. *Separation and Purification Technology* **2005,** 44, (1), 31-36.
175. Yui, T.; Imada, K.; Okuyama, K.; Obata, Y.; Suzuki, K.; Ogawa, K., Molecular and crystal structure of the anhydrous form of chitosan. *Macromolecules* **1994,** 27, (26), 7601-7605.
176. Zivanovic, S.; Li, J.; Davidson, P. M.; Kit, K., Physical, Mechanical, and Antibacterial Properties of Chitosan/PEO Blend Films. *Biomacromolecules* **2007,** 8, (5), 1505-1510.
177. Matienzo, L. J.; Winnacker, S. K., Dry processes for surface modification of a biopolymer: Chitosan. *Macromolecular Materials and Engineering* **2002,** 287, (12), 871-880.
178. Chen, Z. J.; Lu, X. L.; Chan, C. M.; Mi, Y. L., Manipulating the surface properties of polyacrylamide with nitrogen plasma. *European Polymer Journal* **2006,** 42, (11), 2914-2920.
179. Thomas, H. R.; O'Malley, J. J., Surface Studies on Multicomponent Polymer Systems by X-ray Photoelectron Spectroscopy. Polystyrene/Poly(ethylene oxide) Diblock Copolymers. *Macromolecules* **1979,** 12, (2), 323-329.
180. Zhang, C.-H.; Yang, F.-l.; Wang, W.-J.; Chen, B., Preparation and characterization of hydrophilic modification of polypropylene non-woven fabric by dip-coating PVA (polyvinyl alcohol). *Separation and Purification Technology* **2008,** 61, (3), 276-286.
181. Dambies, L.; Guimon, C.; Yiacoumi, S.; Guibal, E., Characterization of metal ion interactions with chitosan by X-ray photoelectron spectroscopy. *Colloids and Surfaces A: Physicochemical and Engineering Aspects* **2000,** 177, (2-3), 203-214.
182. Rjeb, A.; Letarte, S.; Tajounte, L.; El Idrissi, M. C.; Adnot, A.; Roy, D.; Claire, Y.; Kaloustian, J., Polypropylene natural aging studied by X-ray photoelectron spectroscopy. *Journal of Electron Spectroscopy and Related Phenomena* **2000,** 107, (3), 221-230.
183. Krevelen, D. W. V., *Properties of Polymers*. Third ed.; Elsevier Science Publishing Company Inc.: New York, 1990.
184. Kriegel, C.; Weiss, J.; Kit, K., Influence of surfactants on electrospinning of chitosan-poly(ethylene oxide) blend nanofibers. *Abstracts of Papers of the American Chemical Society* **2008**, (042).
185. Deng, Y.; Dixon, J. B.; White, G. N.; Loeppert, R. H.; Juo, A. S. R., Bonding between polyacrylamide and smectite. *Colloids and Surfaces A: Physicochemical and Engineering Aspects* **2006,** 281, (1-3), 82-91.

186. Qian, S. H.; Huang, G. Q.; Jiang, J. S.; He, F.; Wang, Y. T., Studies of adsorption behavior of crosslinked chitosan for Cr(VI), Se(VI). *Journal of Applied Polymer Science* **2000,** 77, (14), 3216-3219.
187. Wang, Q. Z.; Chen, X. G.; Liu, N.; Wang, S. X.; Liu, C. S.; Meng, X. H.; Liu, C. G., Protonation constants of chitosan with different molecular weight and degree of deacetylation. *Carbohydrate Polymers* **2006,** 65, (2), 194-201.
188. Li, J.; Zivanovic, S.; Davidson, M.; Kit, K., Surface properties of chitosan/PEO blend films as affected by film preparation method. *Abstracts of Papers of the American Chemical Society* **2007,** 234.

Appendices

Appendix 1

Chitosan density calculations

Chitosan DDA	Wt of rpt unit (g/mole)	Vol. of chitosan unit cell (cc)	Density (g/cc)	Difference in density between amorphous and crystalline chitosan
80%DDA	169.4	7.44427E-22	1.511258036	0.007449446
70%DDA	173.6	7.44427E-22	1.548727243	0.031462766
67%DDA	174.86	7.44427E-22	1.559968005	0.038441818

Appendix 2

Model Calculations – Effect of % chitosan on metal binding as function of fiber diameter for 80% DDA chitosan blend fibers (theoretical density of chitosan (from appendix 1) = 1.51 g/cc).

95% Chitosan blend fibers

diameter of fiber (nm)	for 95% Chitosan blend fiber surface area of chitosan/g	NH3+ ions for 100% crystalline	NH3+ions (after density correction)	max NH3+ ions being reacted	mass of chromate (g)	mass of chromium (mg)
50	5.03E+05	5.59E+19	5.57E+19	5.34E+19	9.94E-03	9.94
100	2.51E+05	2.80E+19	2.78E+19	2.67E+19	4.97E-03	4.97
200	1.26E+05	1.40E+19	1.39E+19	1.34E+19	2.48E-03	2.48
400	6.29E+04	6.99E+18	6.96E+18	6.68E+18	1.24E-03	1.24
600	4.19E+04	4.66E+18	4.64E+18	4.45E+18	8.28E-04	0.83
800	3.14E+04	3.50E+18	3.48E+18	3.34E+18	6.21E-04	0.62
1000	2.51E+04	2.80E+18	2.78E+18	2.67E+18	4.97E-04	0.50
1200	2.10E+04	2.33E+18	2.32E+18	2.23E+18	4.14E-04	0.41
1400	1.80E+04	2.00E+18	1.99E+18	1.91E+18	3.55E-04	0.35
1600	1.57E+04	1.75E+18	1.74E+18	1.67E+18	3.10E-04	0.31
1800	1.40E+04	1.55E+18	1.55E+18	1.48E+18	2.76E-04	0.28
2000	1.26E+04	1.40E+18	1.39E+18	1.34E+18	2.48E-04	0.25

90% Chitosan blend fibers

diameter of fiber (nm)	for 90% Chitosan blend fiber surface area of chitosan/g	NH3+ ions for 100% crystalline	NH3+ions (after density correction)	max NH3+ ions being reacted	mass of chromate (g)	mass of chromium (mg)
50	4.76E+05	5.30E+19	5.27E+19	5.06E+19	9.41E-03	9.41
100	2.38E+05	2.65E+19	2.64E+19	2.53E+19	4.71E-03	4.71
200	1.19E+05	1.32E+19	1.32E+19	1.27E+19	2.35E-03	2.35
400	5.96E+04	6.62E+18	6.59E+18	6.33E+18	1.18E-03	1.18
600	3.97E+04	4.42E+18	4.39E+18	4.22E+18	7.84E-04	0.78
800	2.98E+04	3.31E+18	3.30E+18	3.16E+18	5.88E-04	0.59
1000	2.38E+04	2.65E+18	2.64E+18	2.53E+18	4.71E-04	0.47
1200	1.99E+04	2.21E+18	2.20E+18	2.11E+18	3.92E-04	0.39
1400	1.70E+04	1.89E+18	1.88E+18	1.81E+18	3.36E-04	0.34
1600	1.49E+04	1.66E+18	1.65E+18	1.58E+18	2.94E-04	0.29
1800	1.32E+04	1.47E+18	1.46E+18	1.41E+18	2.61E-04	0.26
2000	1.19E+04	1.32E+18	1.32E+18	1.27E+18	2.35E-04	0.24

75% Chitosan blend fibers

diameter of fiber (nm)	for 75% Chitosan blend fiber surface area of chitosan/g	NH3+ ions for 100% crystalline	NH3+ions (after density correction)	max NH3+ ions being reacted	mass of chromium (g)	mass of chromium (mg)
50	3.97E+05	4.42E+19	4.39E+19	4.22E+19	7.84E-03	7.84
100	1.99E+05	2.21E+19	2.20E+19	2.11E+19	3.92E-03	3.92
200	9.93E+04	1.10E+19	1.10E+19	1.05E+19	1.96E-03	1.96
400	4.96E+04	5.52E+18	5.49E+18	5.27E+18	9.80E-04	0.98
600	3.31E+04	3.68E+18	3.66E+18	3.52E+18	6.54E-04	0.65
800	2.48E+04	2.76E+18	2.75E+18	2.64E+18	4.90E-04	0.49
1000	1.99E+04	2.21E+18	2.20E+18	2.11E+18	3.92E-04	0.39
1200	1.65E+04	1.84E+18	1.83E+18	1.76E+18	3.27E-04	0.33
1400	1.42E+04	1.58E+18	1.57E+18	1.51E+18	2.80E-04	0.28
1600	1.24E+04	1.38E+18	1.37E+18	1.32E+18	2.45E-04	0.25
1800	1.10E+04	1.23E+18	1.22E+18	1.17E+18	2.18E-04	0.22
2000	9.93E+03	1.10E+18	1.10E+18	1.05E+18	1.96E-04	0.20

50% Chitosan blend fibers

diameter of fiber (nm)	for 50% Chitosan blend fiber surface area of chitosan/g	NH3+ ions for 100% crystalline	NH3+ions (after density correction)	max NH3+ ions being reacted	mass of chromium (g)	mass of chromium (mg)
50	2.65E+05	2.94E+19	2.93E+19	2.81E+19	5.23E-03	5.23
100	1.32E+05	1.47E+19	1.46E+19	1.41E+19	2.61E-03	2.61
200	6.62E+04	7.36E+18	7.32E+18	7.03E+18	1.31E-03	1.31
400	3.31E+04	3.68E+18	3.66E+18	3.52E+18	6.54E-04	0.65
600	2.21E+04	2.45E+18	2.44E+18	2.34E+18	4.36E-04	0.44
800	1.65E+04	1.84E+18	1.83E+18	1.76E+18	3.27E-04	0.33
1000	1.32E+04	1.47E+18	1.46E+18	1.41E+18	2.61E-04	0.26
1200	1.10E+04	1.23E+18	1.22E+18	1.17E+18	2.18E-04	0.22
1400	9.45E+03	1.05E+18	1.05E+18	1.00E+18	1.87E-04	0.19
1600	8.27E+03	9.20E+17	9.15E+17	8.79E+17	1.63E-04	0.16
1800	7.35E+03	8.18E+17	8.14E+17	7.81E+17	1.45E-04	0.15
2000	6.62E+03	7.36E+17	7.32E+17	7.03E+17	1.31E-04	0.13

Appendix 3

Model Calculations – Effect of chitosan DDA on metal binding as function of fiber diameter for 90% chitosan blend fibers.

80% DDA chitosan
Theoretical density of chitosan: 1.51 g/cc (appendix 1)

diameter of fiber (nm)	for 90% Chitosan blend fiber surface area of chitosan/g	NH3+ ions for 100% crystalline	NH3+ions (after density correction)	max NH3+ ions being reacted	mass of chromate (g)	mass of chromium (mg)
50	4.76E+05	5.30E+19	5.27E+19	5.06E+19	9.41E-03	9.41
100	2.38E+05	2.65E+19	2.64E+19	2.53E+19	4.71E-03	4.71
200	1.19E+05	1.32E+19	1.32E+19	1.27E+19	2.35E-03	2.35
400	5.96E+04	6.62E+18	6.59E+18	6.33E+18	1.18E-03	1.18
600	3.97E+04	4.42E+18	4.39E+18	4.22E+18	7.84E-04	0.78
800	2.98E+04	3.31E+18	3.30E+18	3.16E+18	5.88E-04	0.59
1000	2.38E+04	2.65E+18	2.64E+18	2.53E+18	4.71E-04	0.47
1200	1.99E+04	2.21E+18	2.20E+18	2.11E+18	3.92E-04	0.39
1400	1.70E+04	1.89E+18	1.88E+18	1.81E+18	3.36E-04	0.34
1600	1.49E+04	1.66E+18	1.65E+18	1.58E+18	2.94E-04	0.29
1800	1.32E+04	1.47E+18	1.46E+18	1.41E+18	2.61E-04	0.26
2000	1.19E+04	1.32E+18	1.32E+18	1.27E+18	2.35E-04	0.24

70% DDA chitosan

Theoretical density of chitosan: 1.55 g/cc (appendix 1)

diameter of fiber (nm)	Surface area of chitosan/g	NH3+ ions for 100% crystalline	NH3+ions (after density correction)	max NH3+ ions being reacted	mass of chromium (g)	mass of chromium (mg)
50	4.6E+05	5.2E+19	5.062E+19	4.859E+19	9.0E-03	9.04
100	2.3E+05	2.6E+19	2.531E+19	2.430E+19	4.5E-03	4.52
200	1.2E+05	1.3E+19	1.265E+19	1.215E+19	2.3E-03	2.26
400	5.8E+04	6.5E+18	6.327E+18	6.074E+18	1.1E-03	1.13
600	3.9E+04	4.3E+18	4.218E+18	4.050E+18	7.5E-04	0.75
800	2.9E+04	3.2E+18	3.164E+18	3.037E+18	5.6E-04	0.56
1000	2.3E+04	2.6E+18	2.531E+18	2.430E+18	4.5E-04	0.45
1200	1.9E+04	2.2E+18	2.109E+18	2.025E+18	3.8E-04	0.38
1400	1.7E+04	1.8E+18	1.808E+18	1.736E+18	3.2E-04	0.32
1600	1.5E+04	1.6E+18	1.582E+18	1.519E+18	2.8E-04	0.28
1800	1.3E+04	1.4E+18	1.406E+18	1.350E+18	2.5E-04	0.25
2000	1.2E+04	1.3E+18	1.265E+18	1.215E+18	2.3E-04	0.23

67% DDA chitosan

Theoretical density of chitosan: 1.56 g/cc (appendix 1)

diameter of fiber (nm)	Surface area of chitosan/g	NH3+ ions for 100% crystalline	NH3+ions (after density correction)	max NH3+ ions being reacted	mass of chromium (g)	mass of chromium (mg)
50	4.6E+05	5.1E+19	5.001E+19	4.801E+19	8.9E-03	8.93
100	2.3E+05	2.6E+19	2.501E+19	2.401E+19	4.5E-03	4.46
200	1.2E+05	1.3E+19	1.250E+19	1.200E+19	2.2E-03	2.23
400	5.8E+04	6.4E+18	6.252E+18	6.001E+18	1.1E-03	1.12
600	3.8E+04	4.3E+18	4.168E+18	4.001E+18	7.4E-04	0.74
800	2.9E+04	3.2E+18	3.126E+18	3.001E+18	5.6E-04	0.56
1000	2.3E+04	2.6E+18	2.501E+18	2.401E+18	4.5E-04	0.45
1200	1.9E+04	2.1E+18	2.084E+18	2.000E+18	3.7E-04	0.37
1400	1.6E+04	1.8E+18	1.786E+18	1.715E+18	3.2E-04	0.32
1600	1.4E+04	1.6E+18	1.563E+18	1.500E+18	2.8E-04	0.28
1800	1.3E+04	1.4E+18	1.389E+18	1.334E+18	2.5E-04	0.25
2000	1.2E+04	1.3E+18	1.250E+18	1.200E+18	2.2E-04	0.22

Appendix 4

Theoretical chitosan elemental composition

	80%DDA chitosan		70%DDA chitosan		67%DDA chitosan	
Element	**moles**	**At. %**	**moles**	**At. %**	**moles**	**At. %**
N	1	8.77	1	8.403	1	8.34
O	4	35.08	4.3	36.13	4.33	36.11
C	6.4	56.14	6.6	55.46	6.66	55.55
C/N	6.4		6.6		6.66	
C/O	1.6		1.53		1.54	

Theoretical PEO elemental composition

Element	moles	At. %
N	0	0
O	1	33.33
C	2	66.67
C/N	infinite	
C/O	2	

Theoretical PAAm elemental composition

Element	moles	At. %
N	1	20
O	1	20
C	3	60
C/N	3	
C/O	3	

80% DDA pure chitosan film cast from HCl.

Element	Peak BE	At. %
N1s	399.6	5.6
O1s	530.99	28.18
C1s	284.37	61.11
Cl2p	196.49	5.11
C/O	2.17	
C/N	10.91	

Pure PEO film cast from water

Element	Peak BE	At. %
O1s	530.83	32.39
C1s	284.28	66.77
Ca2p ???	346.32	0.53
Cl2p ???	196.76	0.31
C/O	2.07	

Pure PEO espun fiber on non-woven PP

Element	Peak BE	At. %
O1s	531.24	3.74
C1s	283.72	96.26

Pure PAAm film cast from water

Element	Peak BE	At. %
N1s	398.05	13.73
O1s	530.11	18.56
C1s	283.98	67.17
Cl2p ???	196.28	0.54
C/O	3.619073	
C/N	4.892207	

Pure PAAm espun fiber

Element	Peak BE	At. %
N1s	398.13	12.48
O1s	530.28	22.68
C1s	284.08	61.24
Al	73.75	3.14
Cl2p ???	197.18	0.45
C/O	2.700176	
C/N	4.907051	

Calculated surface chitosan wt% for Chitosan/PEO blends with decreasing % chitosan in blend solution and using different molecular weight chitosan

Chitosan molecular wt	% Chitosan in Blend	C/N	wt fraction chitosan in fiber	
			using theoretical # of C	using experimental # of C
HMW	95	10.87	0.63	1.00
	90	14.77	0.48	0.77
	75	27.59	0.27	0.44
	50	179.62	0.04	0.07
LMW	95			
	90	12.85	0.54	0.87
	75	64.39	0.12	0.20
	50			

Calculated surface chitosan wt% for Chitosan/PEO blends with decreasing % DDA chitosan in blend solution in HMWChitosan:PEO (90:10) blends

	% DDA	C/N	wt fraction chitosan in fiber	
			using theoretical # of C	using experimental # of C
before Cr (VI) binding	80%DDA	14.77	0.48	0.77
	70%DDA	15.93	0.46	0.72
	67%DDA	17.81	0.41	0.65
after Cr (VI) binding	80%DDA	18.95	0.38	0.62
	70%DDA	13.71	0.52	
	67%DDA	13.87	0.52	

Calculated surface chitosan wt% for Chitosan/PEO blends with varying fiber diameter (FD) in 80% DDA HMWChitosan:PEO (90:10) blends

	% DDA	C/N	wt fraction chitosan in fiber	
			using theoretical # of C	using experimental # of C
9010 diff.FD before	80	19.13	0.38	0.61
	113	14.77	0.48	0.77
	130	43.41	0.17	0.29
9010 diff.FD after	80	25.84	0.28	0.47
	113	18.95	0.38	0.62
	130	57.37	0.13	0.22

Calculated surface chitosan wt% for Chitosan/PAAm blends

% Chitosan in solution	Spinning solution temperature (°C)	Fiber Diameter (nm)	C/N from XPS	wt fraction chitosan in fiber	
				using theoretical # of C	using experimental # of C
95	RT	155.58	9.87	1.27	0.91
95	40	162.41	10.39	1.30	0.96
95	70	286.49	9.55	1.25	0.88
90	RT	50.85	9.20	1.23	0.85
90	40	63.58	8.83	1.21	0.80
90	70	306.67	8.86	1.21	0.81
75	RT	131.61	8.36	1.18	0.75
75	40	304.49	8.02	1.15	0.70
75	70	315.00	6.85	1.05	0.50

Vita

Keyur Desai was born in 1979 at Mumbai, India. He did his schooling up to 10^{th} grade at Billimoria High School, Panchgani, Maharashtra, India and 12^{th} grade from Jaihind Junior College, Mumbai, India (High School). He obtained a Bachelor's degree in Chemical Engineering from University of Mumbai in summer of 2000. After working as a chemical engineer for two years in Surat, India, Keyur came to the University of Massachusetts, Lowell in spring, 2002 to pursue a MS in chemical engineering. He graduated with master's degree in summer, 2004 and worked for a year there after at The Gillette Company, Boston, MA as process development engineer. In fall, 2005 Keyur joined the materials science and engineering department at The University of Tennessee, Knoxville to pursue a PhD. In fall, 2008 Keyur will have obtained a doctorate in materials science and engineering working under the tutelage of Prof. Kevin M Kit at The University of Tennessee, Knoxville.